Development of Lithium Disilicate Microstructure Graded Glass-Ceramic

Marianne Rose Lindsay

Thesis submitted to the faculty of the Virginia Polytechnic Institute and State University in partial fulfillment of the requirements for the degree of

Master of Science
In
Materials Science and Engineering

David Clark, Chair
G. Q. Lu
Gary Pickrell

May 21, 2012
Blacksburg, Virginia

Keywords: Crystallization, Lithium disilicate glass-ceramic, temperature gradient, microstructure graded material, functionally graded material

Development of Lithium Disilicate Microstructure Graded Glass-Ceramic

Marianne Rose Lindsay

ABSTRACT

The goal of this research was to create a microstructure graded glass-ceramic and investigate the resulting properties as a function of crystallization processing. The desired glass-ceramic was a lithium disilicate material that has a crystallization gradient across the sample, leading to functionally graded properties as a result of the microstructure gradient. Samples were prepared by melting and pouring glass at 1400°C, annealing at 400°C for 48 hours, and nucleating at 480°C for 2 hours. To ensure that crystallization would not occur homogeneously throughout the sample, a temperature gradient was imposed during crystallization. Samples were crystallized on a self-constructed resistance wire furnace that was open to air. Several crystallization processing parameters were tested, including high temperature for a short time and low temperature for a long time. Samples were ground and polished to 0.25 microns before characterization methods were performed. Scanning electron microscopy (SEM) showed the microstructure transition across the sample cross section, with crystals present on the crystalline side and only nuclei present on the glassy side. Raman spectroscopy showed a transformation of the characteristic spectra across the sample cross section, with defined, high-intensity peaks on the crystalline side and broad, low-intensity peaks on the glassy side. Microhardness showed a slight transition in hardness values across the sample cross section, however the variability was too great to draw any conclusions. The characterization methods showed that the desired material was created and the resulting properties were a function of the crystallization processing parameters.

Acknowledgements

I would like to thank my advisor and mentor, Dr. David Clark, for his guidance, help, and knowledgeable advice throughout my research. I really appreciate his concern about the quality of my work, as well as my academic and professional goals. I would also like to thank Ms. Diane Folz for guidance with laboratory work, as well as continuous help and opportunities she provided throughout my study at Virginia Tech. Thank you to the members of my committee, Dr. G. Q. Lu and Dr. Gary Pickrell, for their hard work and helpful advice. I would also like to thank my colleagues, Elizabeth Belcastro, Amanda Krause, and Andrew Kulp, for their useful discussions and laboratory support. I would also like to thank the entire Materials Science and Engineering department staff for their administrative support. I am also indebted to Steve McCartney of the Nanoscale Characterization and Fabrication Laboratory for assistance in using the SEM, and Dr. Robert Bodnar and Charles Farley of the Geosciences Department at Virginia Tech for assistance in using the Raman Spectrometer. Last, but not least, I would like to thank my friends and family for their support, patience, and confidence.

Table of Contents

List of Figures

Page

List of Tables

Page

1. Introduction

1.1 Lithium Disilicate Glass and Glass-Ceramic

Glass-ceramics are polycrystalline materials formed from special glasses [1]. A glass is first created and then transformed into a polycrystalline material through a heat treatment. This heat treatment includes controlled nucleation and crystal growth [1].

Glasses are amorphous in nature, meaning they lack long-range order [2]. In contrast, crystalline materials contain long range order [3]. To describe this further, first consider two simple materials: vitreous silica and crystalline silica. Both materials are identical in composition (SiO_2), but differ in structure.

Vitreous silica is the glassy phase of silica [2]. In this phase, the material lacks long range order, but exhibits short range order. This means that the basic building block of the glass, the silica tetrahedron, is the same throughout the glassy structure. The angle of the bond inside the tetrahedron, the O-Si-O bond, will remain constant. However, the connections of numerous tetrahedrons can vary. The angle of the bond connecting two tetrahedrons, the Si-O-Si bond, can vary between 140° and 180° in vitreous silica [2]. A representation of the Si-O-Si bond angle can be seen in the figure below.

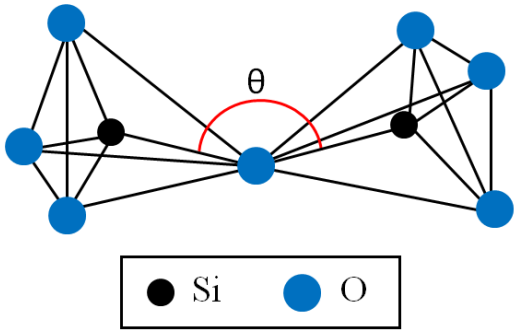

Figure 1.1: Two silica tetrahedrons with the Si-O-Si bond angle shown in red. [Obtained from Kingery et. all, 1975. Modified by author. (Used under fair use, 2012)].

On the other hand, crystalline materials contain long range order [3]. This means that in crystalline silica (quartz), the Si-O-Si bond angle will be the same throughout the material. The figure below is a schematic that shows the presence of long range order in crystalline silica, and the lack of long range order in vitreous silica. Note that in the figure below, the fourth oxygen atom in the tetrahedron is not depicted. In reality, this oxygen would be directly above or below the pictured silicon.

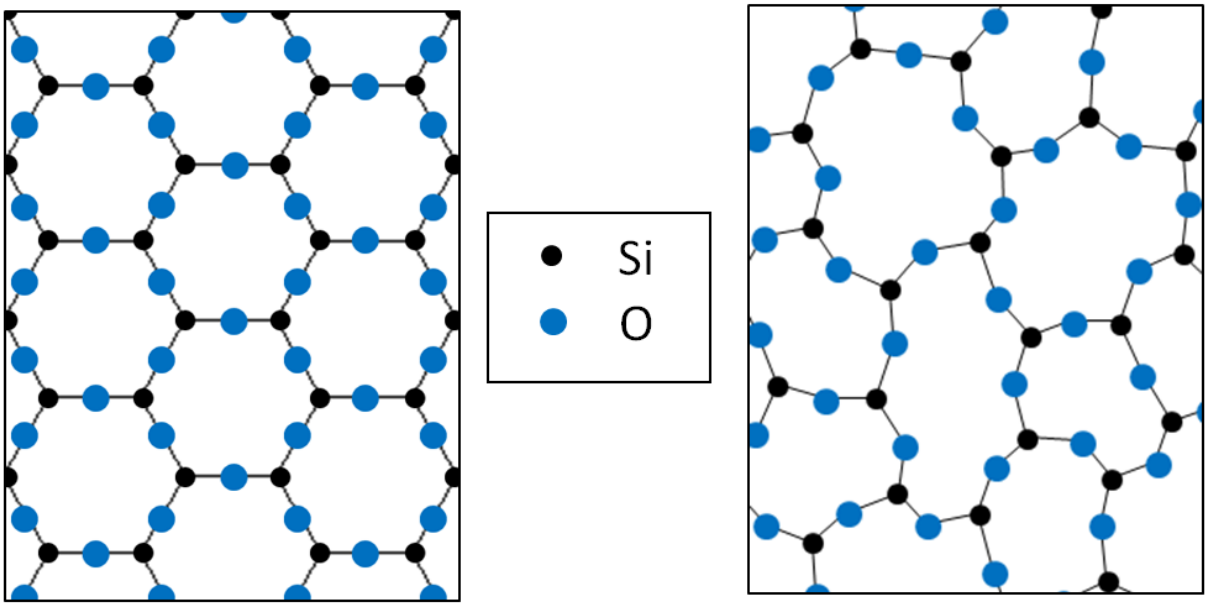

Figure 1.2: 2-Dimensional representation of the structure of silica crystals (left) and glasses (right). [Obtained from Kingery et. all, 1975. Modified by author. (Used under fair use, 2012)].

Now consider a more complicated material system: lithium disilicate. Lithium disilicate glass has two components [2]. The first is silica, which serves as the glassformer. The glassformer is the most abundant material and is the primary source of structure. The second is lithium oxide (Li_2O), which serves as the flux. The purpose of the flux is to lower the processing temperature of the glassformer. In this case, the addition of lithium oxide reduces the processing temperature of the glass from approximately 2000°C to 1100°C [2].

Since silica is the glassformer, the structure of lithium disilicate glass largely resembles the structure of vitreous silica. However, the addition of lithium oxide to silica alters the glass structure slightly [2]. Lithium oxide will infiltrate the structure near an oxygen atom. The addition of the lithium oxide will break one of the Si-O bonds to that oxygen atom, and the lithium oxide will split into two ions (LiO^- and Li^+). The Li^+ ion will bond with the existing oxygen atom (now with only one Si-O bond), and the LiO^- ion will bond with the other silicon atom (now missing an oxygen). The resulting structure will be two oxygen atoms where there used to be one, with two lithium atoms bonded nearby. The addition of lithium oxide causes non-bonding oxygens to form. These non-bonding oxygens are oxygen atoms that only have one Si-O bond [2].

In contrast, the structure of lithium disilicate crystal is very different from the structure of its glassy phase. Crystalline lithium disilicate has a complicated orthorhombic structure that contains corrugated sheets of silica [1]. The figure below is a schematic that shows the presence of long range order in crystalline lithium disilicate,

and the lack of long range order in glassy lithium disilicate. Note that in the crystal portion of the figure (on the left), lithium atoms are layered on top of oxygen atoms, and silicon atoms are not depicted because they are hidden inside the tetrahedron behind oxygen atoms. Also note that in the glassy portion of the figure (on the right), the fourth oxygen atom in the tetrahedron is not depicted. In reality, this oxygen would be directly above or below the pictured silicon.

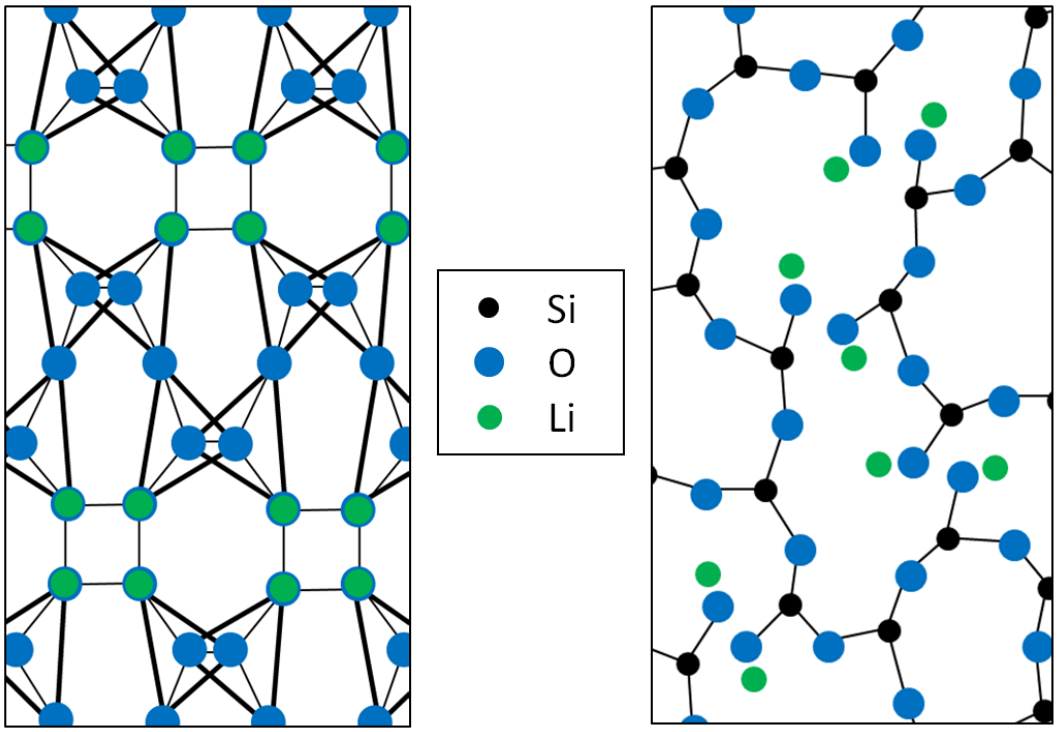

Figure 1.3: 2-Dimensional representation of the structure of lithium disilicate crystals (left) and glasses (right). [Obtained from Mahmoud, 2007 and Fang et. all, 1999. Modified by author. (Used under fair use, 2012)].

In the creation of a lithium disilicate glass-ceramic, the structure of the material would transform from the glassy phase to the crystalline phase. However, glass-ceramics are polycrystalline materials, meaning they contain not one crystal, but numerous crystals packed together [3]. These crystals are called grains and can be in many different

crystallographic orientations. While short range order exists throughout the material, long range order only exists throughout individual grains. A typical heating curve for the creation of a glass-ceramic can be seen in the figure below.

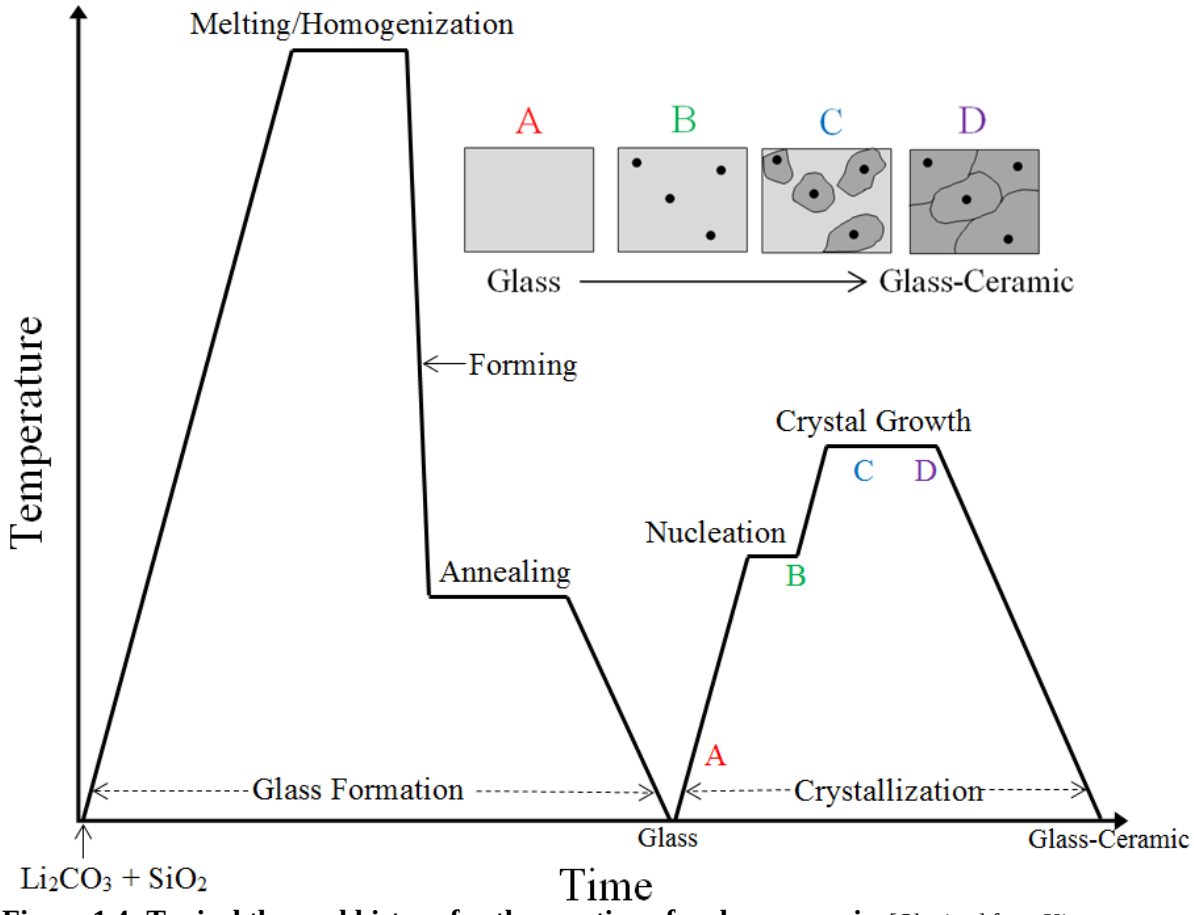

Figure 1.4: Typical thermal history for the creation of a glass-ceramic. [Obtained from Kingery et. all, 1975. Modified by author. (Used under fair use, 2012)].

As can be seen in the figure, the creation of a glass-ceramic begins with the formation of the glass. The raw materials (Li_2CO_3 + SiO_2) are combined and heated to a temperature above the liquidus, releasing CO_2 into the atmosphere. In the case of lithium disilicate, the melting/homogenization temperature is around 1100-1400°C [1]. After a melt has been achieved, the molten glass is poured into a mold, from which it will derive

its shape. The glass is then immediately heated at its annealing temperature (400°C). The purpose of the annealing is to relax stresses that have occurred during the glass pouring and to prevent cracking. After the glass is created, the material can undergo nucleation and crystal growth to transform into a glass-ceramic. The glass is heated to a temperature sufficient to allow spontaneous nucleation to occur in the material and left there until the desired nuclei population is achieved [1]. Then the nucleated glass is heated at the crystallization temperature to allow the crystals to grow from the nuclei. If heating continues, the crystals will continue to grow until 100% crystalline. If heating is prematurely stopped, the result will be a partially crystallized material, where crystallized grains exist within a glassy matrix. Notice from the above diagram that the raw materials can be converted into either an annealed glass (A), a nucleated glass (B), a partially crystallized glass (C), or a fully crystallized glass-ceramic (D). Each of these will exhibit distinctly different properties and could be used in different applications.

Glass-ceramics are used in many applications ranging from stovetops to dental prosthetics. The main benefit of these materials is that they can be easily formed in the glassy state and then transformed into a partially or fully crystalline state. Properties of the resulting glass-ceramic vary considerably depending on the percent crystallization. For example, in the glassy state, the material will appear optically transparent and exhibit only a moderate value of strength. By partially crystallizing, the strength of the material will increase and it will become translucent. When fully crystallized, the material will exhibit high strength and become opaque.

In addition to the amount of crystallization, the size of crystals present can affect the material properties. Both the crystal size and degree of crystallization are controlled by the processing time and temperature [2]. A sparse population of nuclei but extensive crystal growth will result in fewer, larger crystals present in the material. An abundant population of nuclei and minor crystal growth will result in numerous, smaller crystals present in the material. Furthermore, the rate at which nucleation and crystallization occurs is controlled by the temperature of the heat treatment. Below is a graph that shows the dependency of nucleation and crystallization rates on temperature.

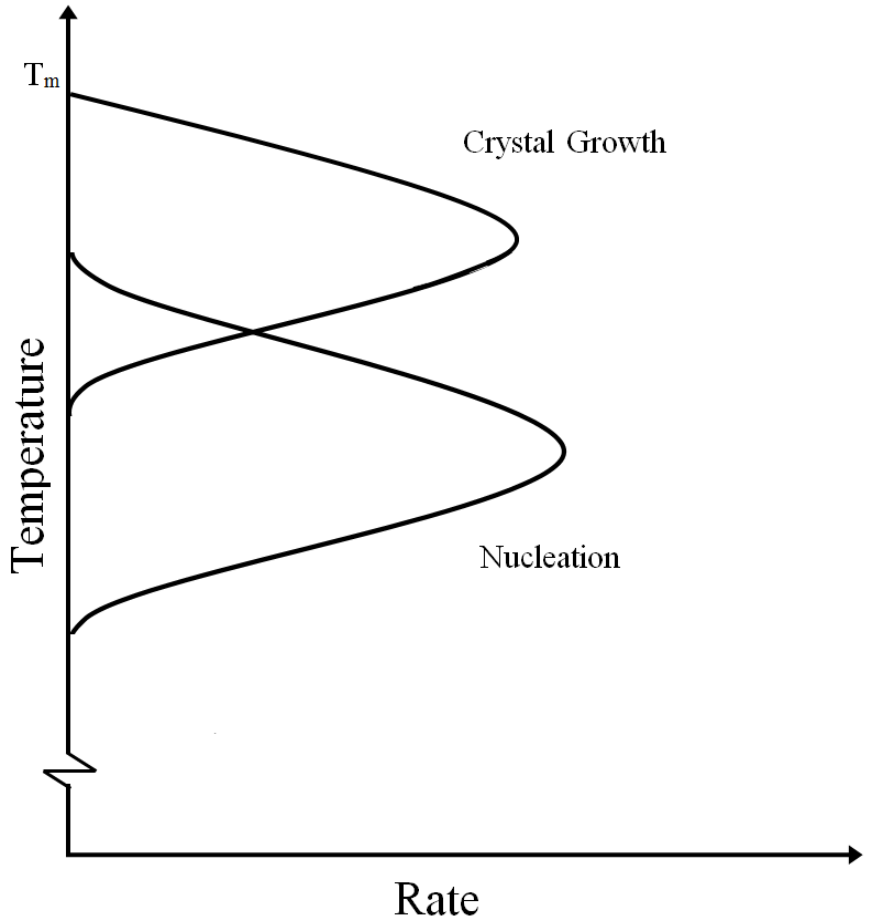

Figure 1.5: The dependence of nucleation and crystallization rate on temperature. [Obtained from Shelby, 2005. Modified by author. (Used under fair use, 2012)].

1.2 Functionally Graded Materials

In some applications, it might be necessary to have a material where properties differ from one side to the other. This material is called a functionally graded material (FGM). A functionally graded material is characterized by the change of properties with changing position in the material [5]. FGMs can be used to avoid unwanted problems at a composite material interface, such as thermal property mismatch, delamination, or unwanted optical reflection [5]. In the place of where a discrete interface would exist, a graded material would have a gradual change in the properties. This could potentially result in elimination of unwanted interfacial issues. FGMs can also be engineered to have designed property profiles that offer unique material performance [5].

It is possible to achieve a functionally graded material by two methods: a chemical gradient and a microstructure gradient [5]. In a chemically-derived FGM, the chemical composition of the material changes in relation to position inside the material. One example of a chemical graded material is a graded index optical fiber, used for telecommunications. In a graded index optical fiber, the amount of dopants added (such as B_2O_3) to the silica preform is gradually changed radially through the fiber cross section [6]. As a result of the gradual change in chemical composition, the material property of refractive index will also experience a gradual change. The resulting material has lower modal dispersion for multiple optical modes traveling through the fiber [6]. A schematic of this chemical graded material can be seen in the figure below.

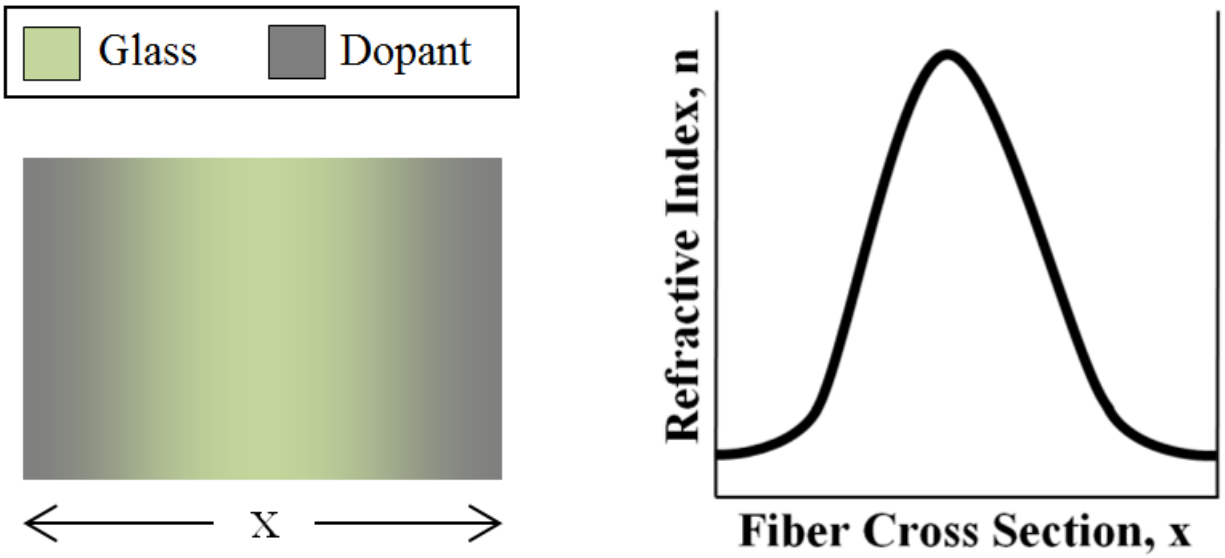

Figure 1.6: Schematic of a graded index optical fiber, a chemical graded material. The gradient in chemical composition causes a gradient in the material property of refractive index. [Obtained from Tilley, 2000. Modified by author. (Used under fair use, 2012)].

The second method of producing a functionally graded material is through a microstructure gradient. In a microstructure-derived FGM, the microstructure changes in relation to position inside the material while maintaining constant chemical composition. One example of a microstructure graded material is a graded density polymer foam. In a graded density polymer foam, the amount of porosity is gradually changed through the foam cross section [5]. As a result of the gradual change in microstructure, the material property of density will also experience a gradual change. The resulting material has high impact strength (due to the dense surface layer) while maintaining low weight [5]. This material could be useful in instrument panels such as in aerospace control panels and automobile dashboards. A schematic of this microstructure graded material can be seen in the figure below.

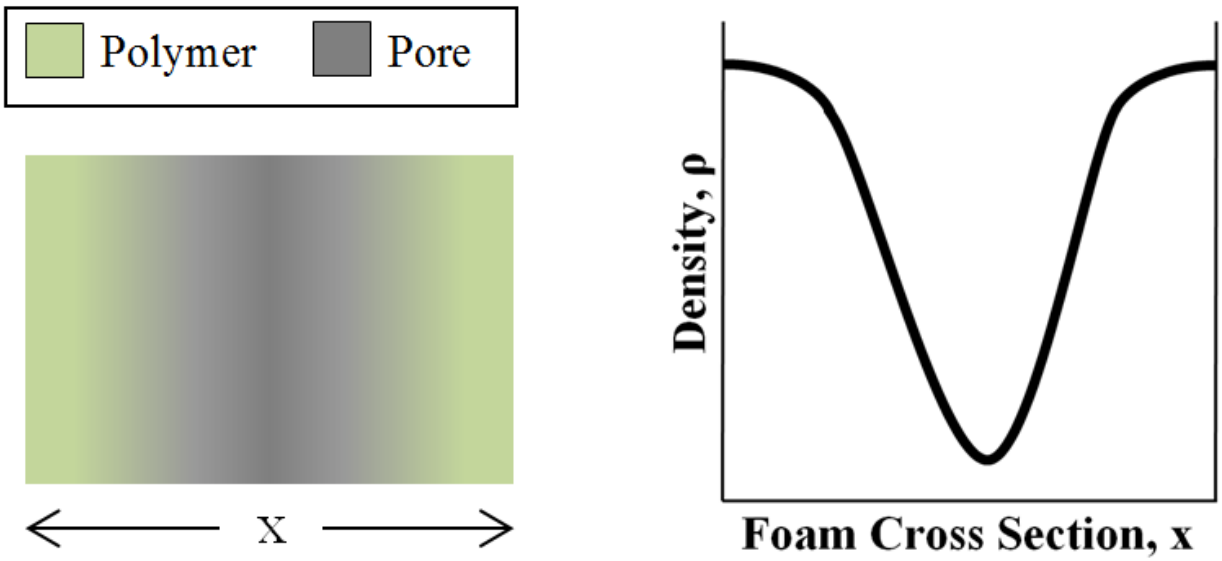

Figure 1.7: Schematic of a graded density polymer foam, a microstructure graded material. The gradient in microstructure causes a gradient in the material property of density.
[Obtained from Neubrand, 2001. Modified by author. (Used under fair use, 2012)].

Functionally graded materials have been successfully produced with a variety of processing methods, including powder, melt, and spray processing [5]. However, there is a lack of information of the reproducibility and reliability of FGMs [5].

1.3 Statement of Work

The goal of this thesis is to develop a processing method for producing microstructure graded materials and then evaluate the resulting properties as a function of position within the sample. The performance of a FGM is strongly influenced by the extension and profile of the property gradient [5]. Therefore, the long term goal of FGM research is to be able to control the material gradient so that different material performances can be achieved. For microstructure graded materials, the key to controlling the property gradient is to control the microstructure gradient. This research

will use the partial crystallization of a glass into a glass-ceramic to create the microstructure gradient. One example of a potential result of using crystallization to create a microstructure graded material can be seen in the figure below. Note that in the figure below, three distinct regions are present: a 100% crystalline phase, a graded phase, and a 100% amorphous phase. The shaded area under the curve depicts a representation of the microstructure present.

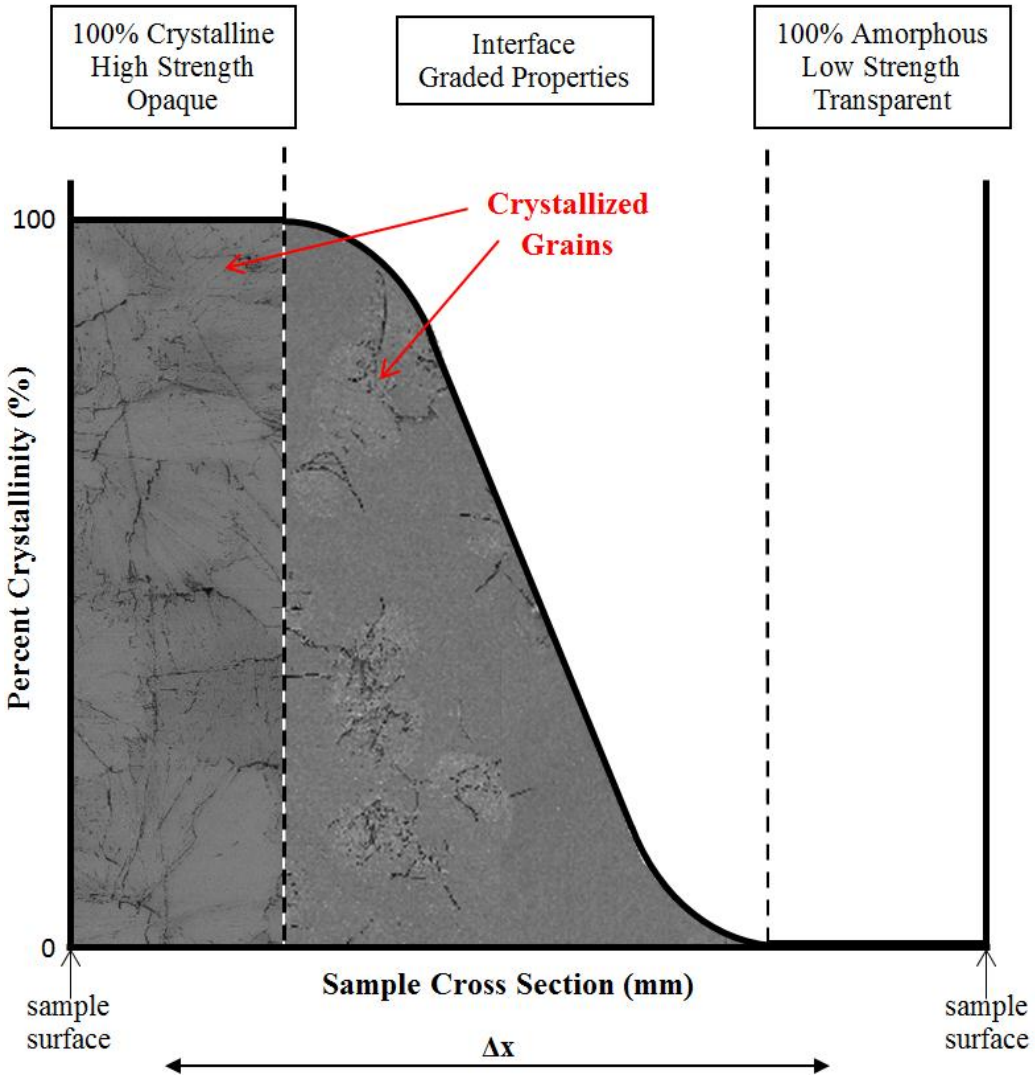

Figure 1.8: Graph of percent crystallinity versus the sample cross section for a microstructure graded material with a steep interface.

It might also be beneficial to have a microstructure graded material with a less steep microstructure gradient. Another example of a potential result of using crystallization to create a microstructure graded material can be seen in the figure below. Note that in the figure below, only one region is present: a graded phase. The shaded area under the curve depicts a representation of the microstructure present.

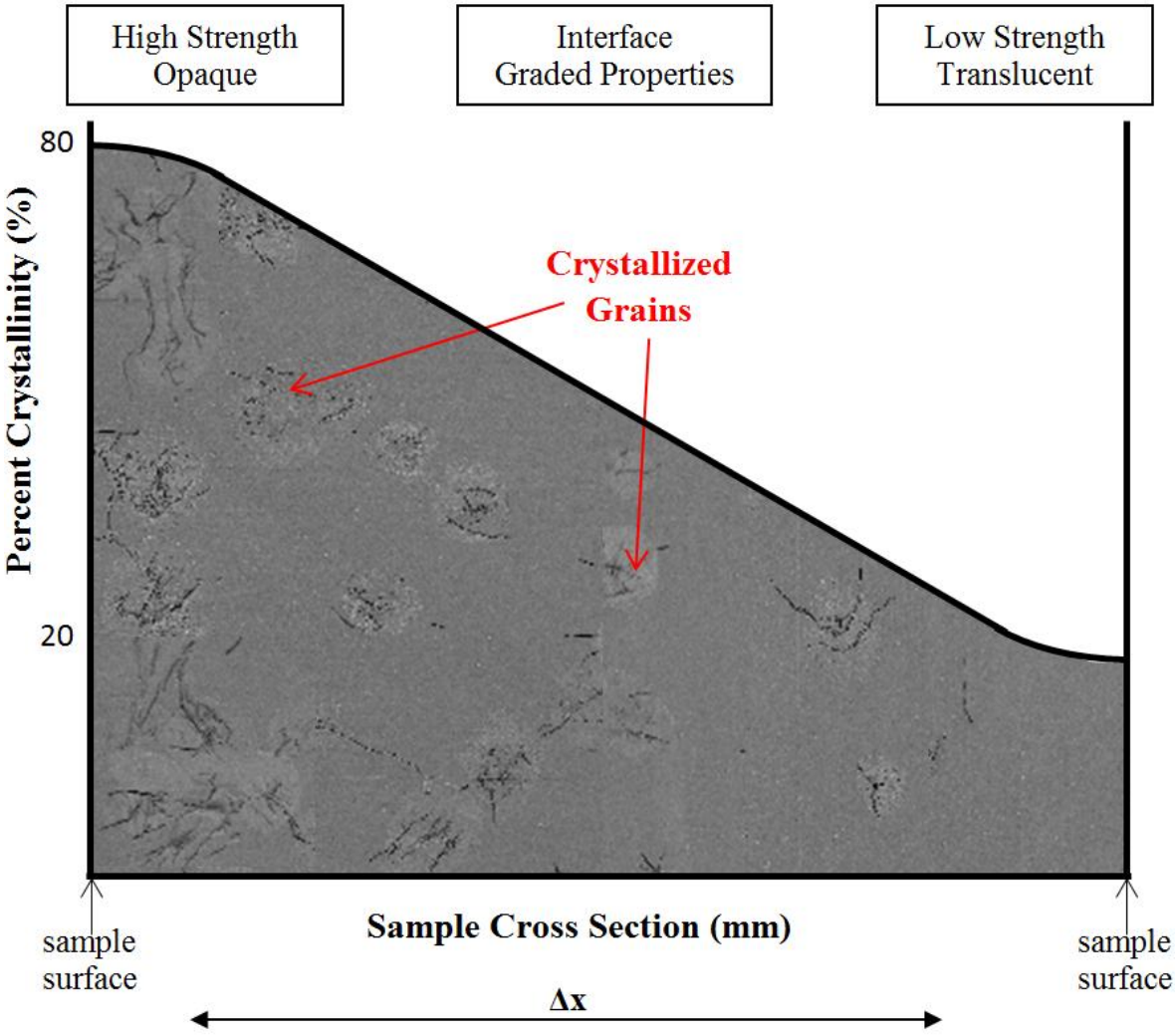

Figure 1.9: Graph of percent crystallinity versus the sample cross section for a microstructure graded material with a shallow interface.

To create an environment in which crystallization would occur on one surface but not homogeneously throughout the sample, a unique processing method is necessary. The processing method that was chosen for this experiment was a temperature gradient imposed during crystallization. If a temperature gradient is imposed across a homogeneously nucleated sample such that temperatures required to initiate crystallization are present at one surface, but not at the opposite surface, a crystallization gradient is possible. This can be seen in the figure below. This study will detail the process developed that involves a temperature gradient imposed across a sample during crystallization to create a microstructure graded glass-ceramic.

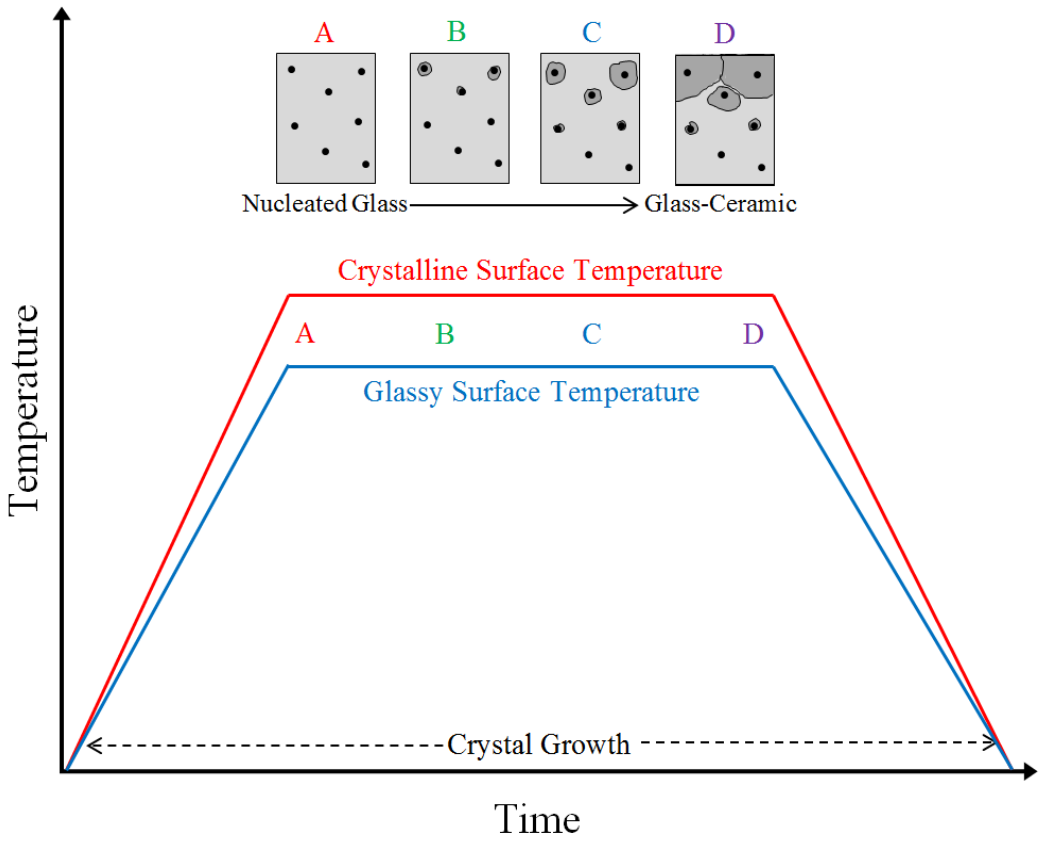

Figure 1.10: Schematic of the creation of a microstructure graded glass-ceramic by imposing a temperature difference across the sample during crystallization.

The goal of this research was to create a lithium disilicate microstructure graded glass-ceramic and investigate the properties as a function of crystallization processing. The objectives of this study were as follows:

- Design and construct a system to fabricate a microstructure graded glass-ceramic.
- Determine experimental parameters necessary to create microstructure graded lithium disilicate glass-ceramic.
- Evaluate the microstructure of the resulting samples as a function of position within the sample using: scanning electron microscopy (SEM) and Raman spectroscopy.
- Using standards and SEM data for percent crystallinity, develop a Raman analysis method to determine crystallization of a microstructure graded material.
- Evaluate the change in microhardness, density, elastic modulus, and thermal expansion coefficient with respect to percent crystallinity for a microstructure graded glass-ceramic.

2. Materials and Experimental Procedure

This section details the procedure and experimental parameters for the partial crystallization of lithium disilicate glass into a glass-ceramic. Glass preparation, crystallization, characterization methods, and change in material properties are described below.

2.1 Glass Formation

The nucleated glass samples used in this experiment had been previously prepared by Morsi Mohamed Mahmoud for his dissertation, "Crystallization of Lithium Disilicate Glass Using Variable Frequency Microwave Processing" [1]. The process by which he formed these glass samples is described below.

Lithium disilicate glass frit (325 mesh-SP1714 Glass Powder-Lot #06179112-P.O. # N18261) was obtained from Specialty Glass, Inc., Florida [1]. This frit was then melted in a covered platinum crucible in an electric furnace (DELTECH, Inc.) with occasional stirring to ensure complete homogenization. This melting cycle was broken up into three components:

1. The temperature was raised slowly to 200°C and held there for 30 minutes to remove any moisture from the frit.
2. The temperature was then raised slowly to 1100°C and held there for one hour to create a congruent melt.

3. The temperature was then raised slowly to 1400°C and held there for four hours to create a low viscosity melt so that the melt could be easily poured into a mold.

The glass melt was cast into a hot graphite mold (400°C) to create rods (60 mm long, 15 mm diameter), and samples were rapidly transferred into a box furnace (Thermolyne-Model 1400) at 400°C for 48 hours. This last step was used to anneal the samples and remove the stress and strain present inside the rods. After annealing, the samples were allowed to furnace cool to room temperature. The glass samples were then heated in an electric furnace (CM furnace-Model 1700) at 480°C for 2 hours to initiate nucleation, and then allowed to furnace cool to room temperature. Shown in the figure below is the entire heating process used by Morsi Mahmoud to prepare the nucleated glass.

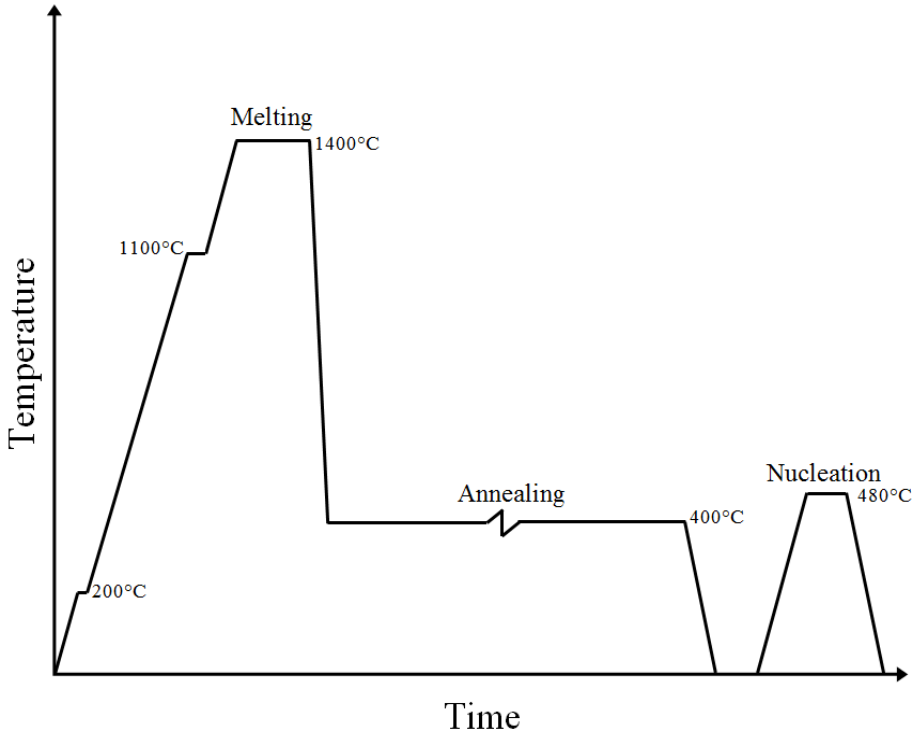

Figure 2.1: Heating conditions for the creation and nucleation of the glass prepared by Morsi Mahmoud. Note that there is a break shown in the graph during annealing. [Obtained from Mahmoud, 2007. Modified by author. (Used under fair use, 2012)].

2.2 Crystallization

The nucleated glass samples were crystallized by two different methods: conventional heating and gradient heating. Before crystallization, the samples were cut into disks (~4 mm thickness) using a low speed (275 rpm) diamond saw (Buehler ISOMET 1000 Precision Saw). The disks were cleaned by ultrasonic waves for about 2 minutes and then rinsed with acetone.

The conventional heating was conducted in an electric furnace (CM furnace-Model 1700) and was used to create homogeneously crystallized samples that were used as standards of crystallization. A 3°C/min ramp rate was used to heat the standards to the temperatures listed in the table below. Note that Standard 1 was not crystallized, but instead characterized in the nucleated glass state.

Table 2.1: Crystallization temperatures and times of standards.

Standard	Crystallization Temperature (°C)	Crystallization Time (hr)
Standard 1	No Crystallization	0
Standard 2	600	0.5
Standard 3	600	1
Standard 4	680	1
Standard 5	680	2
Standard 6	680	100

The gradient heating was conducted in a self-constructed linear gradient furnace and was used to create the microstructure graded samples. The linear gradient furnace

was constructed with Kanthal A1 (Fe-Cr-Al) resistance wire embedded inside a refractory brick. A plate of fused silica separated the resistance wire and the sample. A schematic of the constructed furnace can be seen in the figure below.

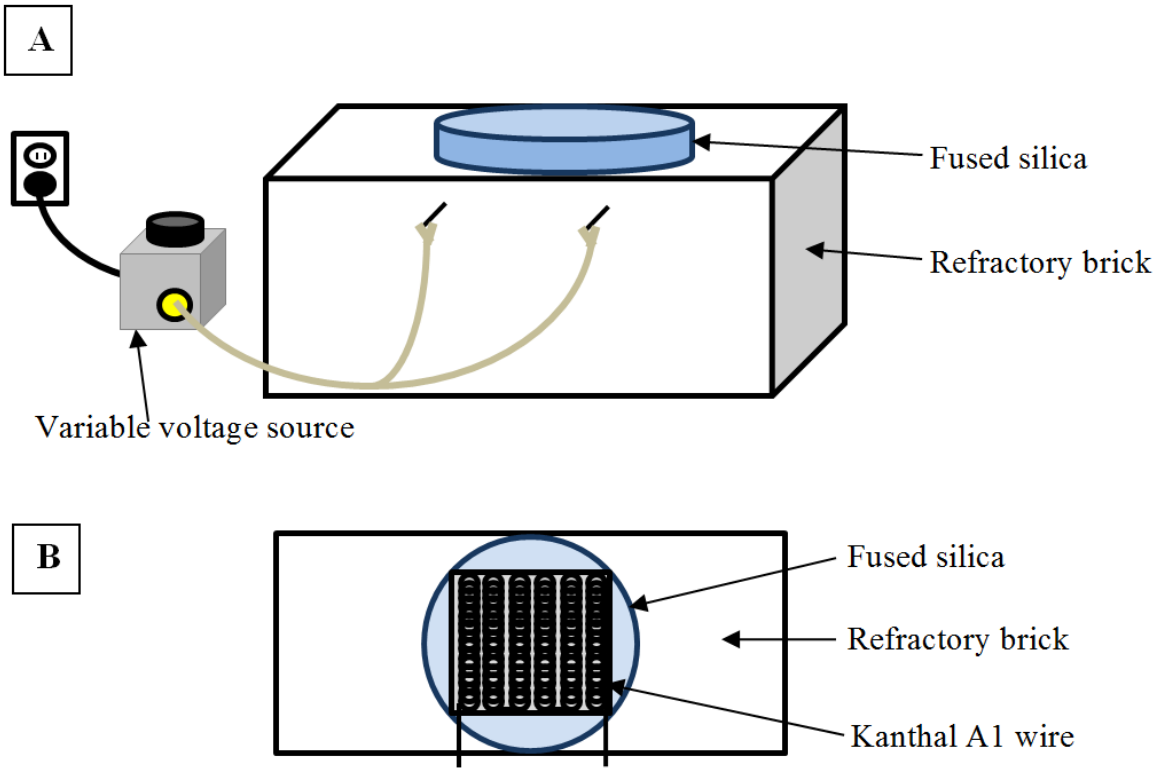

Figure 2.2: Schematic of constructed linear gradient furnace. A) Entire setup. B) Bird's eye view of refractory brick.

The sample was placed upon the fused silica, exposing one surface to the heat created by the resistance furnace. The opposite surface was exposed to the open air, allowing the heat to dissipate and a temperature gradient to be created. Pictures of the entire setup used for gradient heating can be seen below. Also shown is the gradient furnace with a sample being heated.

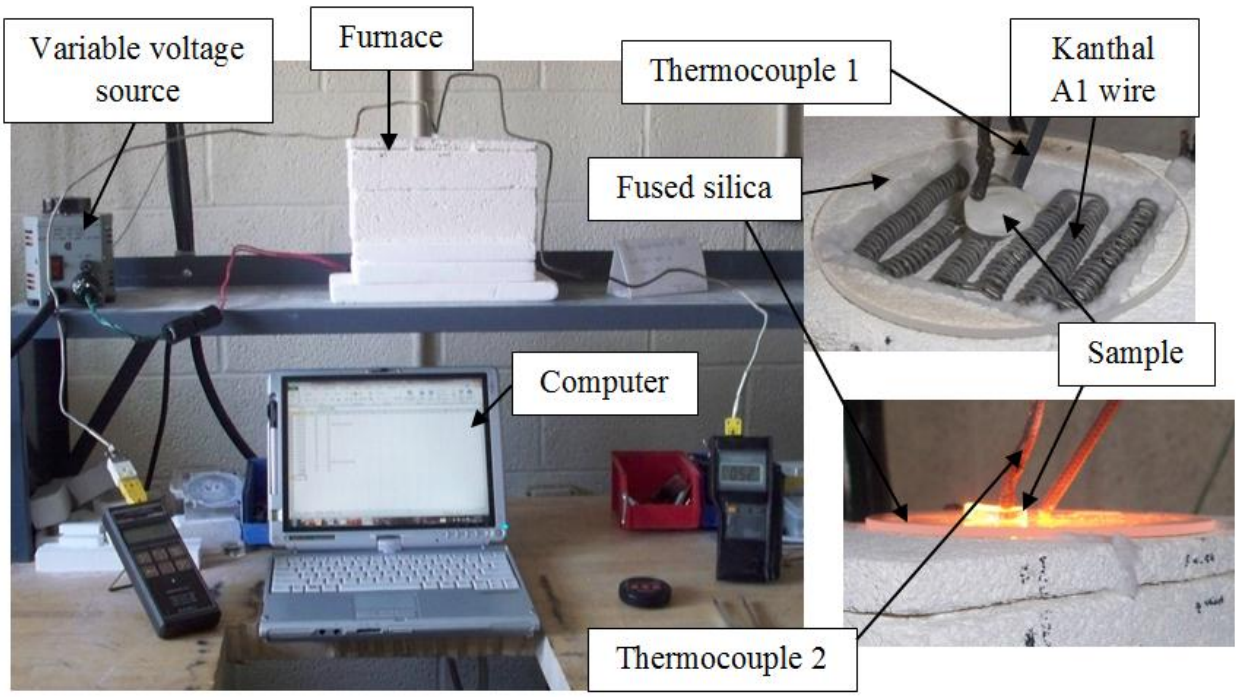

Figure 2.3: Pictures of constructed linear gradient furnace. [Photos by author, 2012].

The samples were crystallized following the information seen in the table below. Note that the temperature gradient reported in the table below takes into account the sample thickness, which was not equivalent for all samples.

Table 2.2: Crystallization temperatures and times of samples.

Sample	Temperature at Crystal Surface (°C)	Temperature at Glass Surface (°C)	Temperature Difference (°C)	Temperature Gradient (°C/mm)	Time at Upper Temperature Range (min)*
Sample 7	613 ± 16	561 ± 24	52	16.6	4
Sample 8	596 ± 24	497 ± 33	99	25.4	6
Sample 9	558 ± 22	468 ± 32	90	33.5	10.5
Sample 10	613 ± 22	513 ± 28	100	26.3	4
Sample 11	672 ± 18	514 ± 38	158	32.2	5

*The time at the upper temperature range is defined as the time spent inside the temperature range given in columns 2 and 3. This time is shown in Figures 2.5-2.9.

The figure below shows a graphical representation of the temperature difference imposed across the samples during crystallization.

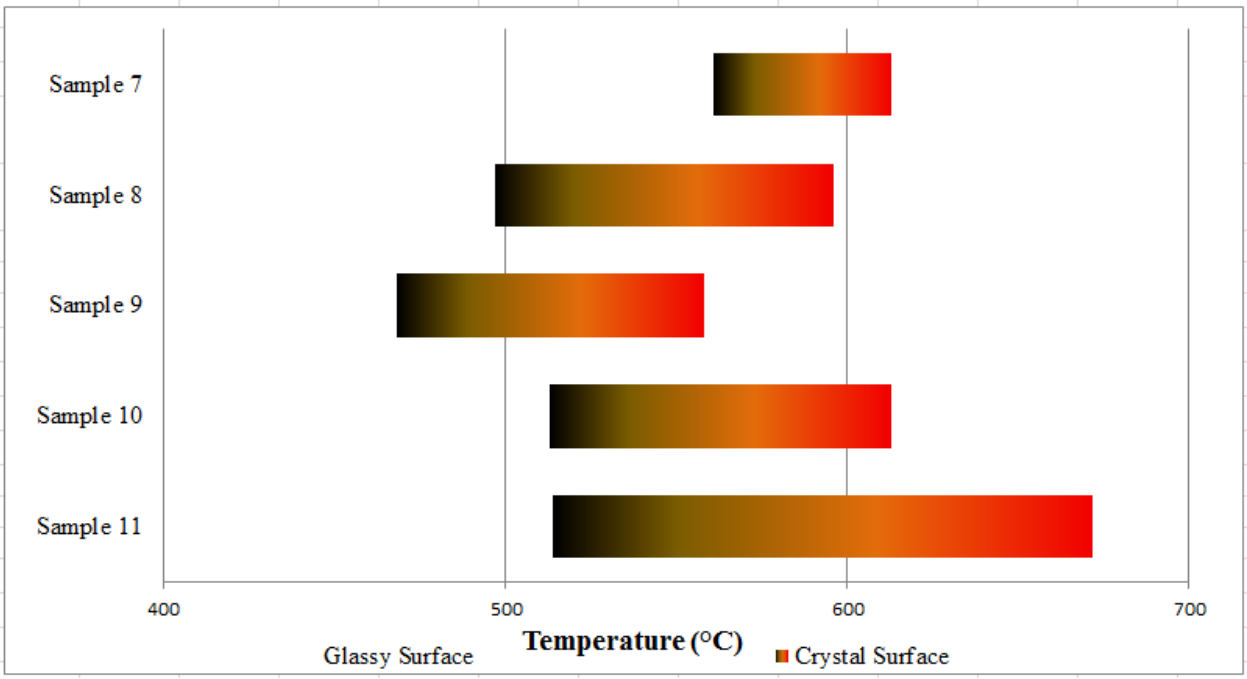

Figure 2.4: Bar graph showing temperature difference imposed across samples during crystallization.

Crystallization heating profiles for all the samples can be seen in the following figures. In the figures below, the red line reports the temperature recorded by Thermocouple 1, the temperature at the crystalline surface. The blue line reports the temperature recorded by Thermocouple 2, the temperature at the glassy surface. Note that for Samples 7, 8, 10, and 11, the cooling rate was controlled by the furnace.

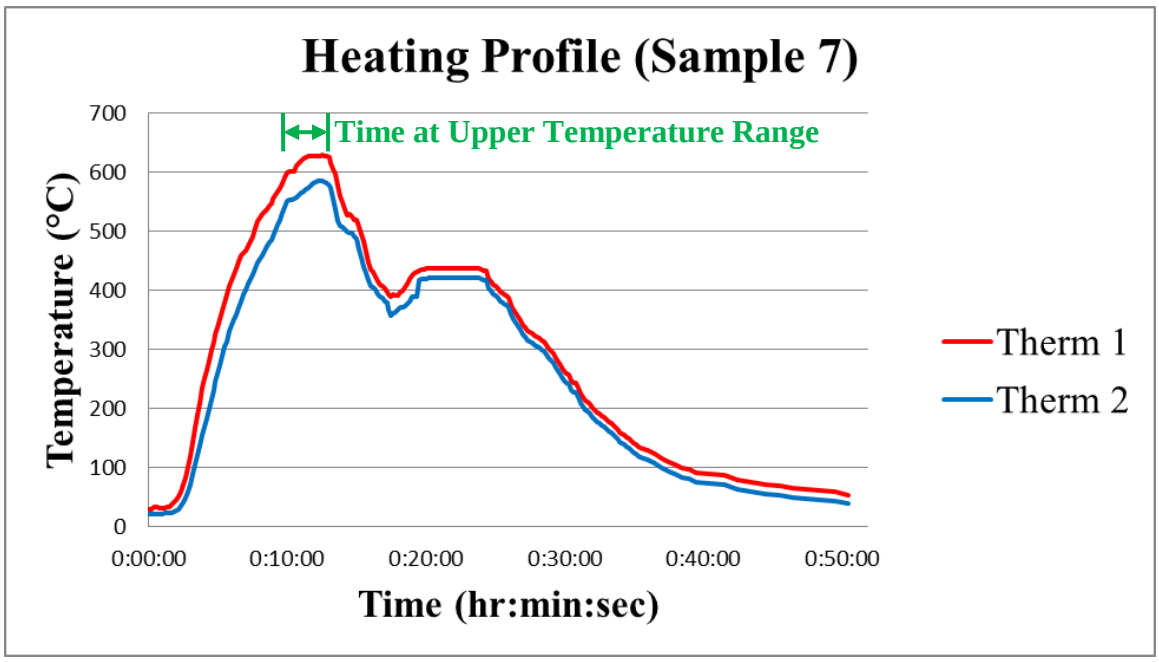

Figure 2.5: Crystallization heating profile for Sample 7.

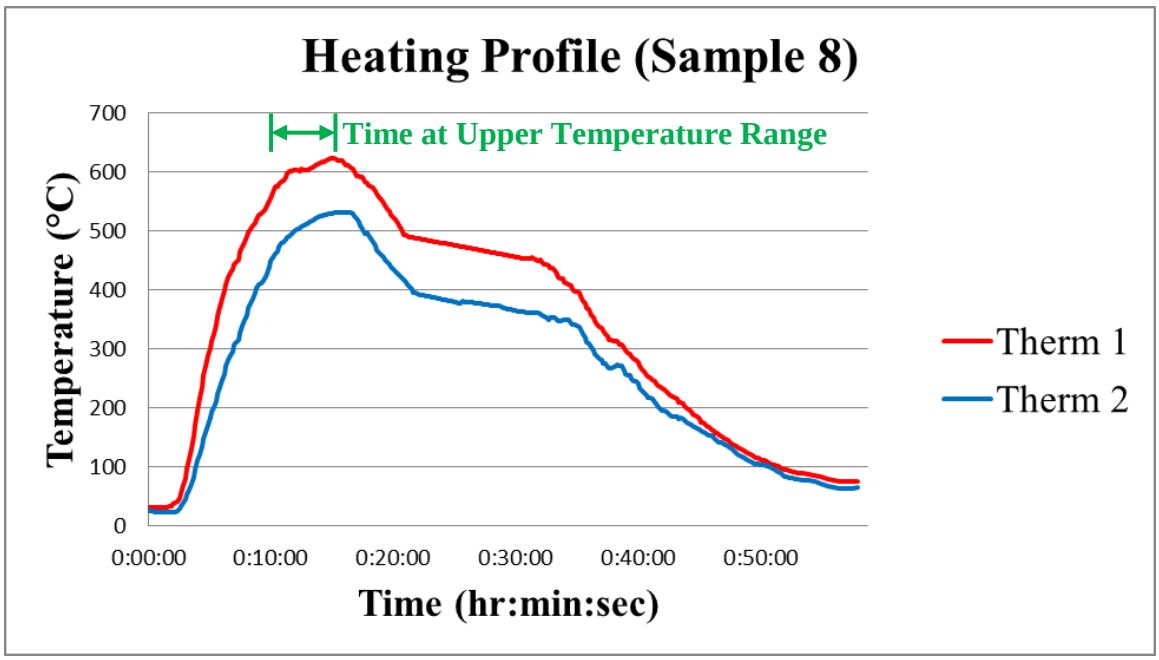

Figure 2.6: Crystallization heating profile for Sample 8.

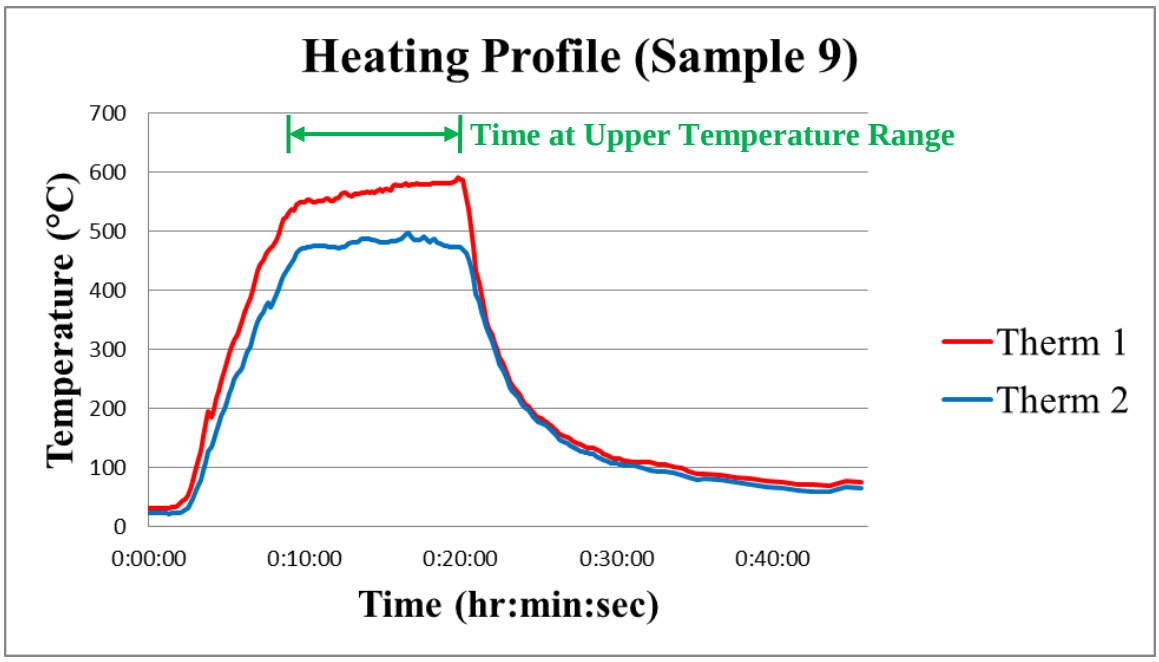

Figure 2.7: Crystallization heating profile for Sample 9.

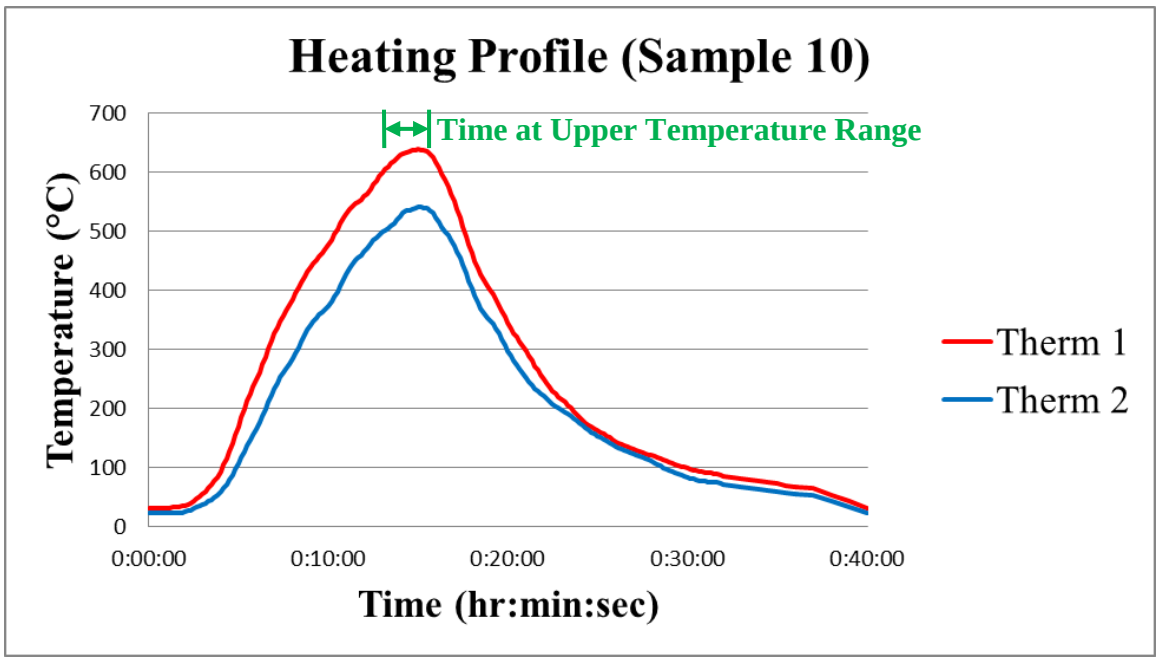

Figure 2.8: Crystallization heating profile for Sample 10.

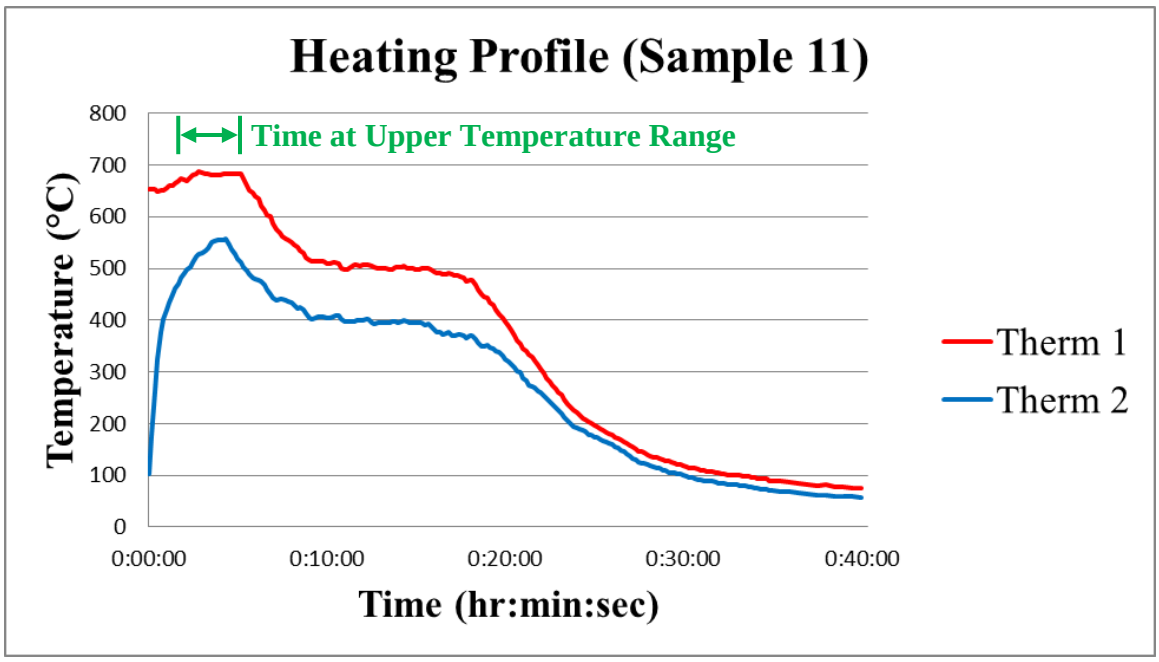

Figure 2.9: Crystallization heating profile for Sample 11.

2.3 Surface Preparation

The homogeneously crystallized standards and microstructure graded samples were polished in preparation for characterization. All standards and samples were first ground with 180 grit silicon carbide abrasive paper to ensure flatness. The standards and samples were then polished gradually using 2 lbs force per specimen for 2 minutes at the following intervals: 240 grit SiC, 320 grit SiC, 400 grit SiC, 600 grit SiC, 15 micron diamond paste on nylon cloth, 6 micron diamond paste on nylon cloth, 3 micron diamond paste on nylon cloth, 1 micron diamond paste on nylon cloth, and 0.25 micron diamond paste on nylon cloth. An automated machine (Buehler-ECOMET 6 Grinder/Polisher) was used for grinding and polishing. The standards and samples were then rinsed with water and dried thoroughly with air.

After microhardness and Raman spectroscopy were performed, but before scanning electron microscopy, select standards and samples were etched with a drop of 50% HF acid for 2 minutes to delineate prominent features. Then the standards and samples were sputter coated with gold/palladium to prevent charging on the surface during electron bombardment.

2.4 Characterization Techniques

Three characterization techniques were chosen to show the materials properties resulting from the microstructure graded glass-ceramics.

2.4.1 Scanning Electron Microscopy (SEM)

Select standards and samples were examined on the polished surfaces. A scanning electron microscope (Model LEO 1550 Gemini Field Emission) was used with accelerating voltage up to 5.0 kV, the InLens Detector, and magnification from 20x up to 2500x. Scanning electron microscopy was used in order to obtain micrographs of the material microstructure. Nuclei and crystals could be observed and measured for size. Overall micrographs were also obtained for use in determining percent crystallinity. SEM analysis was conducted on standards and samples that had been polished, etched in 50% HF, and sputter coated with gold/palladium.

2.4.1.1 Volume Fraction from ImageJ Software

Scanning electron micrographs were analyzed to obtain volume fractions of crystals. Three micrographs were analyzed from each standard, and the volume fractions

from these analyses were used as the percent crystallinity of the standards. The analysis was conducted in a software called Image Processing and Analysis in Java (ImageJ).

ImageJ is a Java-based image processing and analysis software developed by the U. S. National Institutes of Health [7]. This software is public domain. The software was used to edit and analyze SEM micrographs. Editing functions used include contrast manipulation, sharpening, and edge detection. Analysis functions used include the calculation of area and pixel value statistics.

2.4.2 Raman Spectroscopy

Raman spectroscopy produces a wavenumber spectra characteristic to the material, which can be used to determine the molecular structure present inside the material [1]. A Raman spectrometer shines a laser photon beam (usually in the visible spectrum) onto the material, causing the light to be scattered by molecules in the material. When a molecule interacts with the light, it can gain or lose energy, causing a change in energy of the irradiating photon. The change in energy of the photon is characteristic to a particular molecular bond in the material. These energy changes can be compiled to produce a spectrum that can provide information about the type and numbers of molecular bonds present [1].

All standards and samples were examined using Raman spectroscopy. A Raman spectrometer (LabRAM-HR 800, Jobin Yvon Horiba) was used with a 514 nm green Argon laser combined with an Olympus BX41 microscope. A 50x microscope objective lens was used to obtain the Raman spectra of glass, partially crystallized, and completely

crystallized standards. Raman spectra of samples were also collected at various points in sample cross section. The Jobin Yvon Horiba software was also used to calculate the Full Width at Half Maximum, a quantitative value of the width of spectra peaks. Raman spectroscopy was used in order to observe the change in molecular structure from glass to crystalline materials. Raman analysis was conducted on standards and samples that had been polished. The 50x objective leads to an analysis spot size of approximately 3-4 microns. To capture all the features present in a sample, numerous spectra were collected at random spot selection.

2.4.3 Microhardness

Select standards and samples were examined using microhardness. A microhardness tester (LECO, DM-400 Hardness Tester) was used with a 0.5 kg force. Vickers hardness values were obtained for select standards, and for various points in a sample cross section. Microhardness was used in order to observe the change in materials properties in the transition from glass to glass-ceramics, and for application of the Rule of Mixtures. Microhardness testing was conducted on standards and samples that had been polished. The following equation was used to transform the indentation diagonal lengths into a Vickers hardness number [8]:

$$HV = \frac{1.854 * P}{d^2} \qquad (1)$$

where HV is the Vickers hardness number
P is the load applied during testing
d is the indentation diagonal length

2.5 Material Properties and the Rule of Mixtures

In a functionally graded material, the properties of the material change depending upon the location in the material. Because of this, it is important to understand the method that was used to approximate the intermediate properties based upon the extremes. The Rule of Mixtures states that the property of the composite is a function of the volume fraction of the components. The equation for the Rule of Mixtures is as follows [2]:

$$A_{composite} = A_1 * V_1 + A_2 * V_2 \quad (2)$$

where $A_{composite}$ is the property of the composite material
A_1 is the property of phase 1
V_1 is the volume fraction of phase 1
A_2 is the property of phase 2
V_2 is the volume fraction of phase 2

For analysis of this theory, consider four material properties: density (ρ), coefficient of thermal expansion (α), modulus of elasticity (E), and hardness (HV). The true densities of lithium disilicate glass and glass-ceramic are reported in the table below, as found by Helium Pcynometry [1]. The coefficients of thermal expansion are reported in the table below, as found by dilatometry [1]. The moduli of elasticity are reported in the table below, as found by nanoindentation [9]. The Vickers hardness numbers are reported in the table below, as found by microhardness [10, 11]. Note that Equation 2 assumes a linear Rule of Mixtures. Although this equation is not a precise representation for all properties, it can serve to illustrate trends.

Table 2.3: Literature values of density, coefficient of thermal expansion, modulus of elasticity, and hardness for lithium disilicate glass and glass-ceramic.

Material	True Density (g/cm^3)	Thermal Expansion Coefficient (10^{-5} °C^{-1})	Modulus of Elasticity (GPa)	Vickers Hardness (kg/mm^2)
Lithium Disilicate Glass	2.348	3.4	86	530
Lithium Disilicate Glass-Ceramic	2.437	1.23	93	540

Application of the Rule of Mixtures can predict the density, coefficient of thermal expansion, modulus of elasticity, and hardness for a partially crystallized material. The use of Equation 2 would yield the values reported in Table 2.4.

Table 2.4: Application of the Rule of Mixtures to the true density, coefficient of thermal expansion, modulus of elasticity, and hardness for partially crystallized lithium disilicate. Note that "(m)" indicates a measured value from literature and "(c)" indicates a calculated value based on Equation 2.

Crystallinity (%)	True Density (g/cm^3)	Thermal Expansion Coefficient (10^{-5} °C^{-1})	Modulus of Elasticity (GPa)	Vickers Hardness (kg/mm^2)
0	2.348 (m)	3.40 (m)	86 (m)	530 (m)
20	2.366 (c)	2.97 (c)	87 (c)	532 (c)
40	2.384 (c)	2.53 (c)	89 (c)	534 (c)
60	2.401 (c)	2.10 (c)	90 (c)	536 (c)
80	2.419 (c)	1.66 (c)	91 (c)	538 (c)
100	2.437 (m)	1.23 (m)	93 (m)	540 (m)

It is important to be able to approximate the intermediate properties in a functionally graded material to understand the behavior at the graded interface.

3. Results and Discussion

This section entails the results and discussions from the experiment.

3.1 Sample Preparation

The first result from this experiment was the creation of a microstructure graded glass-ceramic. The desired material was prepared using the procedures described above. Examples of these samples can be seen in the figure below. Note that in some samples, the amount of crystallization is not constant throughout the cross section (i.e. there is more crystallization in the center of the sample than closer to the outside). Throughout this research, the samples were analyzed as close to the center of the sample as possible.

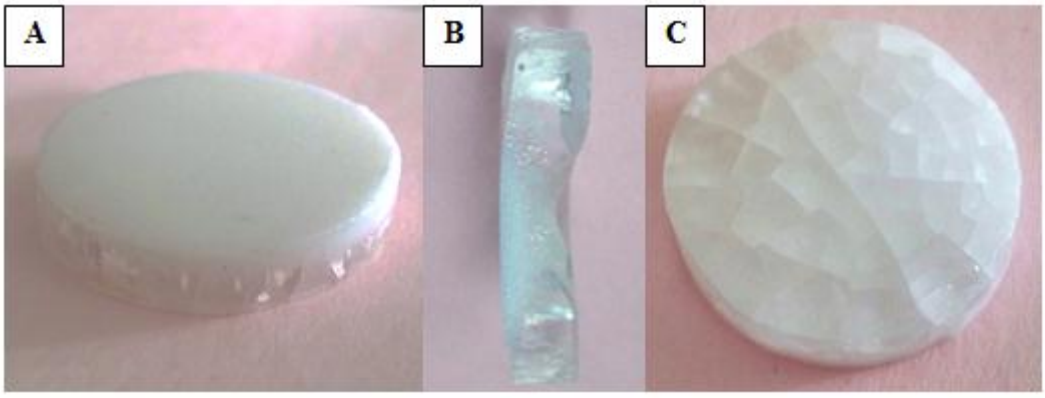

Figure 3.1: Pictures of microstructure graded samples. A) View looking at the crystallized surface of Sample 9. B) View looking at the cross section of Sample 7 with the crystallized region to the left. C) View looking at the glassy surface of Sample 9. [Photos by author, 2012].

As can be seen in the figure above, cracks occurred throughout the glassy portion of the material. The figure below shows pictures of each sample looking at the glassy surface.

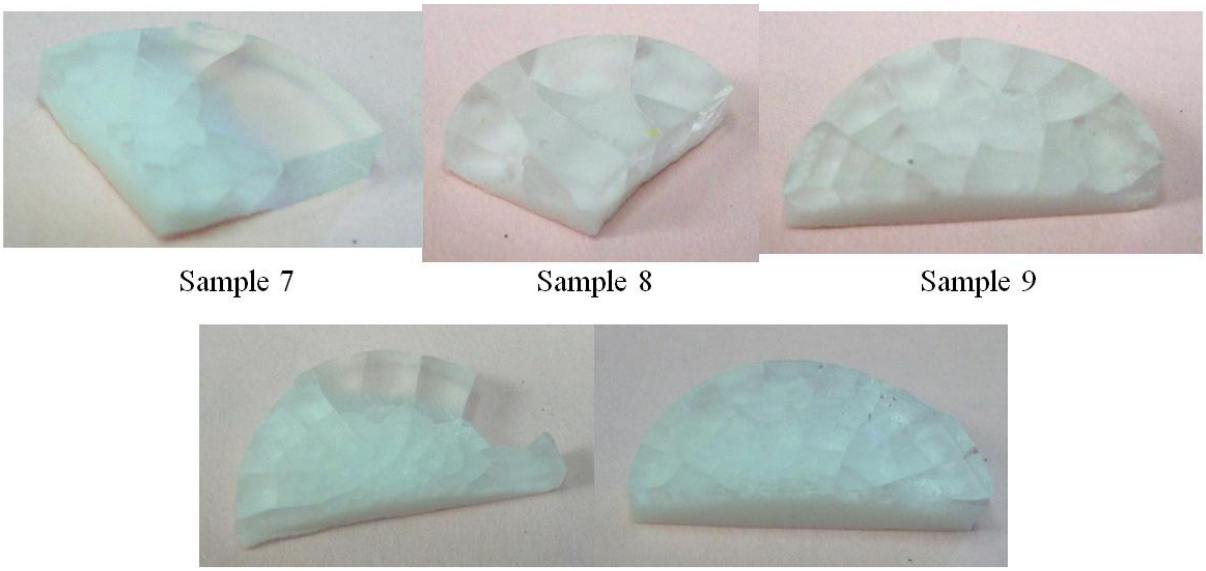

Figure 3.2: Pictures of Samples 7-11 looking at cracks in the glassy phase. [Photos by author, 2012].

The cracking in the glassy phase is believed to be due to different properties in the glass and glass-ceramic, resulting in stress. Cracking will occur when the stress is greater than the fracture stress of either the glass or the glass-ceramic. The fracture stress of glass is about 64 MPa, and for the glass-ceramic is about 215 MPa [12].

As reported in Section 2.5 (Material Properties and the Rule of Mixtures), lithium disilicate glass and glass-ceramic have different densities and coefficients of thermal expansion. The density of the glass is 2.348 g/cm^3, and the density of the glass-ceramic is 2.437 g/cm^3. The density of the glass-ceramic is greater than the density of the glass. The coefficient of thermal expansion of the glass is $3.4*10^{-5}$ $°C^{-1}$, and the coefficient of thermal expansion of the glass-ceramic is $1.23*10^{-5}$ $°C^{-1}$. The coefficient of thermal expansion of the glass is greater than the coefficient of thermal expansion of the glass-ceramic.

The figure below shows representations of these two material properties and the stresses they impose on the graded material. In part A of the figure, a representation is shown of a glass with atoms. This part of the figure is used as a reference of the ideal stress-free state.

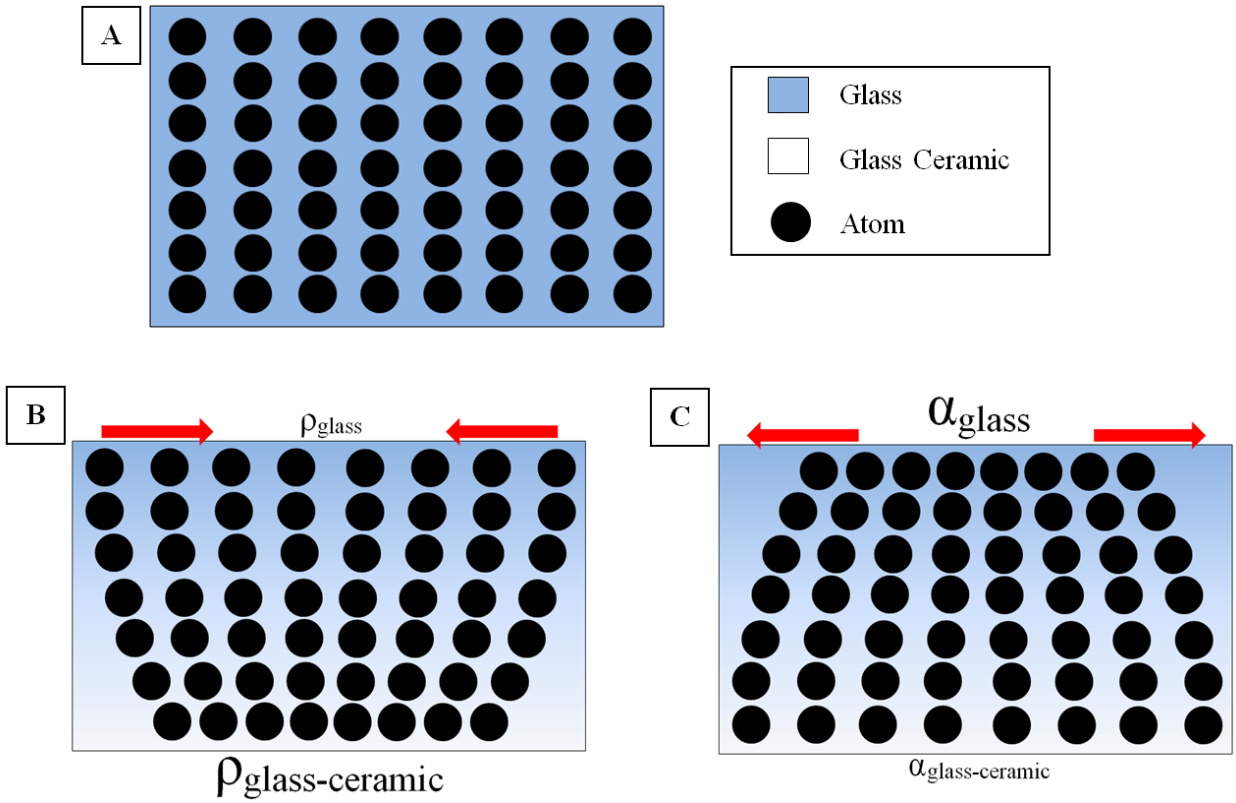

Figure 3.3: Graphic showing stresses imposed on glass surface due to differences in material properties. A) Representation of glass without stresses. B) Representation of compression on glass surface due to densification of crystalline phase. C) Representation of tension on glass surface due to thermal shrinkage of glassy phase.

Part B of the figure shows the result of a higher density in the crystalline phase. When the nucleated glass is heated to the crystallization temperature, crystallization occurs. Since the density is higher in the crystalline phase than in the glassy phase, this crystallization is also accompanied by densification. However, when this densification is

only happening at one surface due to the temperature gradient, the densification occurring at this surface will pull the opposite surface into compression. Since this densification is occurring at well above the annealing temperature of the glass, most of these stresses can likely relax out of the material. Furthermore, compression on the glassy surface tends to close cracks, not open them.

Part C of the figure shows the result of a higher coefficient of thermal expansion in the glassy phase. After the sample has been crystallized and is cooling to room temperature, the sample will shrink, as governed by the coefficient of thermal expansion. However, when there are two different phases present, each material will try to shrink a different amount. Since the glass has a higher coefficient of thermal expansion, it will try to shrink more than the glass-ceramic during cooling. However, the glass-ceramic will oppose this shrinkage and not allow the glassy phase to shrink as much as is thermodynamically stable. This will pull the glassy phase into tension. The difference in coefficient of thermal expansion is likely the cause of the cracking observed in the study. Stresses arising in the material due to the change in coefficient of thermal expansion will be discussed in Section 3.5.3 (Qualitative Stress Analysis).

3.2 Scanning Electron Microscopy (SEM)

Scanning electron microscopy was performed on Standards 1, 2, 3, 4, and 6, as well as on Sample 9.

3.2.1 Microscopy Performed on Standards

Microscopy was first performed on the standards to determine the percent crystallinity of each standard. These results were used to compare the percent crystallinity to the other characterization methods. Micrographs of Standards 1, 2, 3, 4, and 6 can be seen in the figures below. Standard 5 was not analyzed by SEM. Note that the glassy matrix can be seen by the dark gray, and the crystals by the light grey.

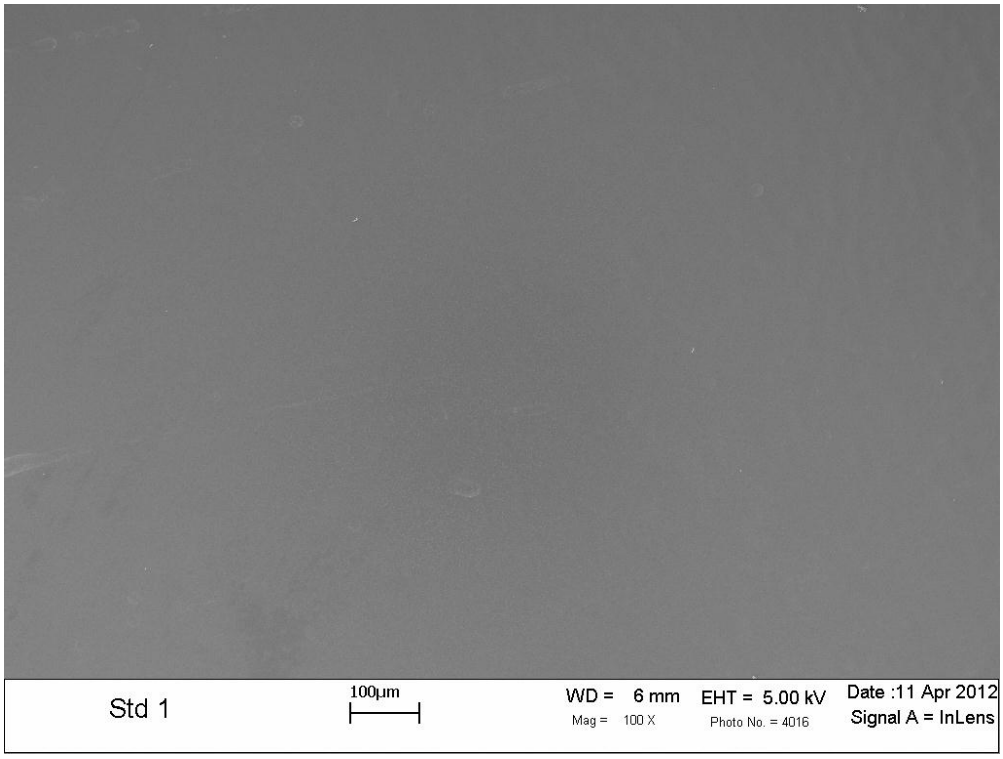

Figure 3.4: Scanning electron micrograph of Standard 1.

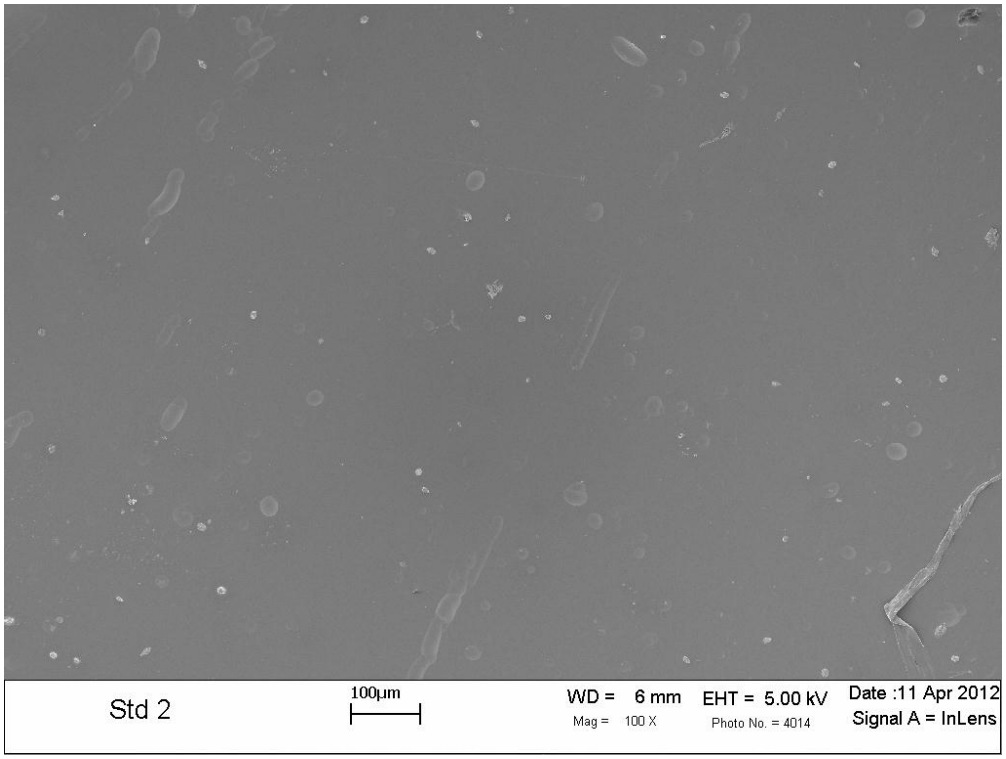

Figure 3.5: Scanning electron micrograph of Standard 2.

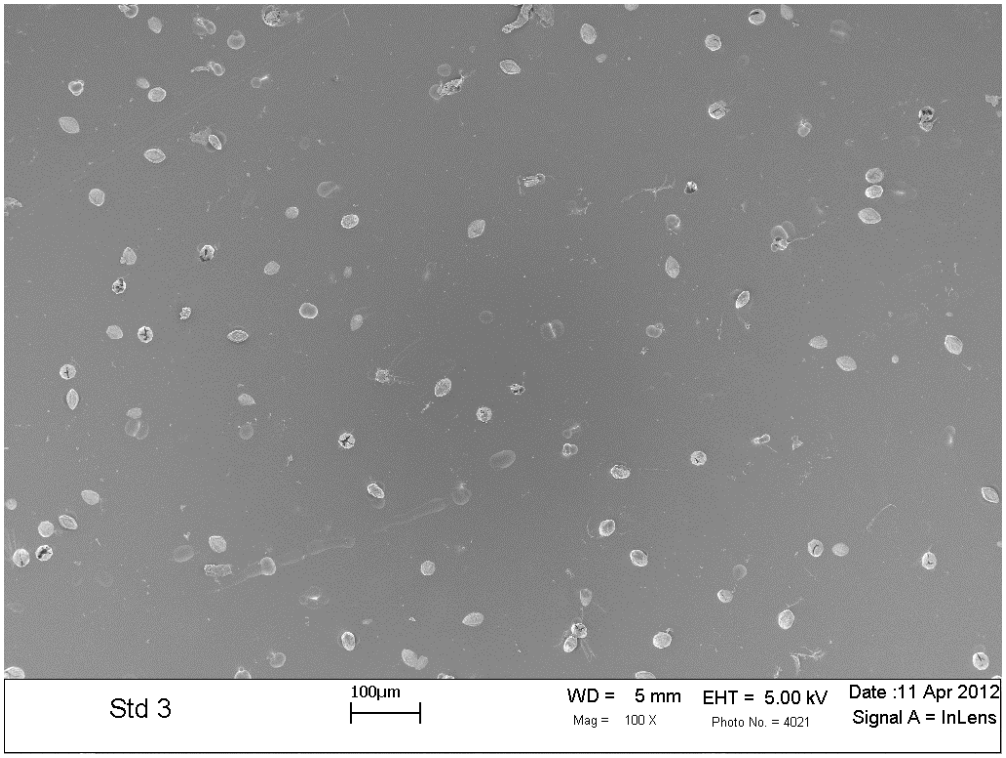

Figure 3.6: Scanning electron micrograph of Standard 3.

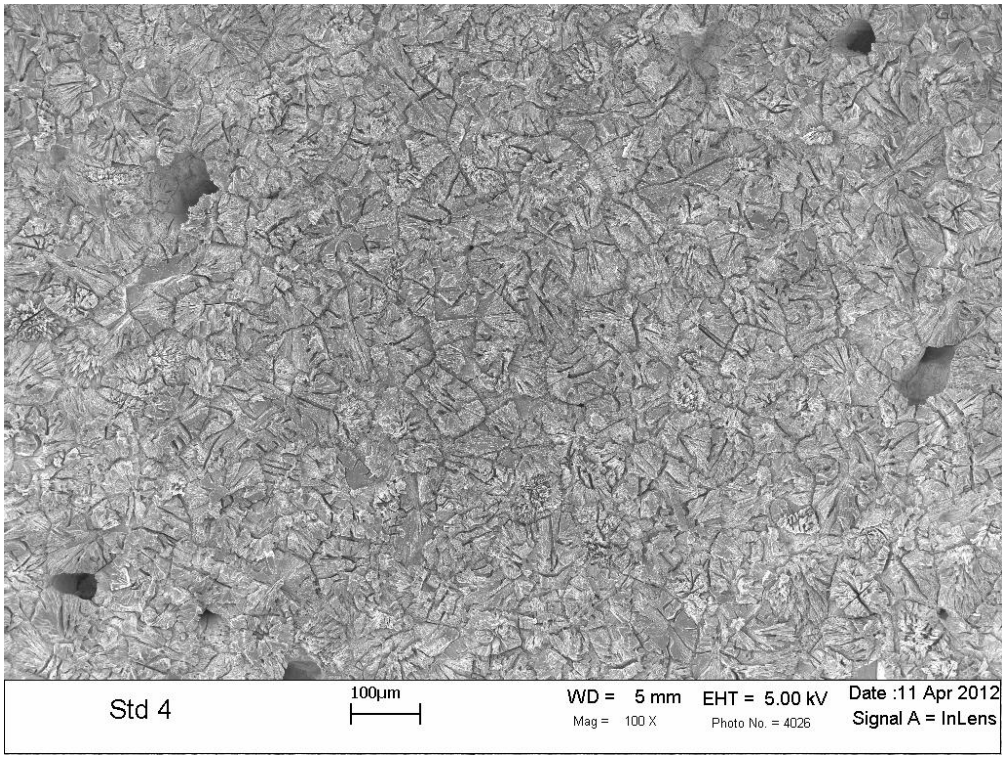

Figure 3.7: Scanning electron micrograph of Standard 4.

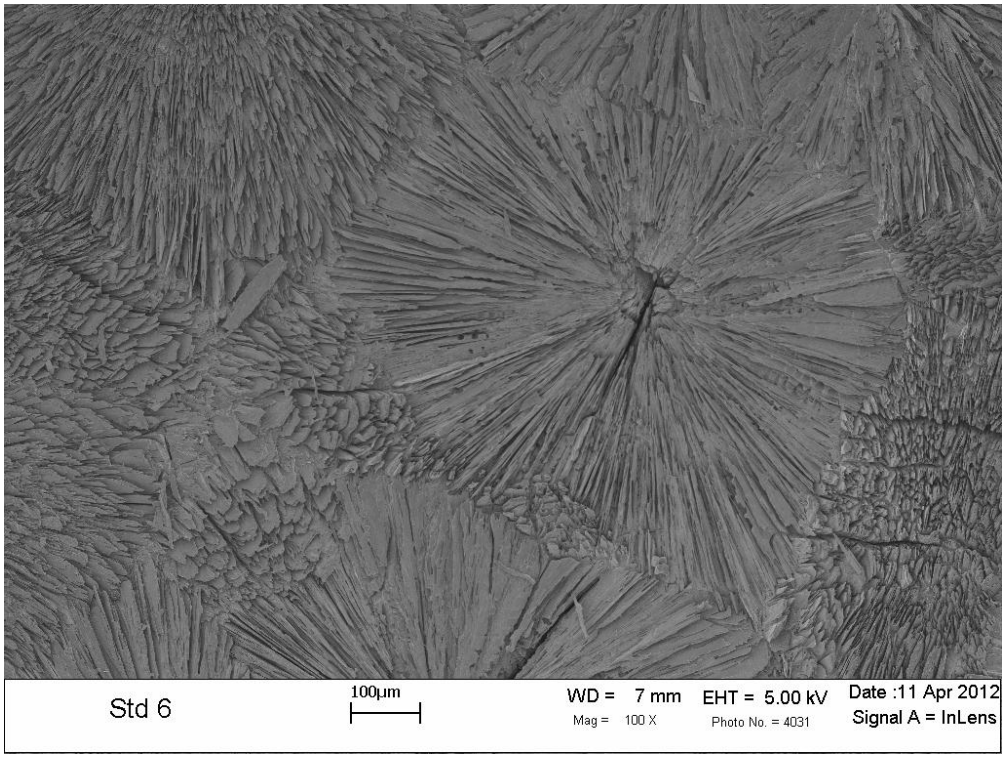

Figure 3.8: Scanning electron micrograph of Standard 6.

Close observation of Figure 3.6 displays some separation voids formed near the crystal/glass interfaces, and some holes inside the crystals. Observation of Figure 3.7 displays larger voids formed in between crystals. This formation of voids could be due to the densification of the crystalline phase. These voids could be potential locations for cracks to initiate if stresses became large enough.

Analysis of the micrographs was performed with ImageJ software to quantify the amount of crystallization present in each standard. Shown below is an example (Standard 3) of how the software transforms the image for analysis.

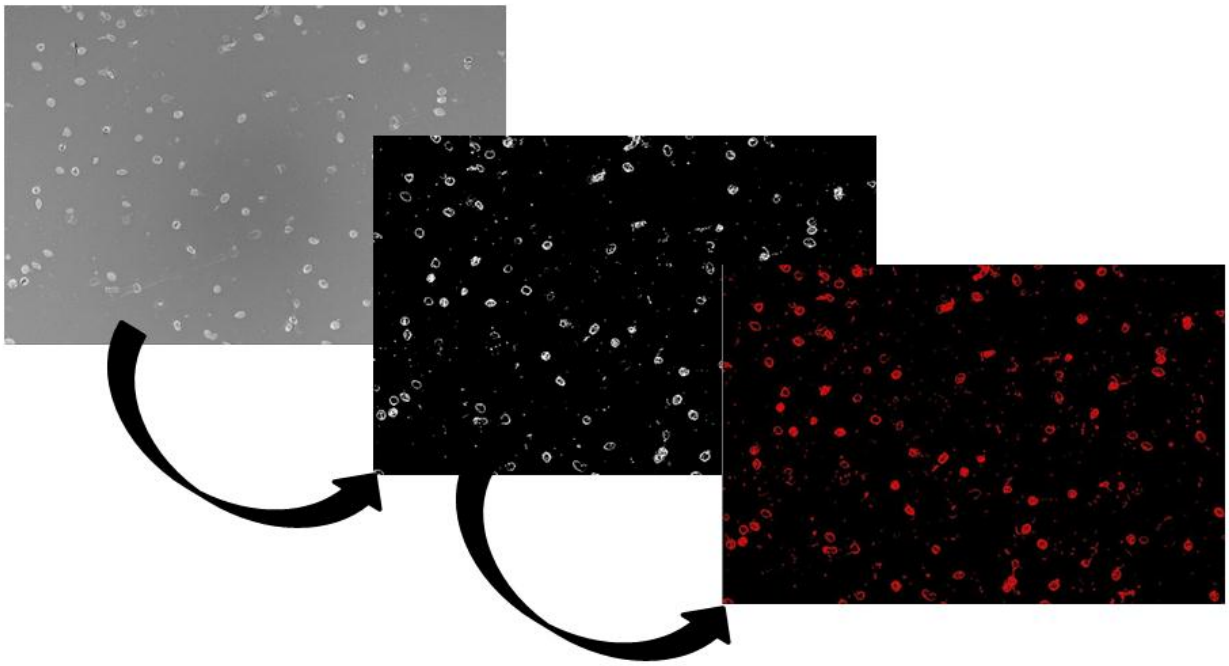

Figure 3.9: Micrograph transformation for data analysis in ImageJ Software.

The image transformation and volume fraction analysis was performed on three micrographs each of Standards 1, 2, 3, 4, and 6. The results of the analysis with ImageJ Software can be seen in the table below. Note that Standard 5 was not analyzed by SEM,

but the percent crystallinity is approximated based upon the other standards. The standard deviation for each standard was found by comparing the ImageJ analysis of three micrographs. In the case of Standard 1, ImageJ analysis of one micrograph reported a slight crystallization (due to the presence of a nuclei), leading to the standard deviation.

Table 3.1: Results of volume fraction analysis by ImageJ Software. Note that the crystallinity of Standard 5 is approximated.

Standard	Crystallization Temperature (°C)	Crystallization Time (hr)	Crystallinity	
			Average (%)	Standard Deviation
Standard 1	No Crystallization	0	0	0.11
Standard 2	600	0.5	35	3.3
Standard 3	600	1	50	3.3
Standard 4	680	1	90	0.9
Standard 5	680	2	~95	
Standard 6	680	100	100	0.3

3.2.2 Microscopy Performed on Sample 9

Sample 9 was also analyzed using microscopy. Micrographs from the sample can be seen below. In the first three micrographs, cracks can be seen in the glassy region of the material. In these figures, the glassy matrix can be seen by the dark gray, and the crystals by the light grey.

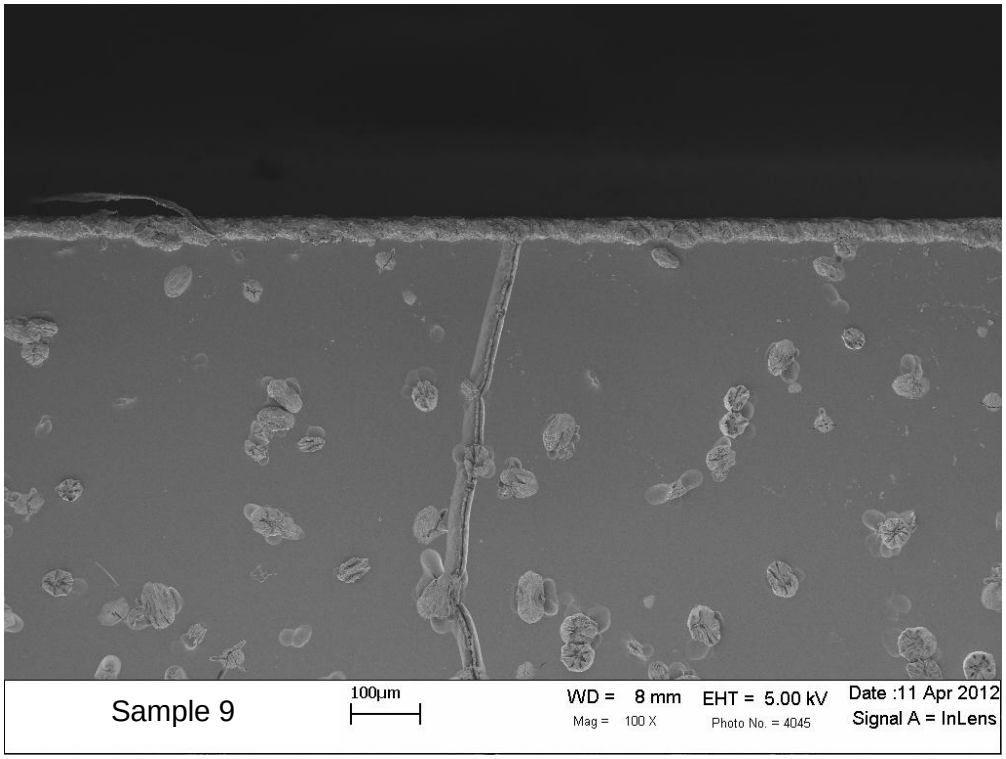

Figure 3.10: Micrograph of Sample 9 centered at location 2.57 mm from the crystal edge.

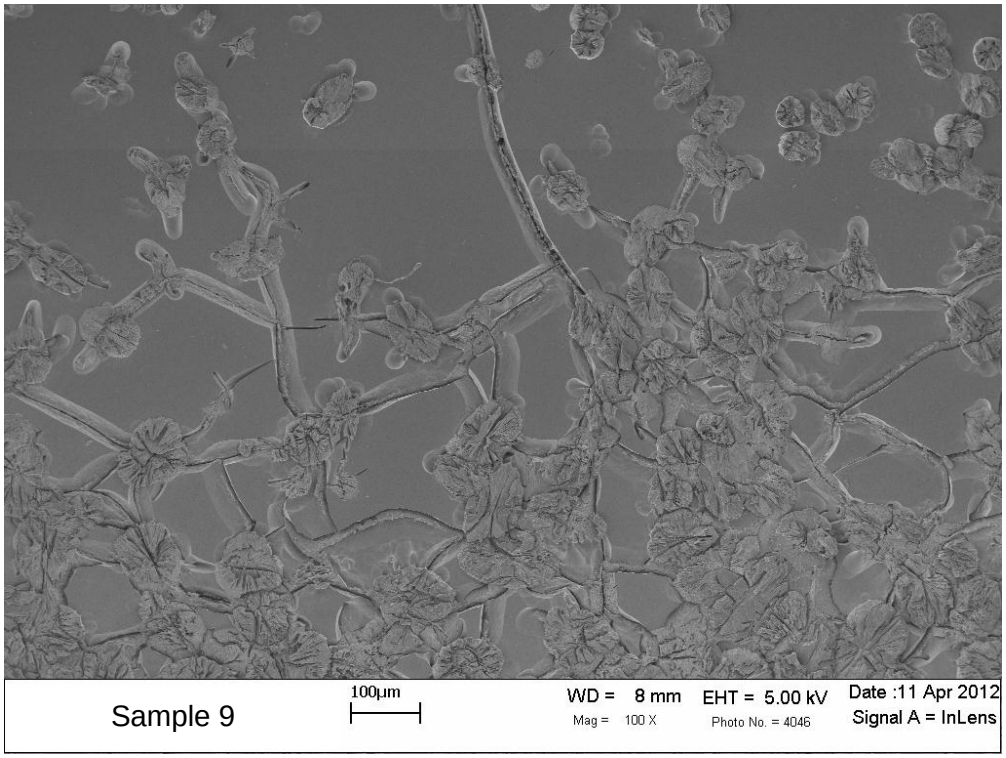

Figure 3.11: Micrograph of Sample 9 centered at location 1.93 mm from the crystal edge.

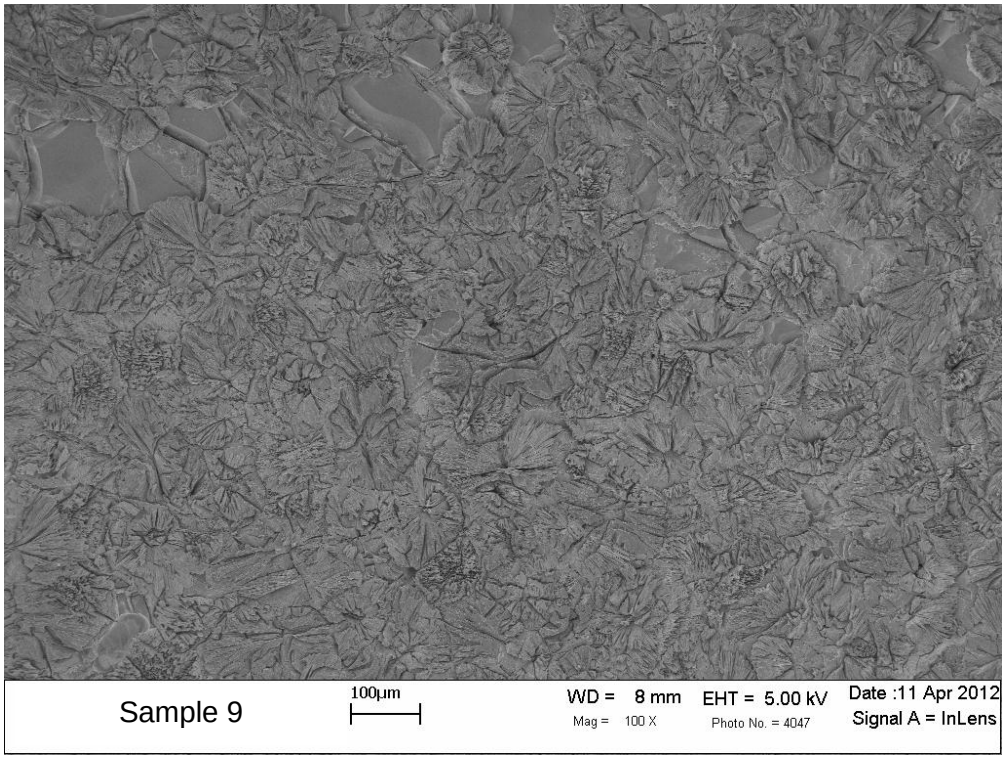

Figure 3.12: Micrograph of Sample 9 centered at location 1.29 mm from the crystal edge.

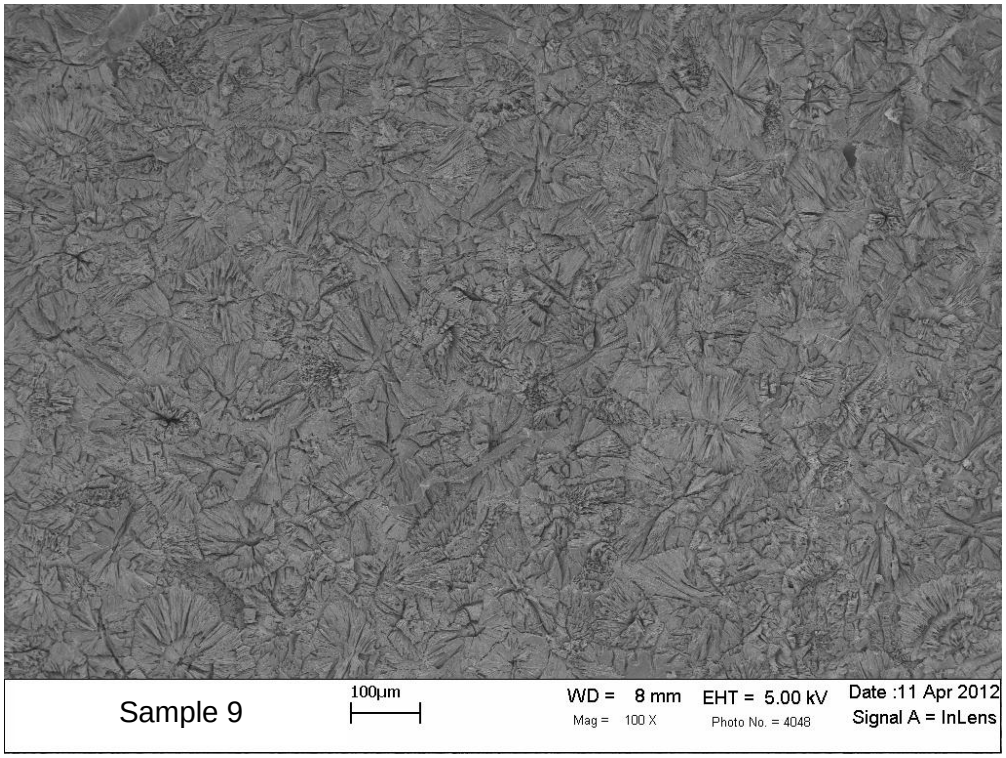

Figure 3.13: Micrograph of Sample 9 centered at location 0.65 mm from the crystal edge.

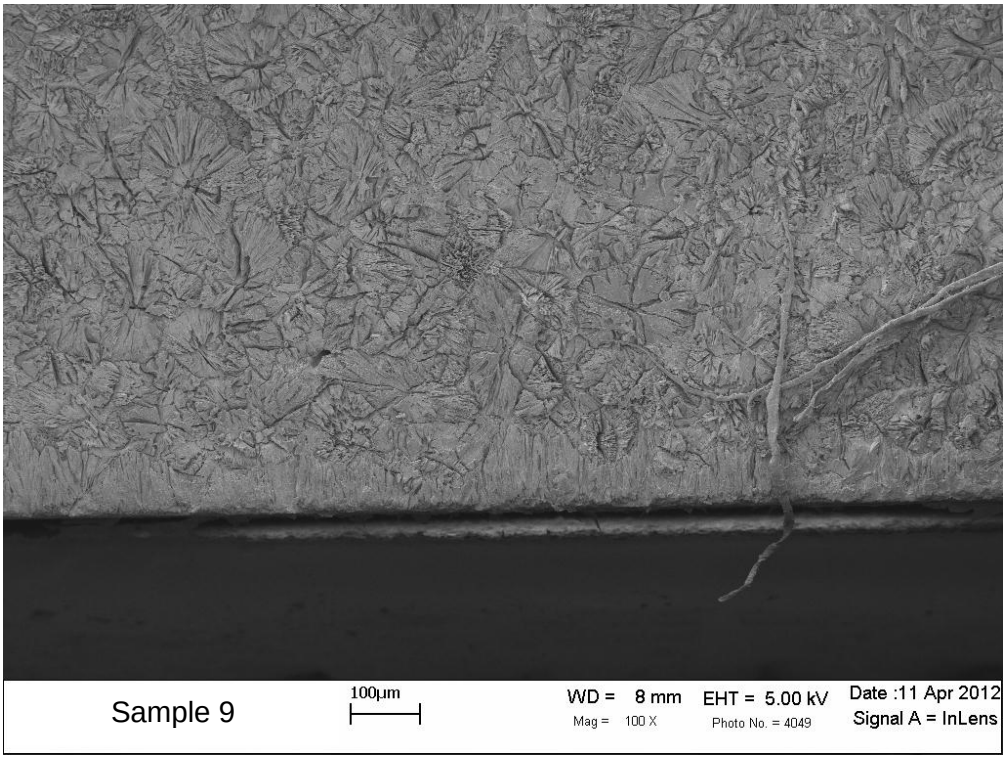

Figure 3.14: Micrograph of Sample 9 centered at location 0.16 mm from the crystal edge.

As seen in the figure above, there is an impurity present on the crystalline surface. This impurity is likely from the sample preparation, possibly a fiber from a paper towel used when drying the samples.

To see the transformation of microstructure through the entire sample cross section, the micrographs above were stitched together, as seen in Figure 3.15. To the right of the figure, the dimension of the cross section thickness can be seen, 2.7 mm. To the left of the figure, the estimated percent crystallinity can be seen. This percent crystallinity has been estimated by analyzing "slices" of the micrographs in the ImageJ software. It is important to note that these are only estimations, not exact values, due to the holistic nature of the software analysis. The software is not equipped to perform a gradient evaluation.

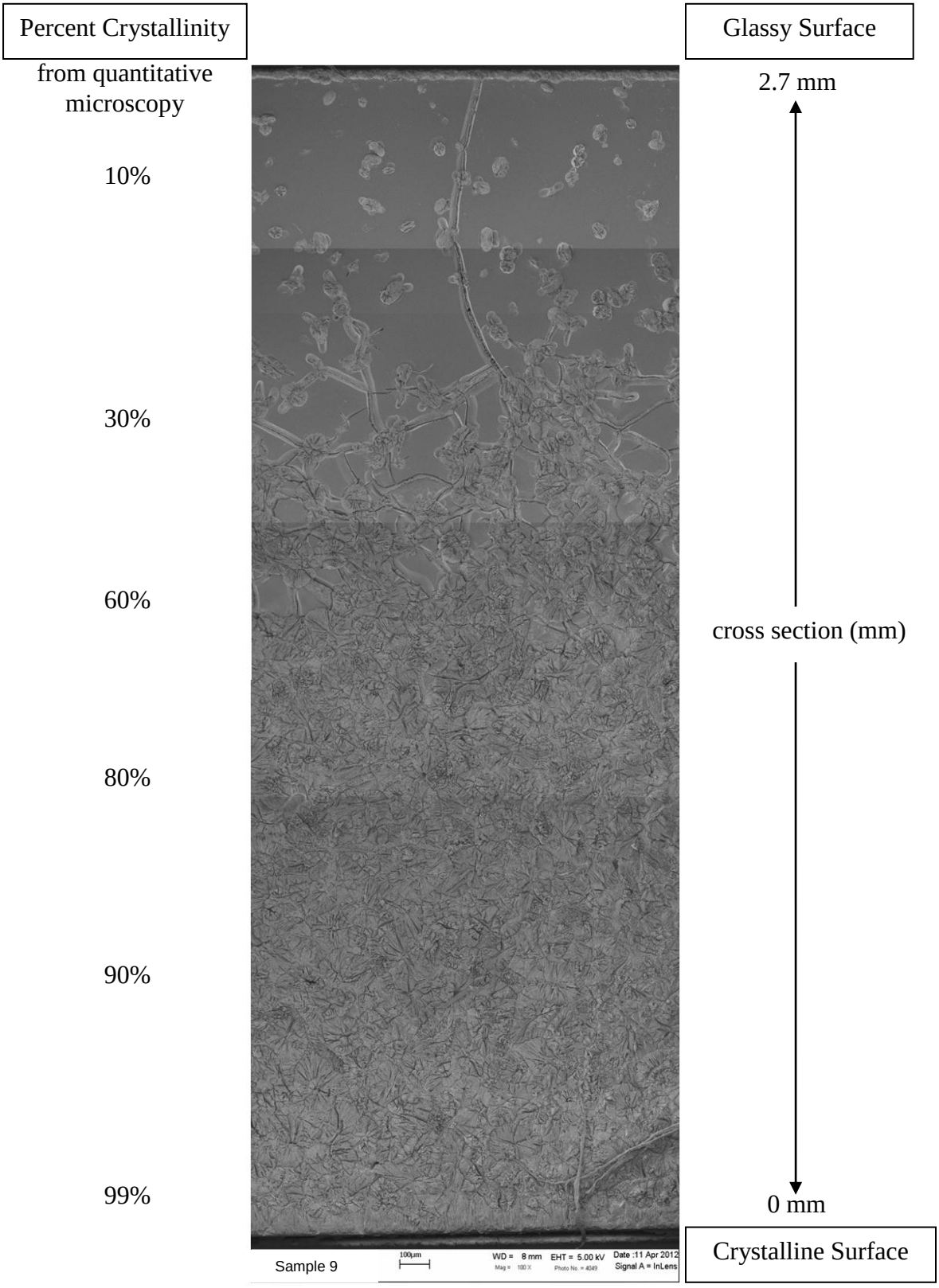

Figure 3.15: Stitched micrographs of Sample 9 throughout sample cross section.

As can be seen in the figure, the crystal population and size change throughout the thickness of the sample. The crystals near the glassy surface are not very populated and are very small. Further down in the figure, crystals become much more populated and appear larger in size. Even further down, the crystals become the dominant phase and the glassy matrix starts to disappear. Close to the crystalline surface, the crystals have grown completely into the surrounding crystals and there is no longer any glassy phase present.

As can be seen in the figure, there are cracks that run through the glassy matrix. There is a large vertical crack close to the glassy surface that runs into the crystalline phase. When this crack enters the crystalline phase, it gets deflected into many smaller cracks. Further down in the figure, as the crystallinity increases, the cracks become more populated but also decrease in length. This is likely due to the crystals acting as crack deflectors. There does not appear to be cracks present when the percent crystallinity exceeds about 60%. The figure also demonstrates why glass-ceramics are usually stronger and tougher than glasses – cracks do not propagate easily in the former. The cracking seen in the figure is the same phenomenon mentioned in Section 3.1 (Sample Preparation).

It is unclear where the cracks initiate from, but one possibility is that these cracks initiate from voids. If voids are forming between the glassy and crystalline phases due to the densification of the crystalline phase, as seen in Figures 3.6 and 3.7, these could be potential sites for crack initiation. As the crack would propagate outwards from these voids, it would only extend into the glassy region since crystals act as crack deflectors.

3.3 Raman Spectroscopy

Raman spectroscopy was used to analyze all Standards and all Samples.

3.3.1 Raman Spectroscopy Performed on Standards

The Raman analysis was first performed on the standards to determine a basis for comparison with percent crystallinity. The Raman spectra of lithium disilicate glass (Standard 1) and glass-ceramic (Standard 6) are shown in Figures 3.16 and 3.17 respectively.

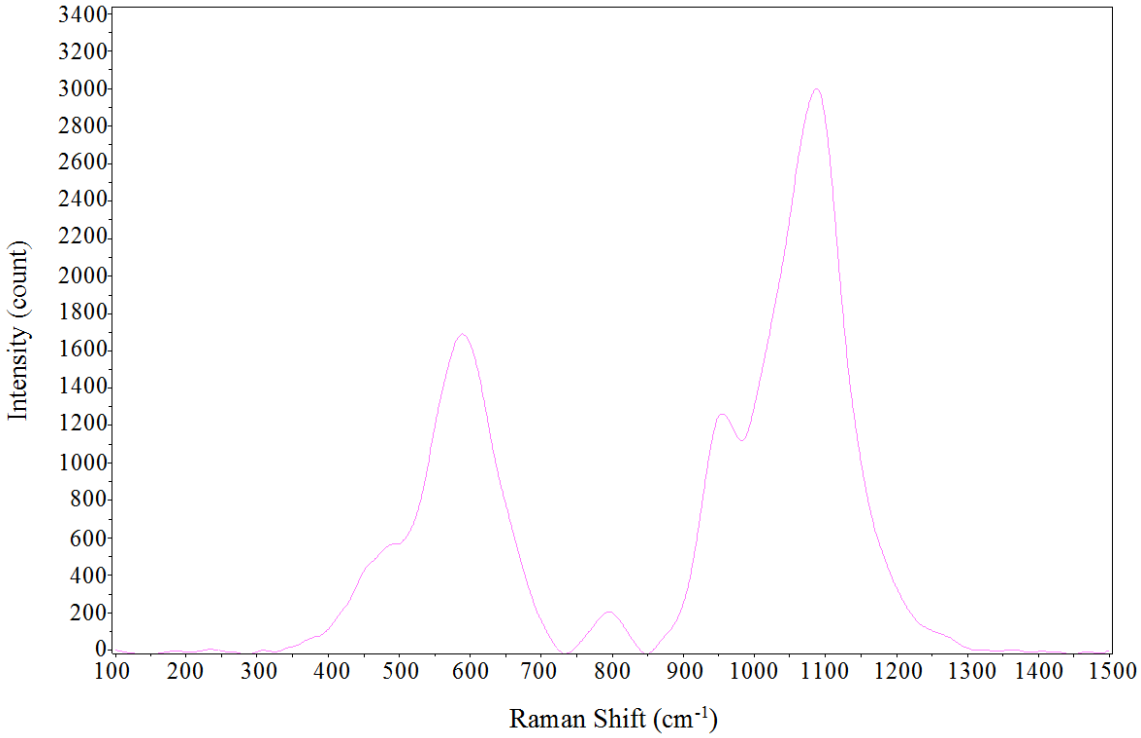

Figure 3.16: Raman spectra of Standard 1 (0% crystallinity).

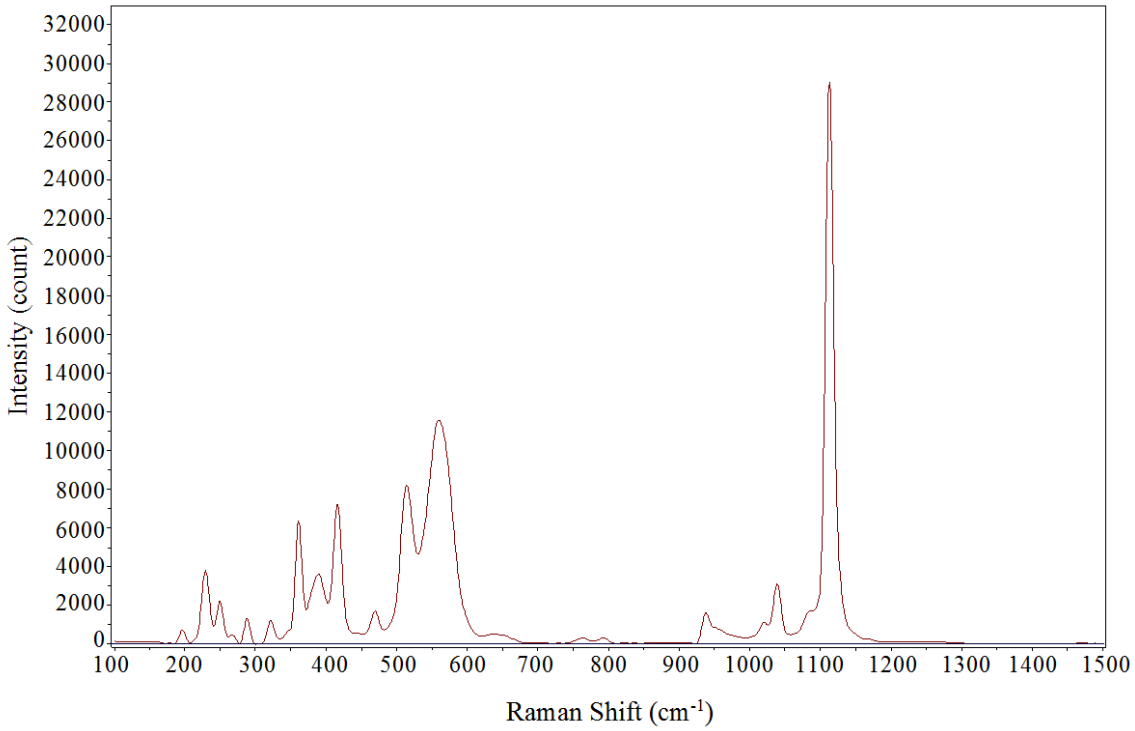

Figure 3.17: Raman spectra of Standard 6 (100% crystallinity).

As can be seen in Figure 3.16, the spectra of the glass shows broad peaks with low intensity. The two major peaks present can be identified by the x-axis location of 587 cm^{-1} and 1086 cm^{-1}. The 587 cm^{-1} peak corresponds to Si-O-Si bending present in the molecular structure of the glass [1]. As can be seen in the figure, the glass contains a wide range Si-O-Si bond angles. The 1086 cm^{-1} peak corresponds to the Si-O stretching in a molecule with one nonbridging oxygen [1]. Seen in the figure, the glass contains many lengths of this Si-O bond.

As can be seen in Figure 3.17, the spectra of the glass-ceramic shows many defined peaks with high intensity. The two major peaks present in the glass can still be seen, however they have shifted. These can be identified by the x-axis location of 551 cm^{-1} and 1110 cm^{-1}. The 551 cm^{-1} peak corresponds to Si-O-Si bending present in the

molecular structure of the glass-ceramic [1]. As can be seen in the figure, the glass-ceramic contains a much more limited range of Si-O-Si bond angles as compared to glass. The 1110 cm^{-1} peak corresponds to the Si-O stretching in a molecule with one nonbridging oxygen [1]. Seen in the figure, the glass-ceramic contains very few lengths of this Si-O bond.

From the comparison of Figures 3.16 and 3.17, it can be seen that during the transformation from glass to glass-ceramic, peaks should sharpen, grow in intensity, and shift slightly in x-axis location. This can be seen by the stacked spectra of all the standards seen in the figure below.

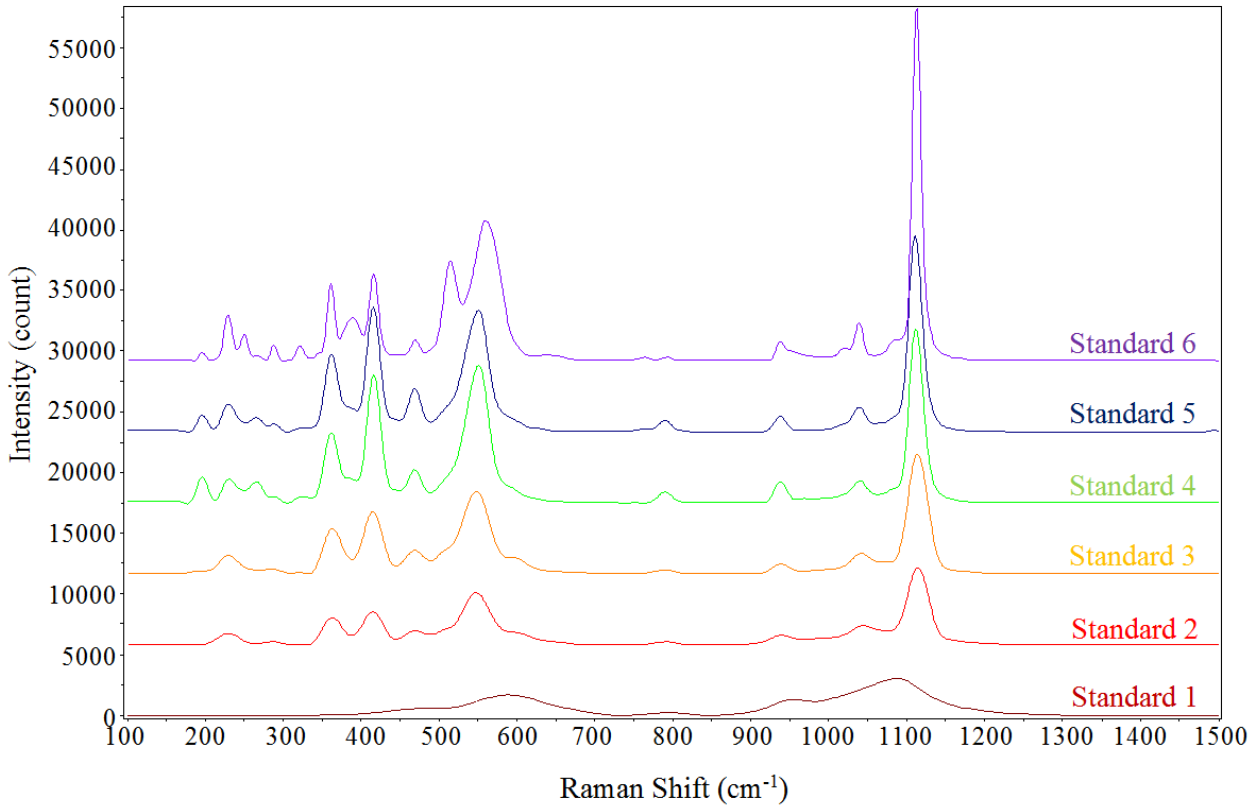

Figure 3.18: Raman spectra of all standards. The spectra are labeled by the colored text on the right.

The Full Width at Half Maximum for the spectra peaks of the standards is reported in the table below.

Table 3.2: Full Width at Half Maximum for all standards.

Standard	Crystallinity (%)	Full Width at Half Maximum			
		587-551 cm^{-1} Peak		1086-1110 cm^{-1} Peak	
		Average	Standard Deviation	Average	Standard Deviation
Standard 1	0	125	4.7	107	2.7
Standard 2	35	42	1.9	20	1.9
Standard 3	50	41	1.5	19	1.2
Standard 4	90	38	1.9	15	<0.1
Standard 5	~95	32	3.3	12	1.9
Standard 6	100	29	4.5	11	0.8

Comparison of the Raman Full Width at Half Maximum average for the 1086-1110 cm^{-1} peak and percent crystallinity of the standards yields the graph seen below. This graph will be used to calculate the percent crystallinity of samples based upon the Raman spectra.

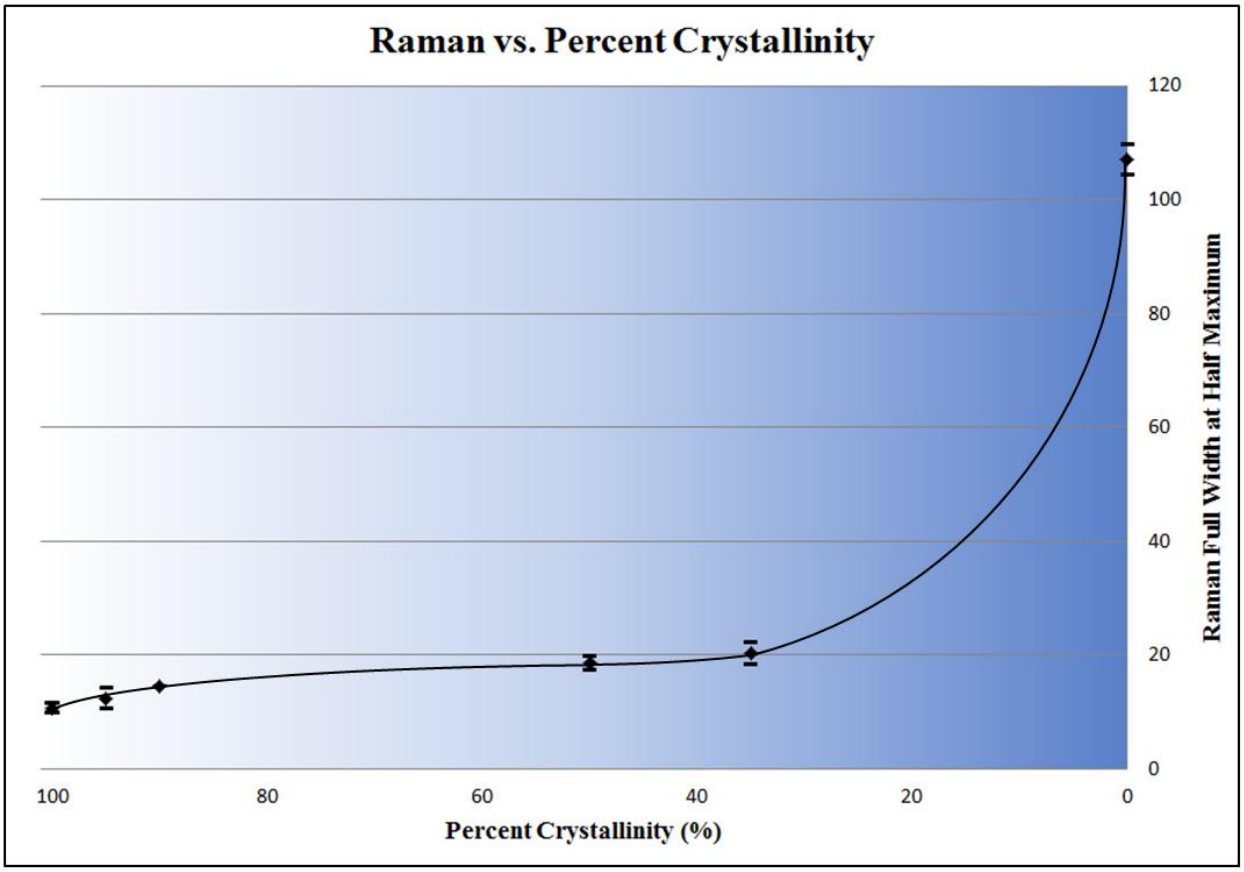

Figure 3.19: Graph of Raman spectra 1086-1110 cm^{-1} peak width versus crystallinity derived from the standards.

3.3.2 Raman Spectroscopy Performed on Samples

The samples were also analyzed using Raman analysis throughout the sample cross section. Spectra taken at various points throughout the sample cross section showed a similar transformation in Raman peaks as the standards. An example of the spectrum transformation throughout the sample cross section can be seen in the figure below.

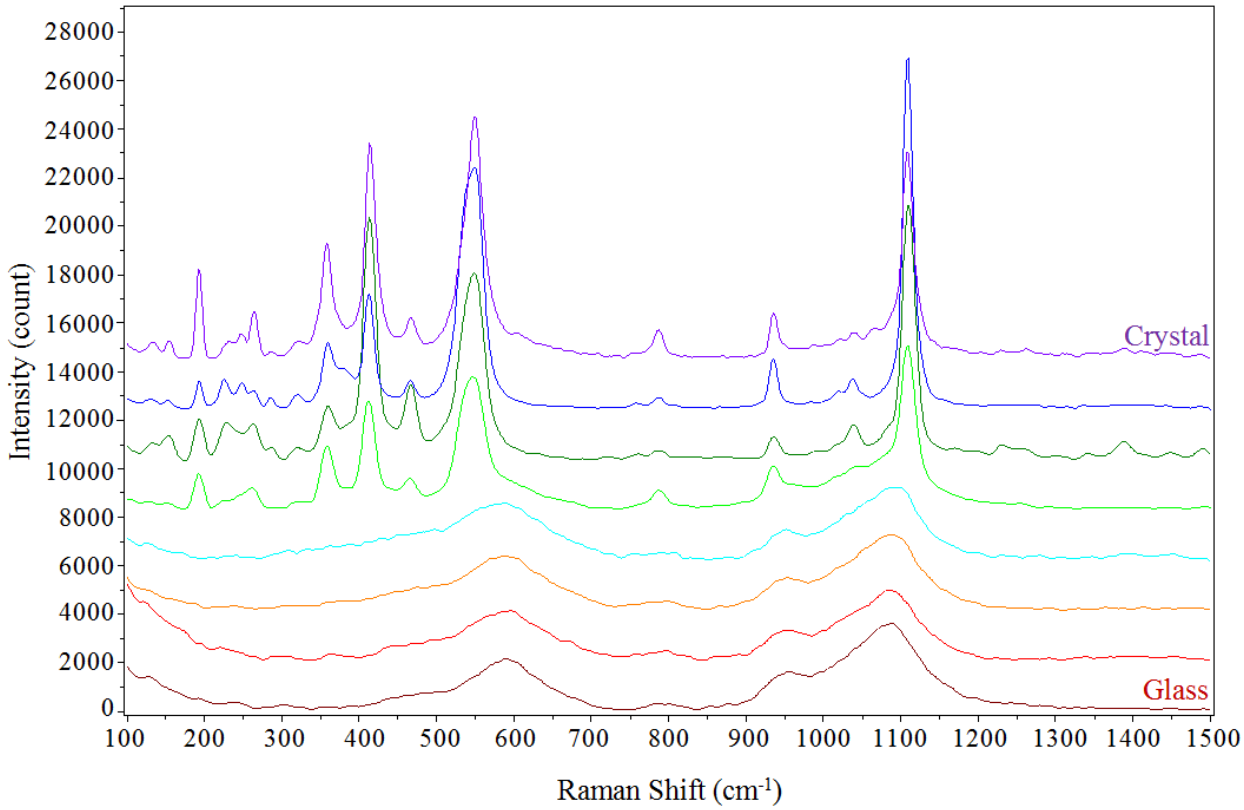

Figure 3.20: Raman spectra of points across Sample 10. The two spectra taken closest to the surfaces are labeled by the colored text on the right.

The peak Full Width at Half Maximum was analyzed from the spectra taken throughout the sample cross sections. This data was converted to a graph of 1086-1110 cm^{-1} peak width versus analysis position. The Raman profile graph for each sample can be seen in the figures below.

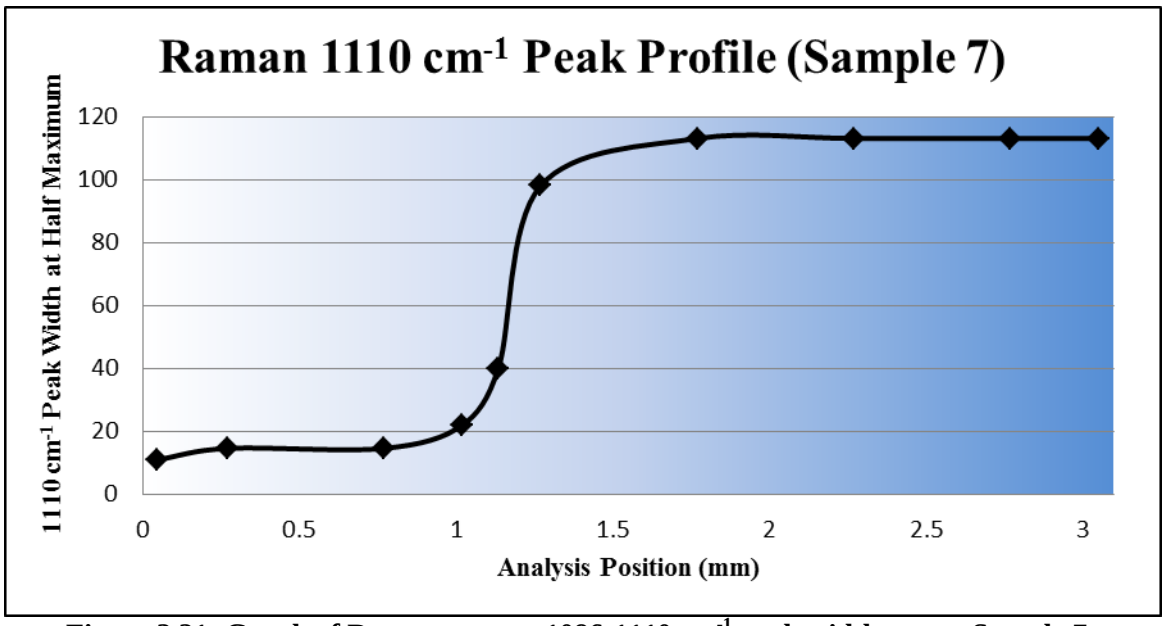

Figure 3.21: Graph of Raman spectra 1086-1110 cm^{-1} peak width across Sample 7.

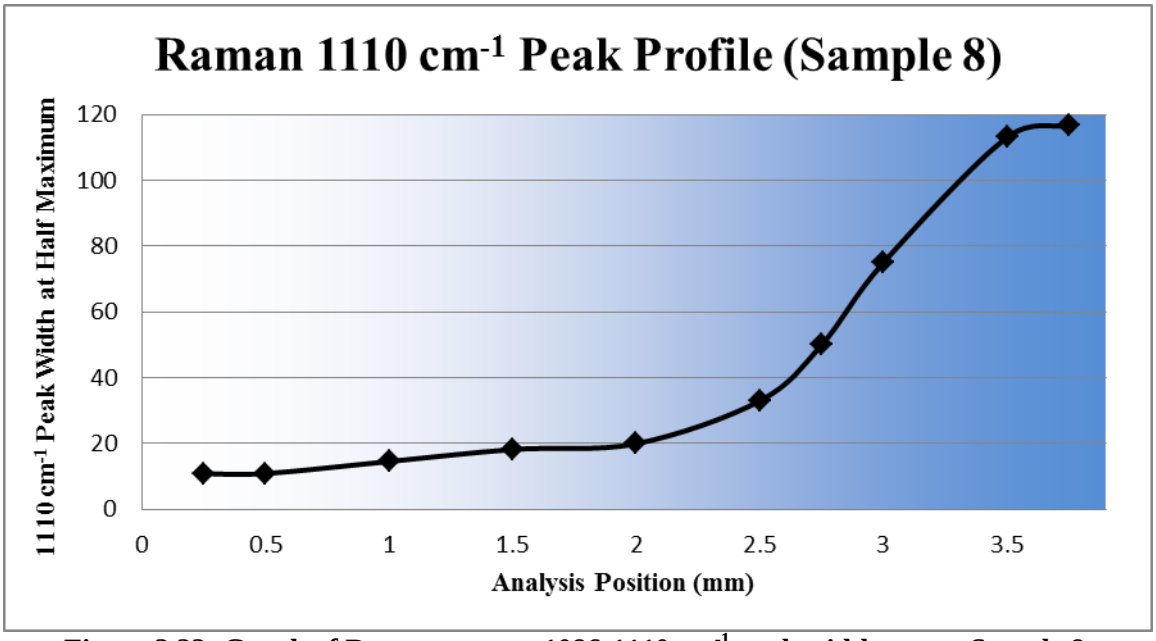

Figure 3.22: Graph of Raman spectra 1086-1110 cm^{-1} peak width across Sample 8.

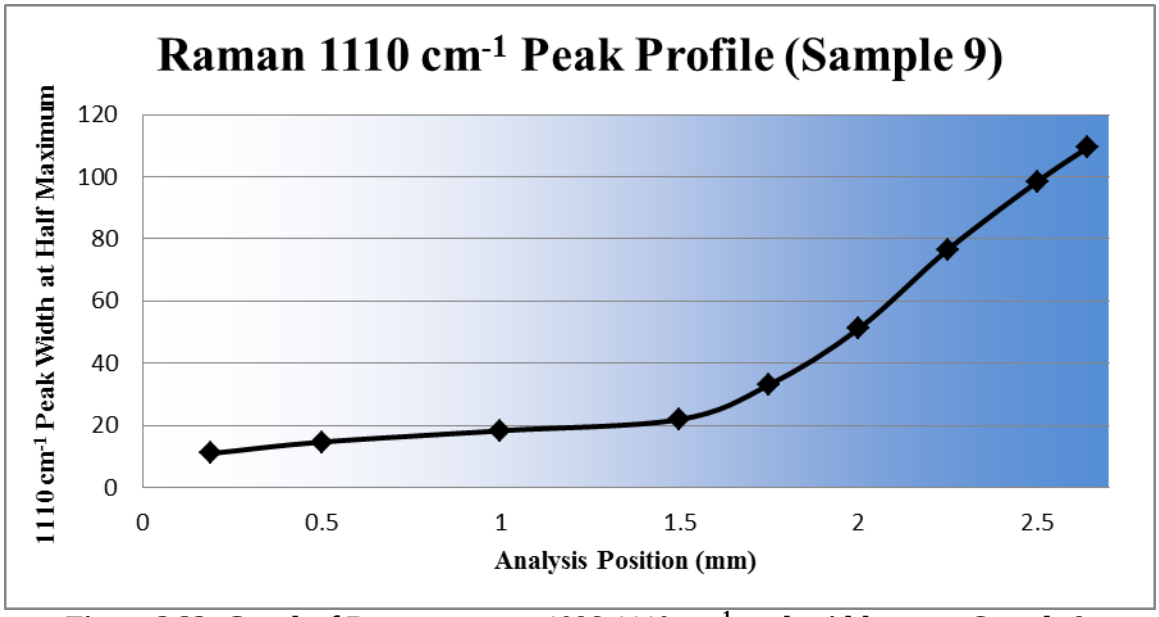

Figure 3.23: Graph of Raman spectra 1086-1110 cm^{-1} peak width across Sample 9.

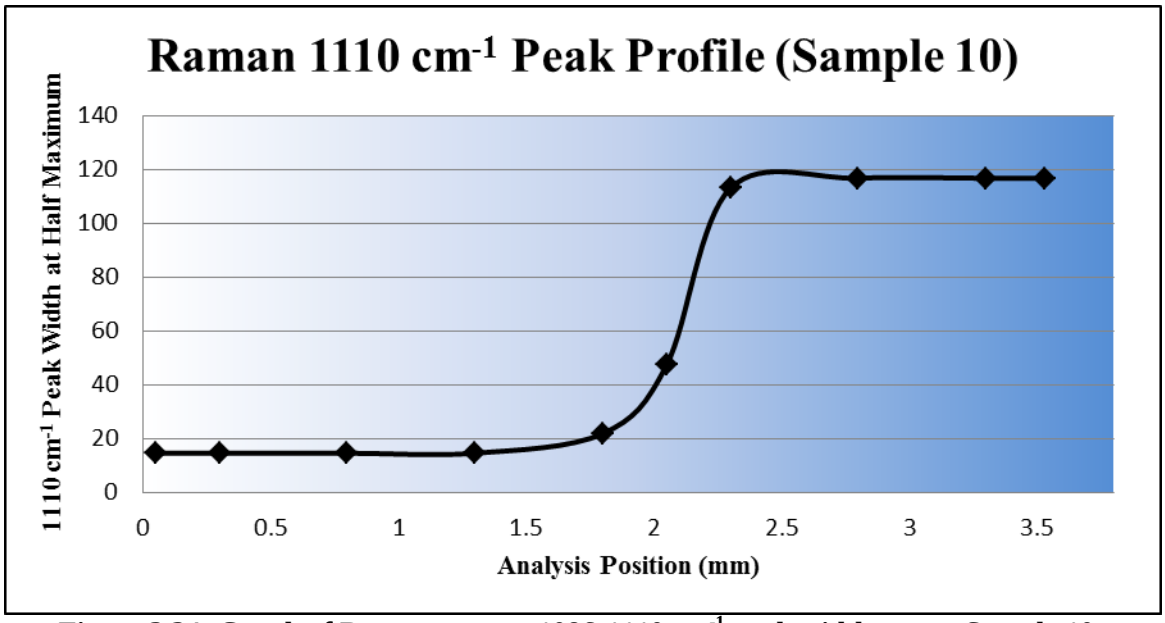

Figure 3.24: Graph of Raman spectra 1086-1110 cm^{-1} peak width across Sample 10.

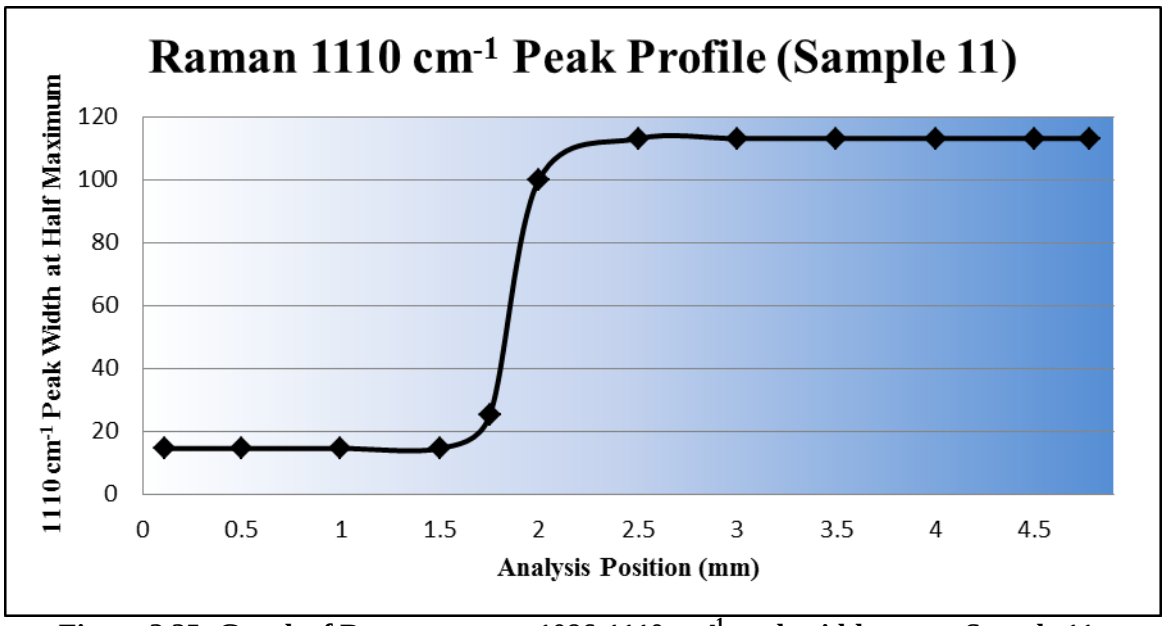

Figure 3.25: Graph of Raman spectra 1086-1110 cm^{-1} peak width across Sample 11.

Comparison of the analysis done on each sample and the analysis done on the standards can lead to percent crystallinity graphs for each sample. By comparing the data presented in Figure 3.19 and the Raman peak profile for each sample, a crystallinity profile graph can be obtained. The crystallinity profiles for all the samples can be seen in the figures below. The crystallinity profile for sample 9 is repeated to show the scanning electron micrographs in the background of the graph.

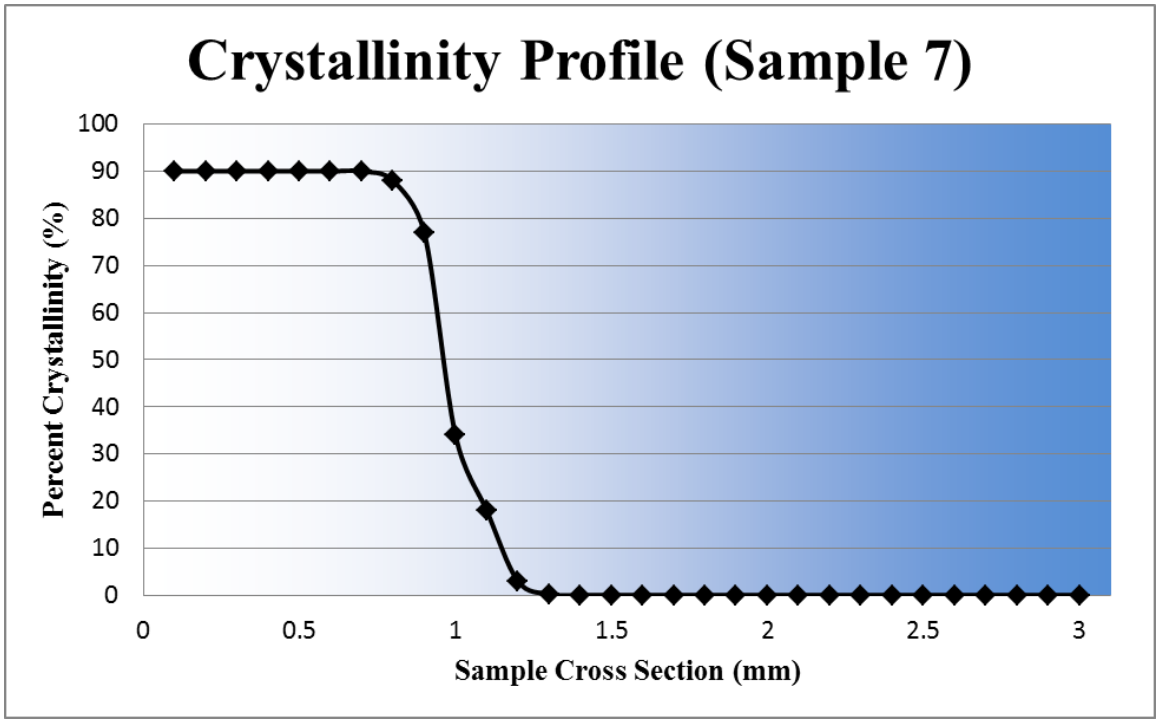

Figure 3.26: Graph of percent crystallinity across Sample 7 using Raman spectroscopy.

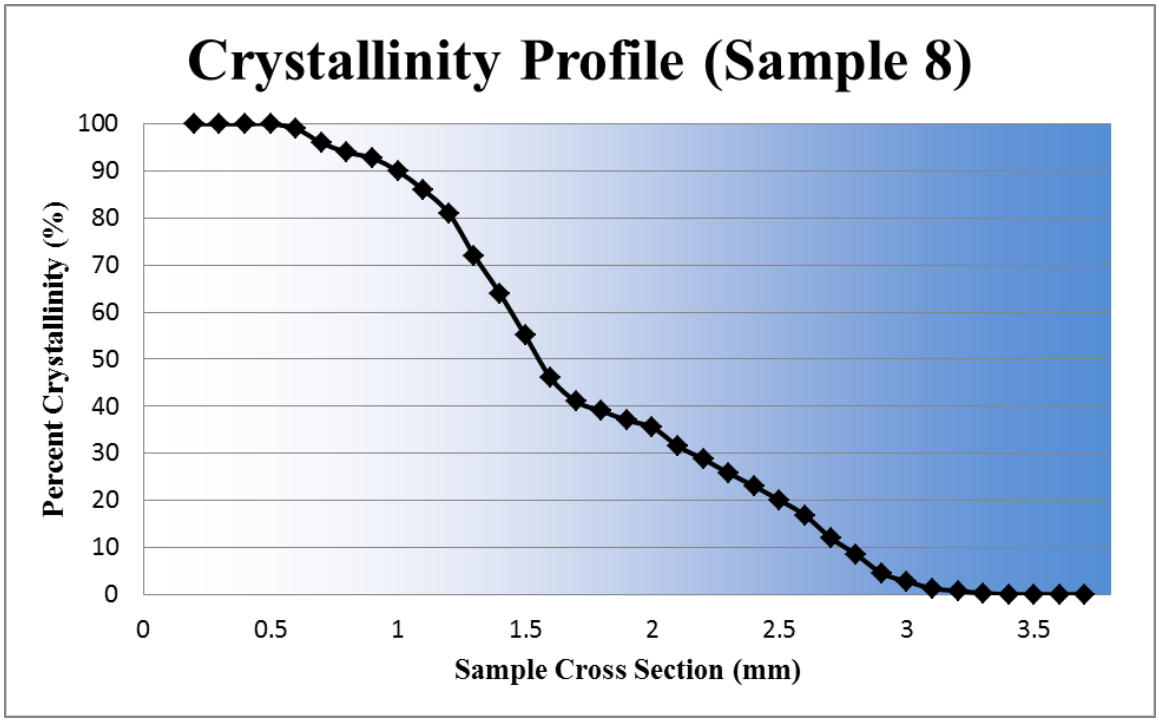

Figure 3.27: Graph of percent crystallinity across Sample 8 using Raman spectroscopy.

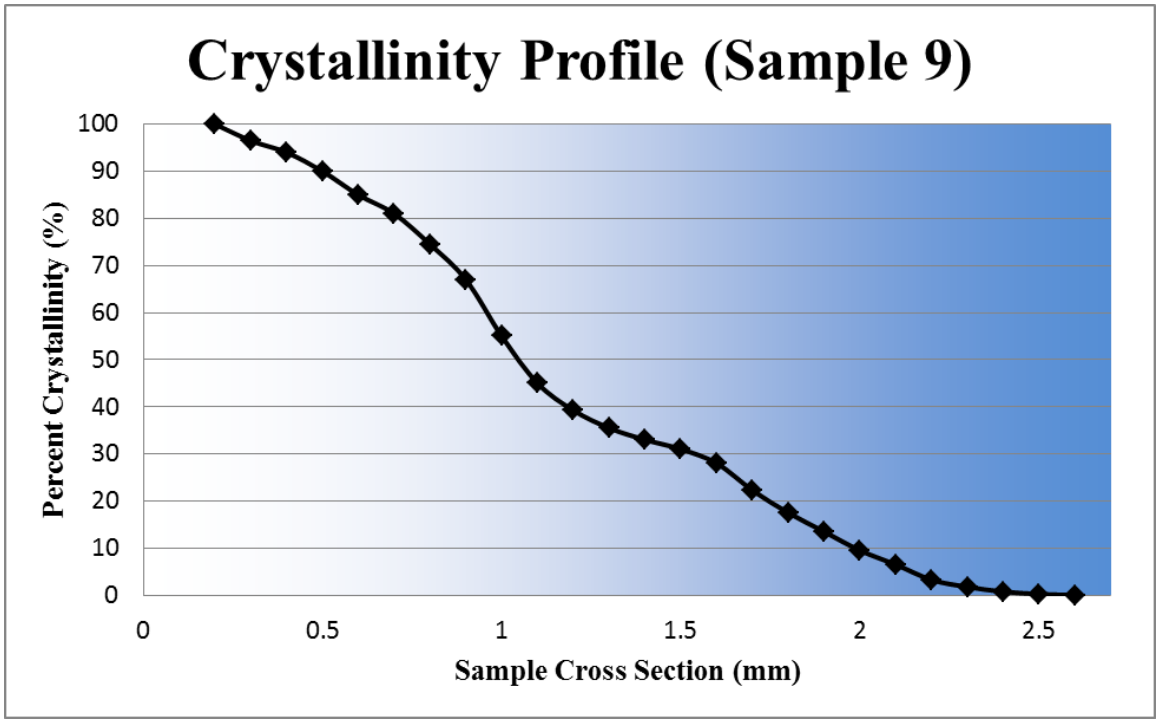

Figure 3.28: Graph of percent crystallinity across Sample 9 using Raman spectroscopy.

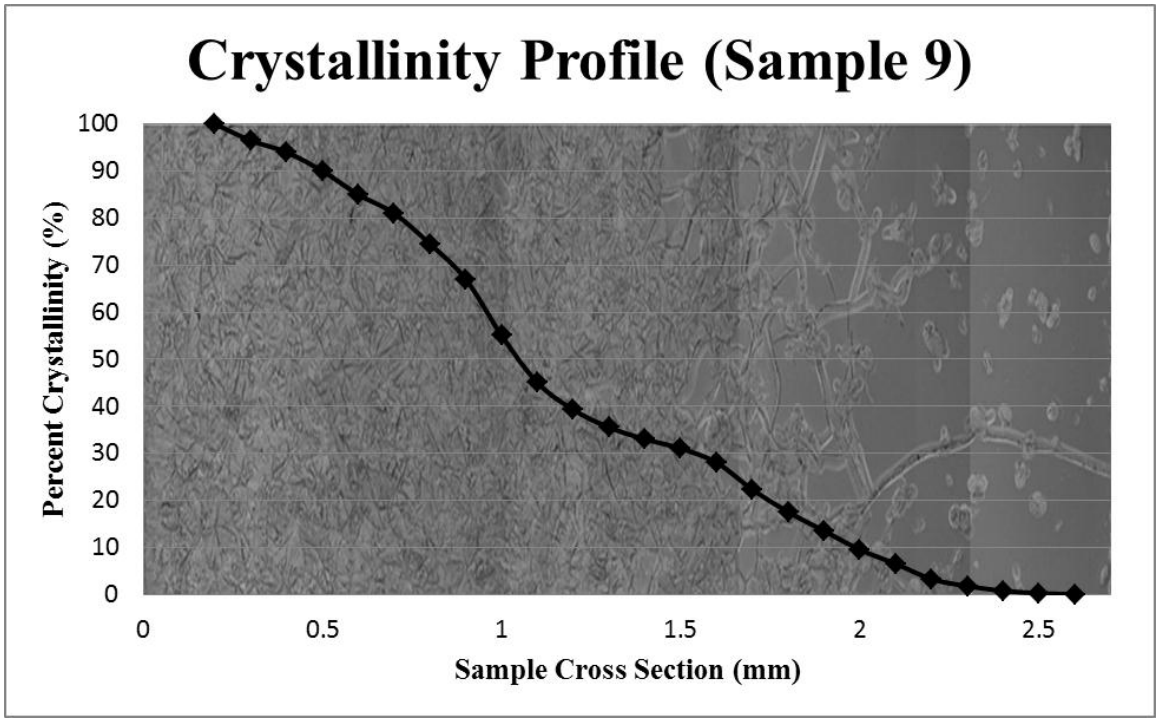

Figure 3.29: Graph of percent crystallinity across Sample 9 with scanning electron micrographs in the background.

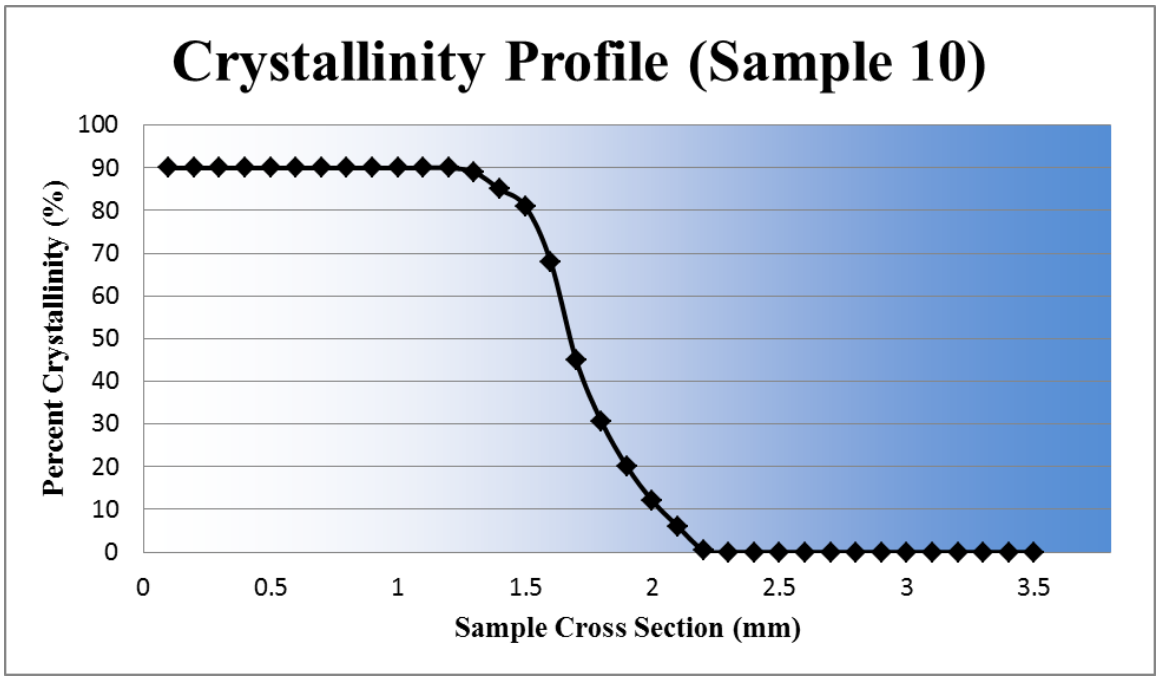

Figure 3.30: Graph of percent crystallinity across Sample 10 using Raman spectroscopy.

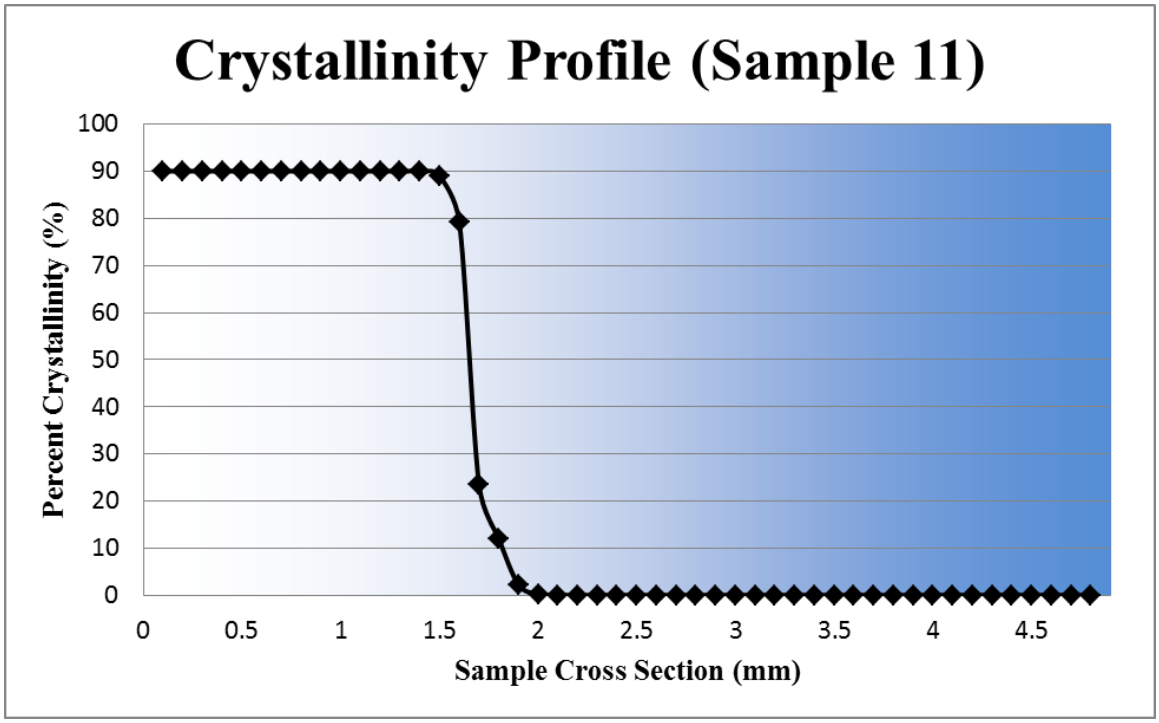

Figure 3.31: Graph of percent crystallinity across Sample 11 using Raman spectroscopy.

3.4 Microhardness

Microhardness was performed on Standards 1, 2, 3, and 6 and on Sample 10.

3.4.1 Microhardness Performed on Standards

The microhardness was first performed on the standards to determine a basis for comparison with percent crystallinity. The results can be seen in the table below. Note that the measured values resemble the literature values reported in Section 2.5 (Material Properties and the Rule of Mixtures). These values from literature were lithium disilicate glass: 530 kg/mm^2, and lithium disilicate glass-ceramic: 540 kg/mm^2 [10, 11].

Table 3.3: Hardness values of select standards.

Standard	Crystallinity (%)	Vickers Hardness	
		Average (kg/mm^2)	Standard Deviation
Standard 1	0	538	6
Standard 2	35	546	8
Standard 3	50	551	16
Standard 6	100	577	254

From the comparison of the hardness values for the different standards, it can be seen that hardness values should increase slightly with increasing crystallinity. However, it can also be seen that the variation in hardness values (reported in the table as standard deviation) also increases as crystallinity increases. In the 100% crystalline standard, the standard deviation is over six times larger than the difference in hardness with increasing crystallinity. This means that a hardness value at a given point in the 100% crystalline

sample could in actuality be either larger or smaller than the 0% crystalline standard. The great variation and the small difference in hardness between the glass and glass-ceramic makes it difficult to draw conclusions about the trend in hardness with increasing crystallinity.

The trend of increasing variation with increasing crystallinity is believed to be due to the heterogeneous nature of a polycrystalline material. In a glass, the material is homogeneous on a large scale. However, in a polycrystalline material, when the crystals form and grow, they can grow in many different crystallographic orientations. Different crystallographic orientations will have different affinities for being deformed. This affinity is due to the orientation of the crystal's slip planes. The slip plane's orientation in relation to the crystal structure of the material will remain constant. However, with changing crystallographic orientations, the slip plane's orientation in relation to the load applied will change. When performing hardness testing on different crystallographic orientations, the indenter could align parallel with a slip plane during one test, and perpendicular to a slip plane during the next test, producing very different hardness results. It is believed that the variability in hardness values found while testing the polycrystalline standards is due to different crystallographic orientations in the material.

Microcracks or voids due to the densification of the crystalline phase could also play a role in the observed variation. The difference in density between the glass and glass-ceramic causes voids to form in the polycrystalline material, as seen in Figure 3.7. These voids appear to become more prevalent as the percent crystallinity increases. The

relation of these voids to the indenter would contribute to differing amounts of plastic deformation upon loading, therefore affecting the hardness values.

3.4.2 Microhardness Performed on Sample 10

Sample 10 was also analyzed using microhardness throughout the sample cross section. Hardness tests performed at various points throughout the sample cross section showed similar results to the standards. The hardness profile across Sample 10 can be seen in the figure below. In the same figure, the hardness averages and standard deviations measured from the 100% crystalline and 0% crystalline standards can be seen in gold on the vertical axes. The calculated hardness profile based upon literature values can also be seen in purple (calculated from Equation 2 and reported as a function of percent crystallinity) [10, 11]. The crystallinity profile of Sample 10 can also be seen in red.

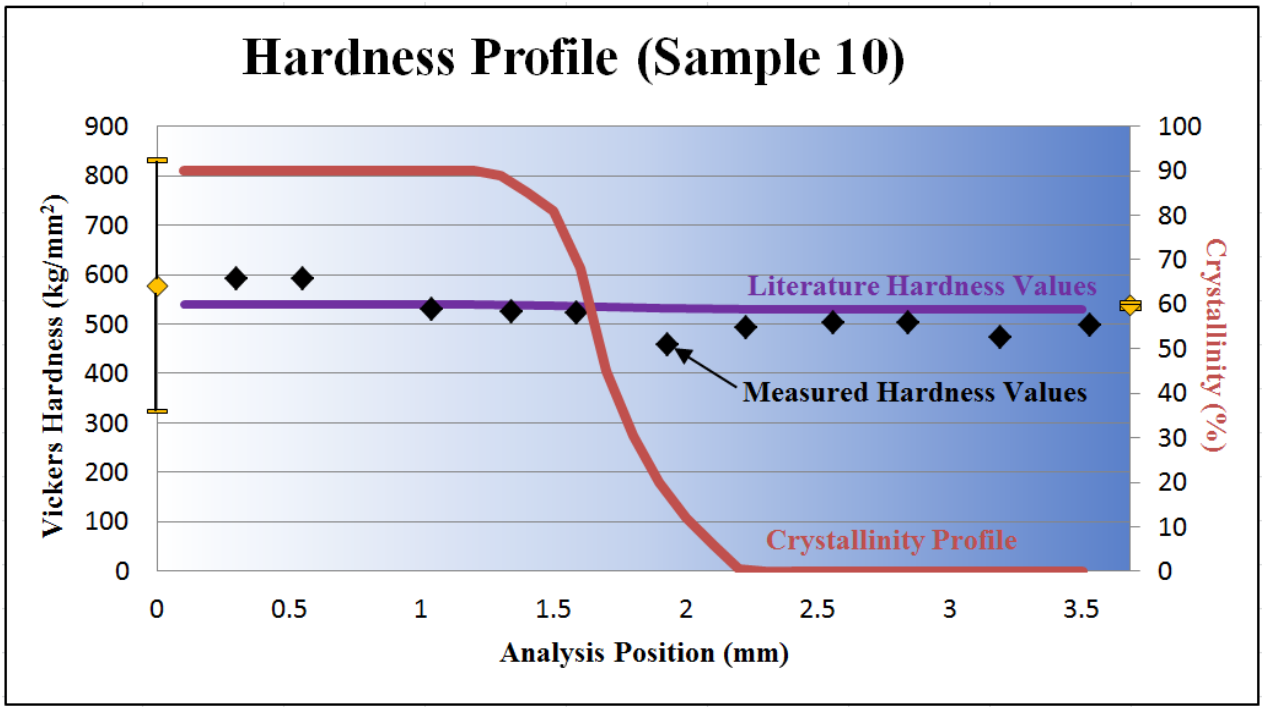

Figure 3.32: Graph of Vickers hardness across Sample 10 (black diamonds). The averages and standard deviations measured from Standard 1 and 6 are shown in gold on the vertical axes. The calculated hardness profile based upon literature values is shown in purple. The crystallinity profile of Sample 10 is shown in red.

As seen above, with increasing crystallinity (moving from right to left in the graph), the hardness values increase slightly. However, because of the variation present in the 100% crystalline standard, conclusions cannot be made about the trend in the hardness values.

3.5 Sample Analysis

This section examines all the characterization results to analyze the created microstructure graded glass-ceramics.

3.5.1 Heating Parameter Analysis

One goal of this experiment was to determine how processing parameters affect the resulting microstructure graded glass-ceramic. By comparing the heating parameters applied during crystallization (temperature at crystallization surface, temperature gradient, time of crystallization), and the crystallization profiles developed from the Raman spectroscopy data, trends can be seen.

Sample 10 was crystallized at a high temperature (613°C) with a moderate temperature gradient (26.3°C/mm) for a short time (4 minutes). This resulted in a crystallization profile (shown in Figure 3.30) that has three distinct regions: 1) a region with 90% crystallinity and a width of 1.2 mm; 2) a region with a crystallinity gradient and a width of 1.1 mm; and 3) a region with 0% crystallinity and a width of 1.5 mm. This crystallinity profile resembles the proposed steep interface seen in Figure 1.8. By looking at the sample pictures in Figure 3.2, it can also be seen that Sample 10 resulted in abundant cracking in the glassy phase. A representation of the crystallinity profile, microstructure, and cracking present in Sample 10 can be seen in Figure 3.33.

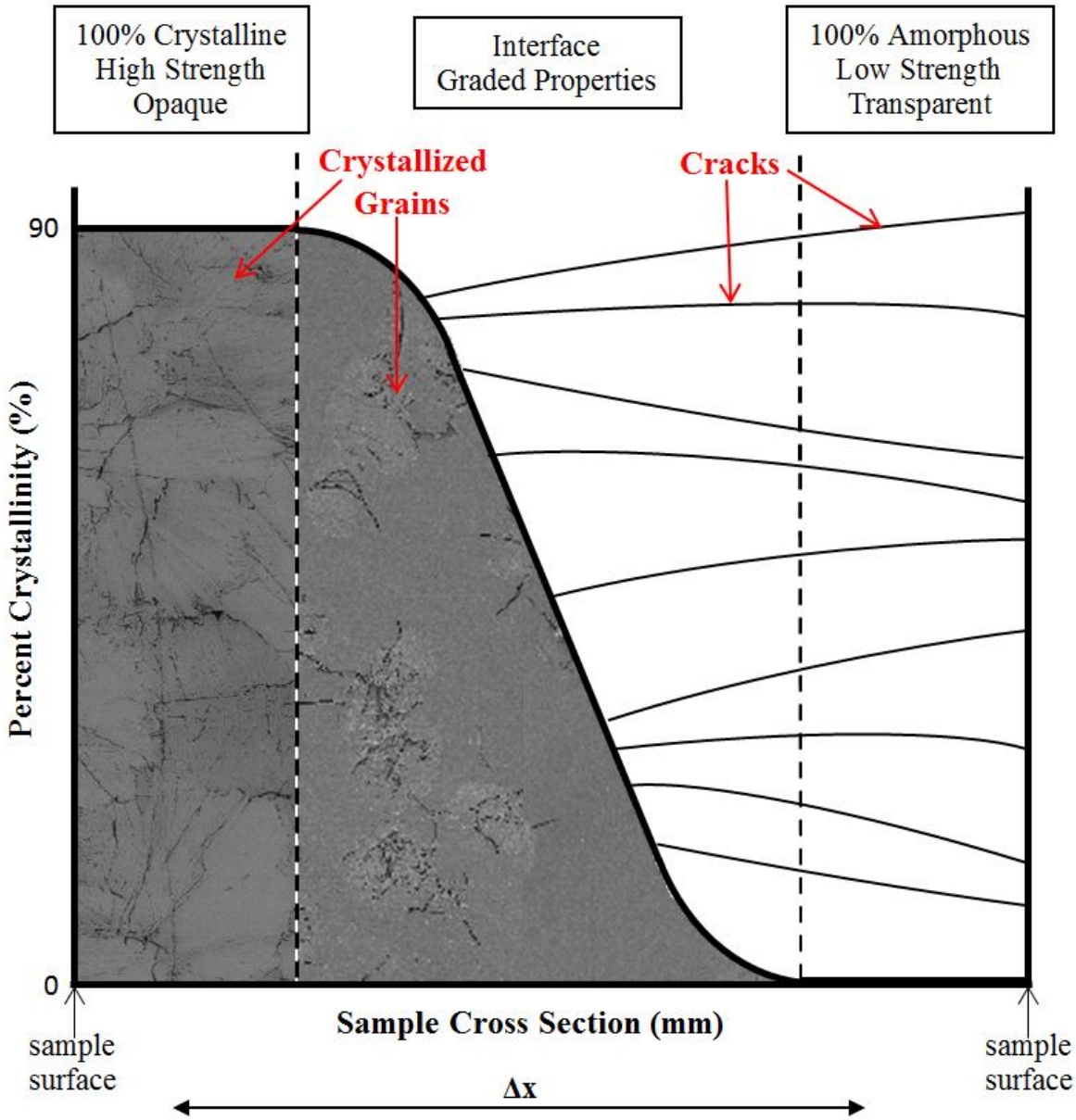

Figure 3.33: Graph of percent crystallinity versus the cross section for Sample 10.

In contrast, Sample 9 was crystallized at a low temperature (558°C) with a high temperature gradient (33.5°C/mm) for a long time (10.5 minutes). This resulted in a crystallization profile (shown in Figure 3.28) that has only one region: a region with a shallow crystallinity gradient from 100% crystallinity to 0% crystallinity and a width of 2.7 mm. This crystallinity profile resembles the proposed shallow interface seen in Figure

1.9. By looking at the sample pictures in Figure 3.2, it can also be seen that Sample 9 resulted in a lesser extent of cracking than Sample 10. A representation of the crystallinity profile, microstructure, and cracking present in Sample 9 can be seen in Figure 3.34.

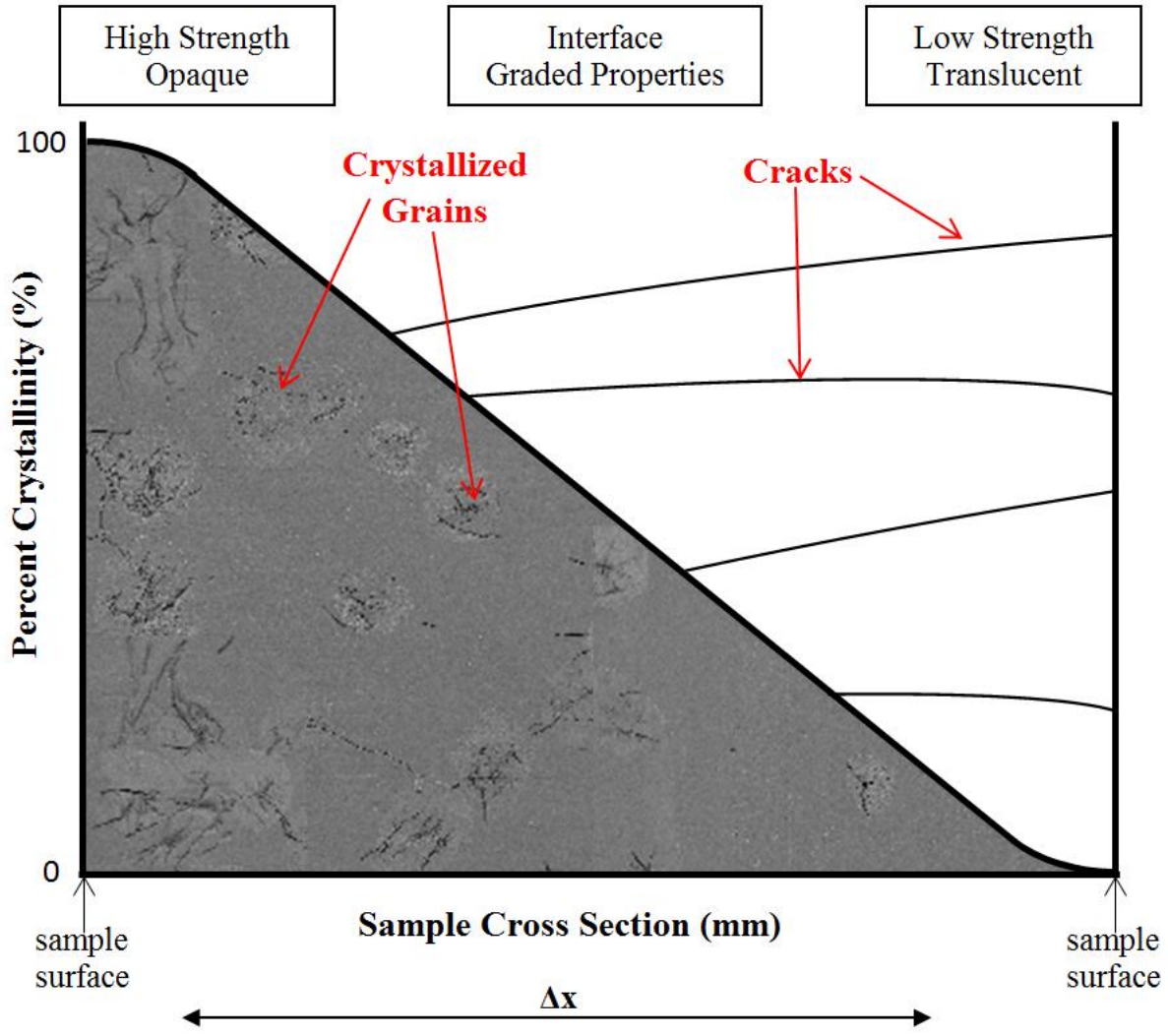

Figure 3.34: Graph of percent crystallinity versus the cross section for Sample 9.

The table below shows a comparison between the processing parameters and the resulting crystallinity gradient for each sample. The crystallization gradient was

quantified by dividing the change in percent crystallinity (Δ%) by the gradient width (Δmm).

Table 3.4: Processing parameters and crystallization gradients of samples.

Sample	Temperature at Crystal Surface (°C)	Temperature Gradient (°C/mm)	Time at Upper Temperature Range (min)	Crystallization Gradient (%/mm)
Sample 7	613 ± 16	16.6	4	128.6
Sample 8	596 ± 24	25.4	6	34.5
Sample 9	558 ± 22	33.5	10.5	41.7
Sample 10	613 ± 22	26.3	4	81.8
Sample 11	672 ± 18	32.2	5	180.0

From the experimental results, it can be concluded that the crystallization heating parameters can control the resulting microstructure graded glass-ceramic. The slope of the crystallization gradient is a result of the experimental parameters. Processing parameters of high temperature and moderate temperature gradient for a short time lead to a steep crystallization gradient. Processing parameters of low temperature and high temperature gradient for a long time lead to a shallow crystallization gradient.

3.5.2 Property Profile Analysis

As discussed in Section 1.2 (Functionally Graded Materials), a functionally graded material is characterized by the change of properties with changing position in the material. To evaluate the FGMs created, three properties were plotted versus the cross section of Samples 9 and 10. These three properties were density, elastic modulus, and

coefficient of thermal expansion. As discussed in Section 2.5 (Materials Properties and the Rule of Mixtures), these material properties will change as a function of percent crystallinity. Therefore, the property profiles can be created for a FGM based upon the crystallinity profile of the sample.

Since density and percent crystallinity are linearly related, the crystallinity profile and density profile of a sample have a direct correlation. A steep crystallinity profile will lead to a steep density profile. Similarly, a shallow crystallinity profile will lead to a shallow density profile. Shown below is the relationship between the percent crystallinity and density for Sample 10. This sample displays a steep density gradient.

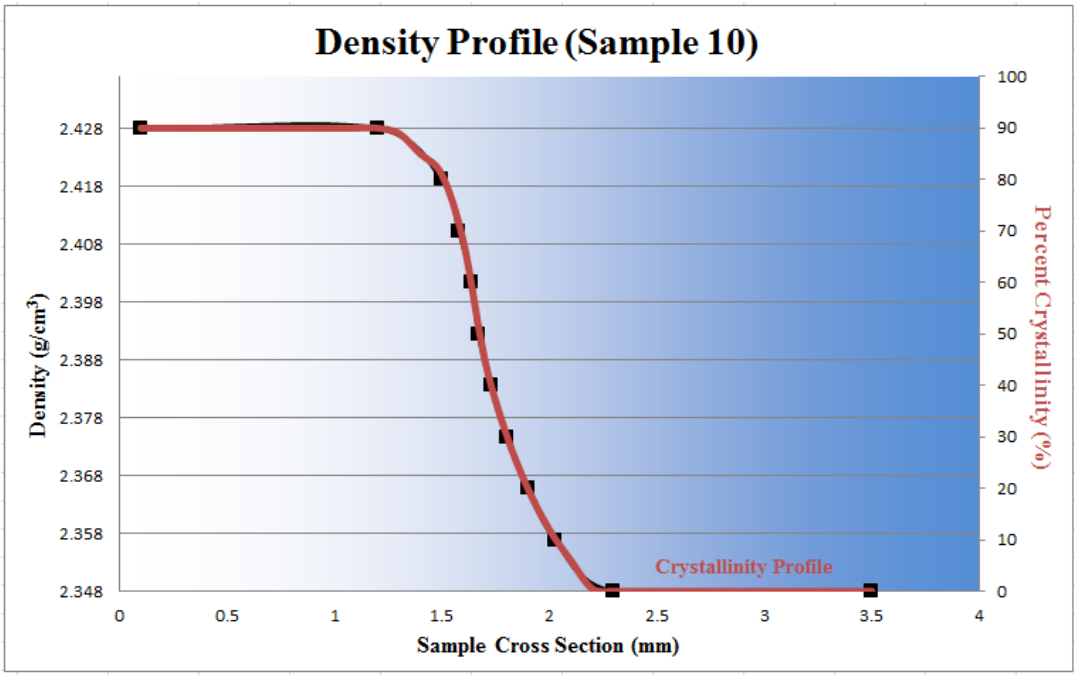

Figure 3.35: Graph of percent crystallinity and density versus cross section for Sample 10. The crystallinity is shown in red and the density is shown in black. The two lines overlap each other, as expected.

Shown below is the relationship between the percent crystallinity and density for Sample 9. This sample displays a shallow density gradient.

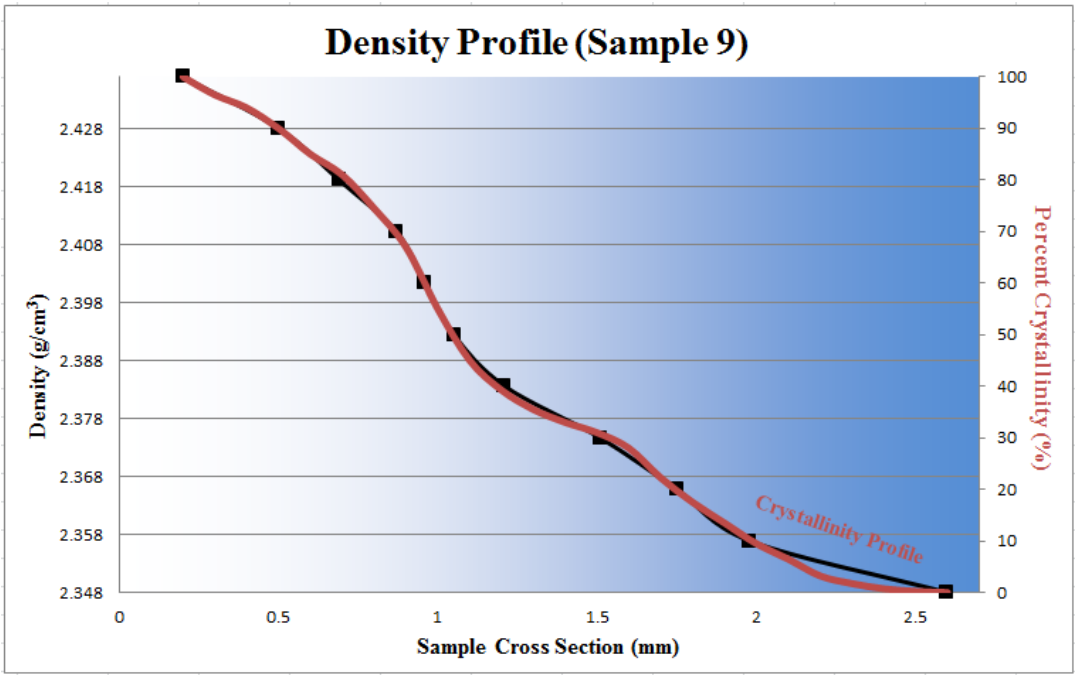

Figure 3.36: Graph of percent crystallinity and density versus cross section for Sample 9. The crystallinity is shown in red and the density is shown in black. The two lines overlap each other, as expected.

Since elastic modulus and percent crystallinity are linearly related, the crystallinity profile and elastic modulus profile of a sample have a direct correlation. A steep crystallinity profile will lead to a steep elastic modulus profile. Similarly, a shallow crystallinity profile will lead to a shallow elastic modulus profile. Shown in Figure 3.37 is the relationship between the percent crystallinity and elastic modulus for Sample 10. This sample displays a steep elastic modulus gradient.

Since the coefficient of thermal expansion increases with decreasing crystallinity, the trend of the thermal expansion is inversely related to the trend of crystallinity.

However, a steep crystallinity gradient will lead to a steep coefficient of thermal expansion gradient because the two are linearly related. Shown in Figure 3.37 is the relationship between the percent crystallinity and coefficient of thermal expansion for Sample 10. This sample displays a steep thermal expansion gradient.

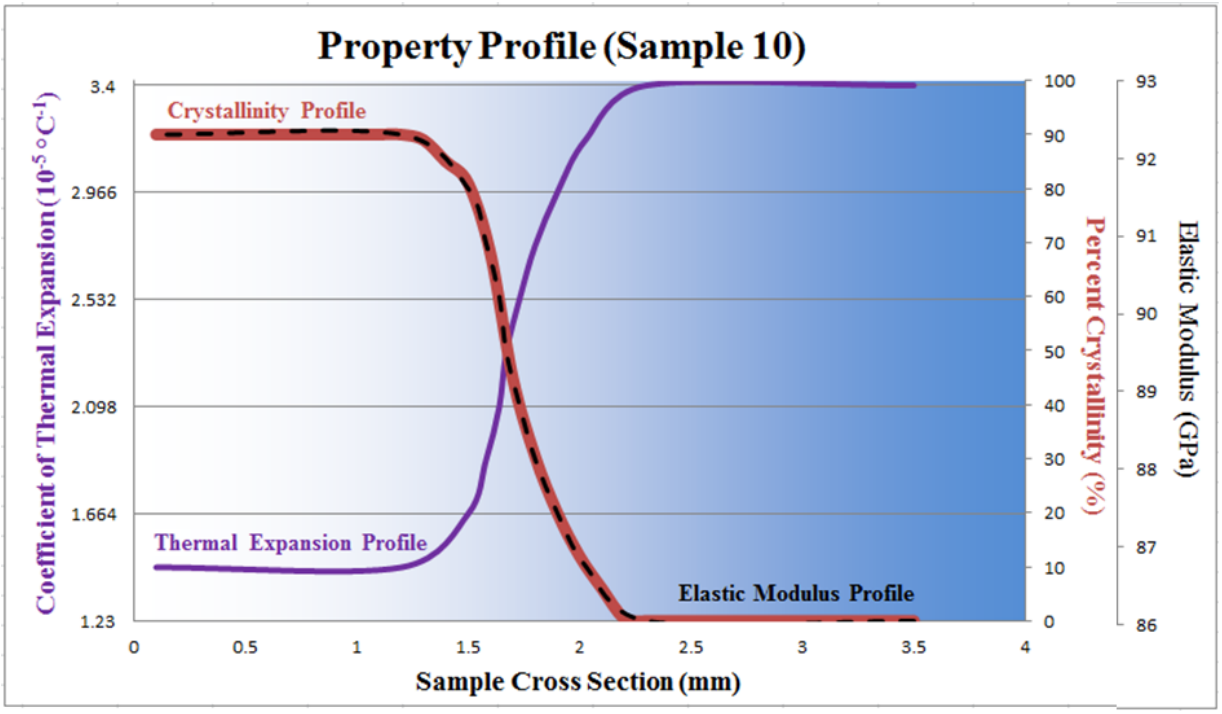

Figure 3.37: Graph of percent crystallinity, coefficient of thermal expansion, and elastic modulus versus cross section for Sample 10. The crystallinity is shown in red, the coefficient of thermal expansion is shown in purple, and the elastic modulus is shown in black (dotted line overlapping crystallization).

Shown below is the relationship between the percent crystallinity, elastic modulus, and coefficient of thermal expansion for Sample 9. This sample displays a shallow property gradient.

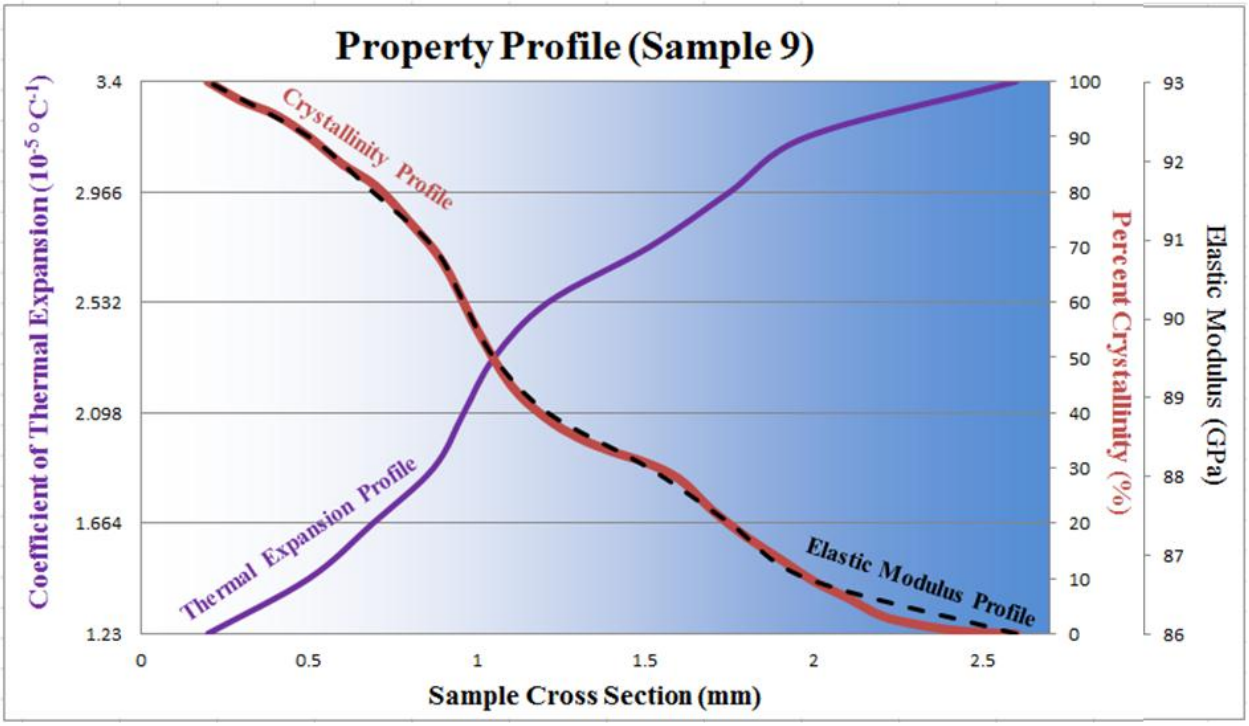

Figure 3.38: Graph of percent crystallinity, coefficient of thermal expansion, and elastic modulus versus cross section for Sample 9. The crystallinity is shown in red, the coefficient of thermal expansion is shown in purple, and the elastic modulus is shown in black (dotted line overlapping crystallization).

As there could be specific applications for both steep and shallow gradients of material properties, it is important to understand how the crystallization profile affects the property profiles.

3.5.3 Qualitative Stress Analysis

As stated is Section 3.1 (Sample Preparation), cracking is believed to occur due to the difference in coefficient of thermal expansion between the glassy and crystalline phases. To understand the cause of the cracks, the stresses that arise due to the difference in coefficient of thermal expansion must be understood.

The stresses present in a body arising from a difference in coefficient of thermal expansion can be modeled by the following equation [3]:

$$\sigma_{right} = \frac{E}{1-\mu}(T_o - T')(\alpha_{right} - \alpha_{left})\frac{A_{left}}{A_{total}} \quad (3)$$

where σ_{right} is the stress imposed on the right body
E is the modulus of elasticity of the right body
μ is Poisson's ratio of the right body
T_o is the temperature at which the material is stress free
T' is the temperature to which the material is cooled
α_{right} is the coefficient of thermal expansion of the right body
α_{left} is the coefficient of thermal expansion of the left body
A_{left} is the cross sectional area of the left body
A_{total} is the cross sectional area of the entire material

Note that Equation 3 only calculates the stresses due to the difference in coefficient of thermal expansion. In reality, the stresses present in the material could be due to many factors.

To explore this, consider three cases with a discrete interface between lithium disilicate glass (0% crystalline) and crystal (100% crystalline). Case 1 has an equal cross sectional area of the glass and crystal. Case 2 has a small region of glass on a large body of crystal, and Case 3 has a small region of crystal on a large body of glass. Schematics of these cases can be seen in Figure 3.39.

From analysis of Equation 3, it can be seen that many inputs will remain constant for the three cases presented. The elastic modulus, Poisson's ratio, and change in coefficient of thermal expansion will remain constant since these are material properties.

If all three cases are assumed to undergo to the same thermal cycling, then T_o and T' will also remain constant throughout the three cases.

This means that the only difference between the calculated stresses in the three cases will be due to the geometric factor, A_{left}/A_{total}. For Case 1, since the cross sectional areas of the two bodies are equal, this geometric factor will equal 0.5. For Case 2, since the cross sectional area of the right body is smaller, this geometric factor will be larger. A larger geometric factor will lead to a larger stress present in the right body. For Case 3, since the cross sectional area of the left body is smaller, this geometric factor will also be smaller. A smaller geometric factor will lead to a smaller stress present in the right body.

The stress present in the left body will be found by assuming a zero overall stress state in the material. This means that if the right body has a tensile force, the left body must have an equal and opposite compressive force. Where the sizes of the two bodies differ, the stress present in the larger body will be distributed over a greater area than in the smaller body, resulting in a smaller stress in the larger body. For example, if the larger body is four times the size of the smaller body, the stress present in the larger body will be one fourth the stress in the smaller body.

Analysis of the cases presented would result in the stress states seen in the figure below. In the figure, a tensile stress is represented by a positive number, and a compressive stress is represented by a negative number.

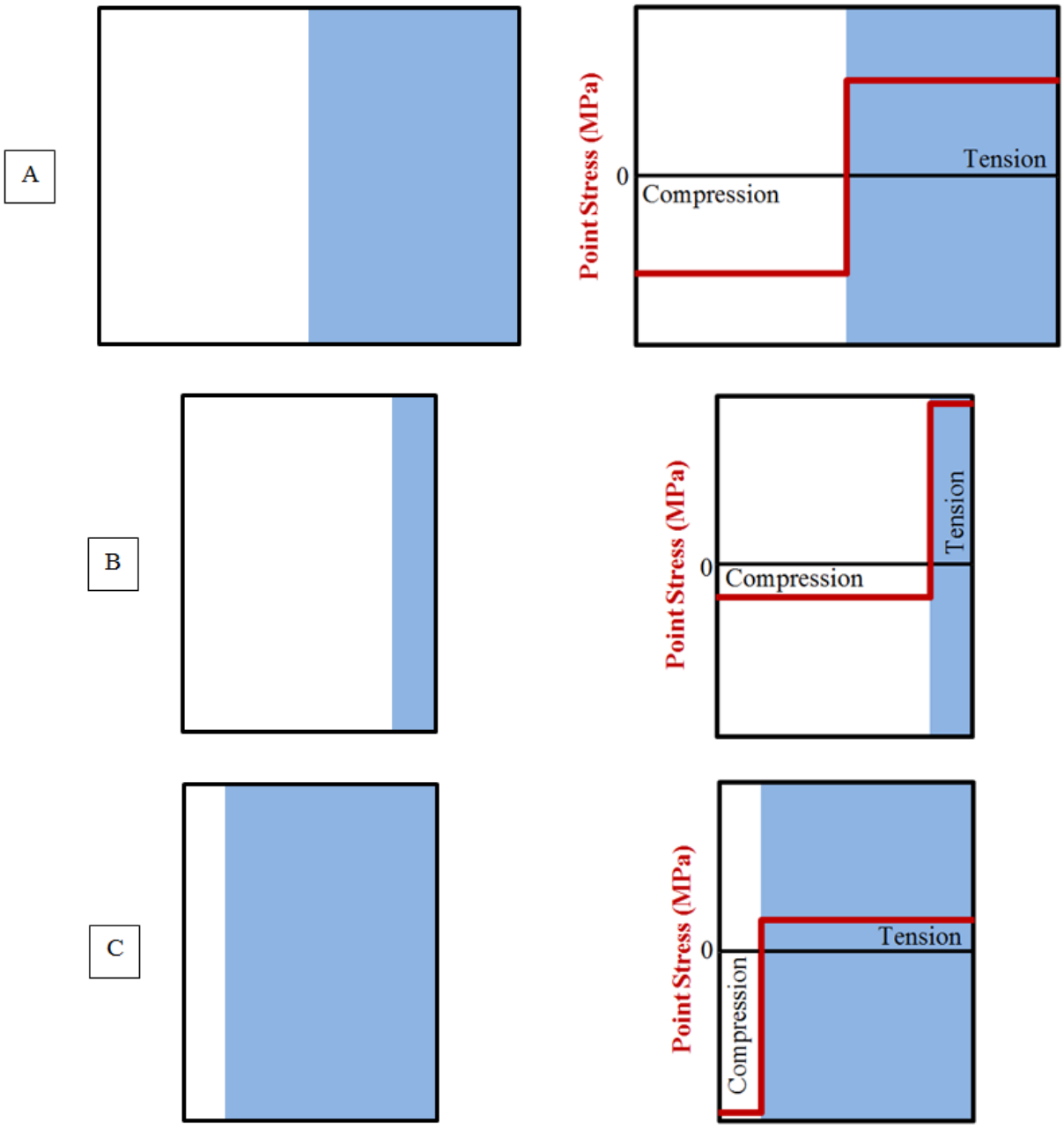

Figure 3.39: Schematic of the cases analyzed (left) and results of calculations (right). A) Case 1 (discrete interface, equal parts). B) Case 2 (discrete interface, thin glass). C) Case 3 (discrete interface, thin crystal).

The result of Case 1 (a discrete interface with equal parts glass and crystal) is moderate compressive stress in the crystal and moderate tensile stress in the glass. In this

case, the stresses present in the two bodies are equal since the two bodies are equally sized.

The result of Case 2 (a discrete interface with a thin glass region) is low compressive stress in the large crystal body and extreme tensile stress in the thin glass body. In this case, the stress present in the glass is significantly higher than the stress in the crystal because the glass body is smaller. This case could result in cracks opening in the glass region due to the extreme tensile force.

The result of Case 3 (a discrete interface with a thin crystal region) is extreme compressive stress in the thin crystal region and low tensile stress in the large glass body. In this case, the stress present in the glass is significantly smaller than the stress in the crystal because the glass body is larger. This case is less likely to result in cracks opening in the material due to the lowered tension in the glass. Cracks are not likely to open in the crystal body due to the extreme compression closing the cracks. The pairing of a thin crystal region and a large glass body could be preferable for crack prevention.

As seen in the cases above, stress changes drastically from compression to tension at a discrete interface. However, the materials created in this research resulted in graded interfaces. To understand the stresses at a graded interface, consider two additional cases. Case 4 has a large crystal body adjacent to a steep graded interface, similar to Sample 10. Case 5 has a shallow graded interface, similar to Sample 9. Schematics of these cases can be seen in Figure 3.40.

Analysis of graded interfaces will require additional assumptions. First, this analysis will consider the graded interface to be composed of discrete elements of linearly-decreasing crystallinity (i.e. an element with 100% crystallinity adjacent to an element with 80% crystallintiy for Case 4). The elements analyzed in each case is shown in Figure 3.40.

Second, some material property inputs into Equation 3 will change depending upon the percent crystallinity of the element. These material properties (coefficient of thermal expansion and elastic modulus) will be assumed to follow the linear Rule of Mixtures (shown in Section 2.5). Other inputs will remain constant throughout the material (Poisson's ratio and thermal cycling). In Cases 4 and 5, all elements will be assumed to have equal cross sectional areas, fixing the geometric factor at 0.5 for all elements.

Third, the stress of the element is equal to the summation of the calculated stress (from Equation 3) and the stress state of the adjacent element to the left. For example, if the left element has a stress of -100 MPa, and the calculated stress for the right element is +50 MPa, the reported stress for the right element would be -50 MPa.

The fourth assumption will involve the calculation of the compressive forces. As can be seen in Cases 1-3, the integral of the curve when the material is in tension equals the integral when the material is in compression. The integral can be seen graphically by the area of the region bounded by the curve and the axis (i.e. the rectangle between the red line and the x-axis). This equivalence of the tensile integral and the compressive

integral shows the equal and opposite forces. The equating of the integrals will be applied for the graded interfaces to obtain a zero overall stress state in the material. The compressive stress in the left-most element will be fixed so that the area above the curve (when in compression) and below the curve (when in tension) are equal.

Analysis of Cases 4 and 5 would result in the stress states seen in the figure below. In the figure, a tensile stress is represented by a positive number, and a compressive stress is represented by a negative number.

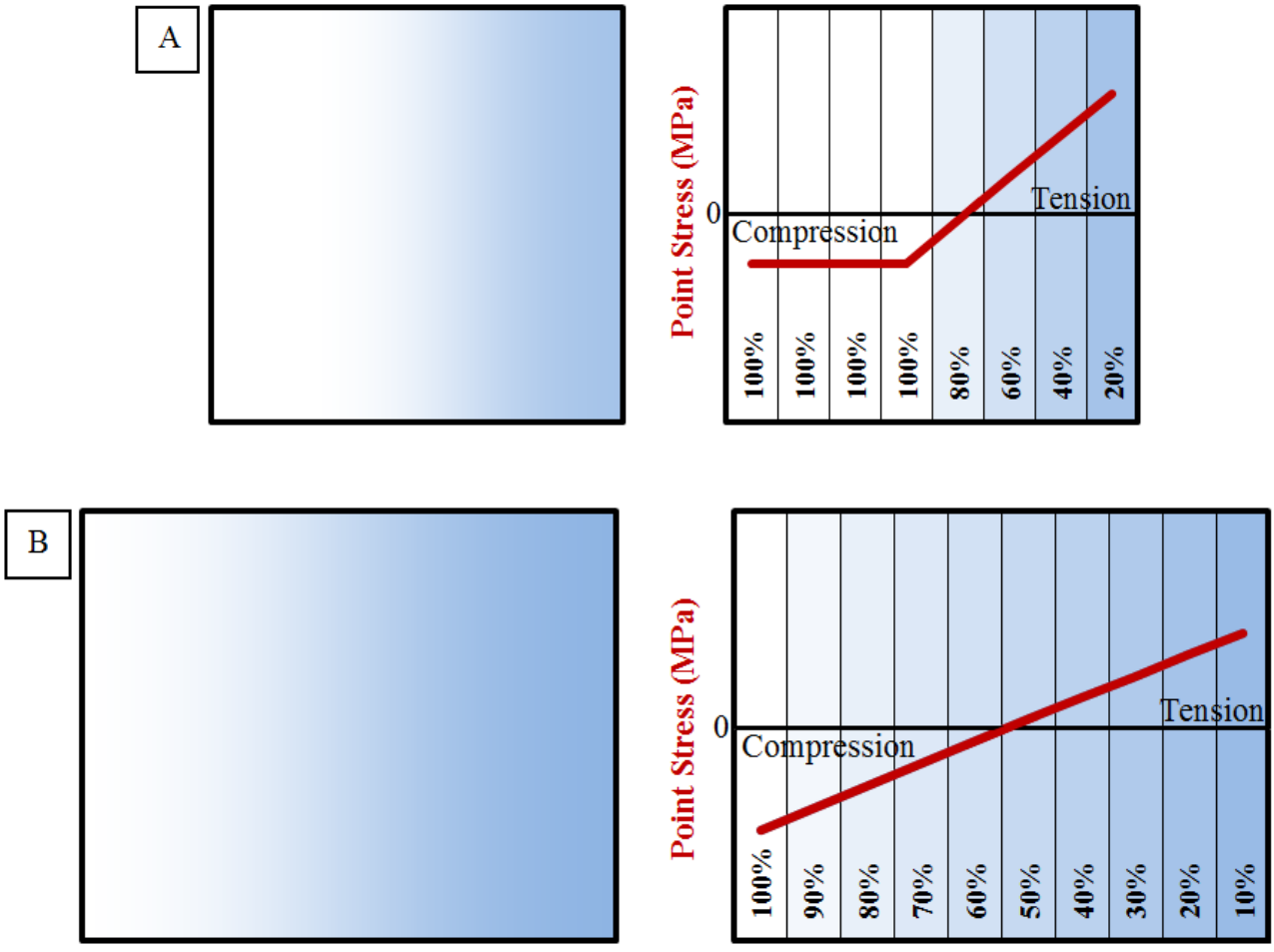

Figure 3.40: Schematic of the cases analyzed (left) and results of calculations (right). A) Case 4 (crystal region with steep graded interface). B) Case 5 (shallow graded interface).

The stress profiles of Cases 4 and 5 show a similar relationship to Cases 1-3. Near the 100% crystalline phase, the samples are in compression. Near the 0% crystalline phase, the samples are in tension. In contrast, the change in stress state is gradual, instead of instantaneous. The stress in the material gradually increases (towards tension) with decreasing crystallinity.

The result of Case 4 (crystal region with steep graded interface) is a constant low compressive stress in the crystal with a linearly increasing stress in the graded interface. In the graded interface, the change in stress is spread out over a distance. In Case 4, the extreme values of compression and tension are spaced between five elements.

The result of Case 5 (shallow graded interface) is a shallow linearly increasing stress. When compared to Case 4, the change in stress is spread out over an even greater distance. In Case 5, the extreme values of compression and tension are spaced between ten elements.

Cases 4 and 5 were analyzed to model the stresses present in Samples 9 and 10. Both of the cases resulted in high tensile forces near the glassy phase. These tensile forces can exceed the fracture strength of the glass, 64 MPa [12]. This could lead to the cracks opening in the glassy phase.

Note that this analysis is based on a two-dimensional semi-quantitative evaluation. These calculations approximate the stress for an element due to the difference in thermal expansion coefficient between that element and the adjacent element. This procedure is not appropriate for determining the exact stress in the material. Instead, it

can be used to show the trends in stresses due to changes in thermal expansion coefficients.

In the created microstructure graded glass-ceramics, cracks opened in the glassy phase because the fracture strength of the glass was exceeded. If the stresses in the samples are similar to the stresses modeled in Cases 4 and 5, the differences in coefficient of thermal expansion between lithium disilicate glass and crystal contributed to the stresses that exceeded the fracture stress.

It is unclear where these cracks initiate from, but one possibility is the voids that form due to the densification of the crystalline phase. These voids forming in between the glassy and crystalline phases could be sites of extreme stress, leading to crack initiation. Another possibility for crack initiation is from the surface of the glass. Surface defects could be formed from material handling and open from the tension due to the thermal expansion mismatch.

4. Summary and Conclusions

The following conclusions correspond to the objectives discussed earlier in Section 1.3 (Statement of Work).

- A linear gradient resistance wire furnace was designed and constructed.
- Application of a temperature gradient imposed across a sample during crystallization resulted in a lithium disilicate microstructure graded glass-ceramic.
    - Different crystallization heating parameters resulted in varying crystallinity gradients.
        - High temperature, moderate temperature gradient, and short time resulted in a steep crystallization gradient (as seen in Sample 10)
        - Low temperature, high temperature gradient, and a long time resulted in a shallow crystallization gradient (as seen in Sample 9)
    - The samples created using the procedures described above resulted in cracking throughout the glassy region.
        - This cracking is likely due to the difference in coefficient of thermal expansion present across the sample, causing stresses that exceed the strength of the glass.

- Scanning electron microscopy and Raman spectroscopy were used to evaluate the microstructure of the resulting samples throughout the cross section.
    - Scanning electron microscopy was used to show the microstructure of the standards and one sample. The micrographs were analyzed with ImageJ Software to quantify the amount of crystallization present.
    - Raman spectroscopy was used to determine the molecular bonds present in the material.
- In conjunction with the SEM data, a method was developed to quantify the percent crystallization based upon the Raman spectra.
    - A set of standards were analyzed with both scanning electron microscopy and Raman spectroscopy to create a data correlation between spectra peak Full Width at Half Maximum and percent crystallinity.
    - Samples were analyzed by Raman spectroscopy to collect various spectra throughout the sample cross section. These spectra were analyzed to determine the spectra peak Full Width at Half Maximum at the various points.
    - The sample peak widths were correlated with the standard data to determine the amount of crystallinity present.

- Material properties of microhardness, density, elastic modulus, and thermal expansion coefficient were evaluated with respect to percent crystallinity.
    - Microhardness testing was performed on several standards and one sample. However, the variation in data was too great and the difference in hardness too small to draw any conclusions on the trend of the material property with respect to percent crystallinity.
    - Density, elastic modulus, and thermal expansion coefficient values for a lithium disilicate glass and glass-ceramic were reported. The Rule of Mixtures was applied to show the trend of these material properties with respect to percent crystallinity. The density and elastic modulus of lithium disilicate increases with increasing present crystallinity. The thermal expansion coefficient of lithium disilicate decreases with increasing present crystallinity. These material properties were also plotted with respect to cross section for Samples 9 and 10.

In addition to the objectives of this study, a model was developed from literature research to create a possible explanation for the sample cracking. This model involved application of a composite equation into a two-dimensional semi-quantitative analysis using literature reported material property values. This model shows that a thermal property mismatch leads to stresses present in the material that can exceed the strength of the glass.

Preferential crystallization as a means to create a microstructure graded material provided a useful method for controlling properties without altering the chemical

composition. If research were to continue on this topic to produce a crack free material, microstructure graded glass-ceramics could be useful in many potential applications. With more sophisticated processing equipment, parameters could be controlled to create a wide range of functionally graded materials.

5. Future Work

This experiment has proven that it is possible to create a microstructure graded glass-ceramic by imposing a temperature gradient across the material during crystallization. However, there are many areas of research that could expand on this topic.

The most obvious is the bulk creation of a microstructure graded glass-ceramic without resulting in cracking through the glassy phase. Further exploration could develop the experimental parameters necessary to create a stress-free material. Perhaps a temperature gradient furnace could be used to more precisely control the temperature gradient during crystallization. The temperature gradient directly controls the resulting crystallization gradient. There could be a crystallization gradient, and therefore a thermal expansion gradient, that would result in a gradual enough change that would not cause cracks upon cooling.

Another method to produce a crack free sample could be to further explore the stresses created in the material due to the crystallization gradient. The use of Finite Element Analysis could analyze the stresses arising in the material on the scale of atomic layers. This method could eliminate the need for assumptions (as was done in this work) and make the analysis more accurate. Exploration of these stresses as a function of percent crystallinity could discover the maximum crystallization gradient possible to produce a crack-free sample.

If a crack-free material can be created, it could be possible to take advantage of the compression in the crystalline phase due to the thermal expansion differences (stresses due to thermal expansion differences were shown in Section 3.5.3). An example of this would be a material where 100% crystallinity exists on both surfaces of the material and 0% crystallinity inside the cross section. If a microstructure graded "sandwich" were to be created, the center of the material would be in tension, but both surfaces of the material would be in compression. A large glassy region in the center and thin crystalline regions on the surfaces would result in low tension in the glass and extreme compression in the crystal (as seen in Case 3 in Section 3.5.3). The compression on the surface of the material could result in enhanced strength values while not exceeding the fracture strength of the glass.

Another area of future research could be to study the individual contributions of crystallization temperature, temperature gradient, and time on the resulting crystallization gradient. If the exact contribution of each parameter is determined, then materials can be created with specified gradient slopes and thicknesses. This will help to gather the knowledge necessary for implementation into specific applications.

A possible area of future research is to impose a temperature gradient during nucleation instead of, or in addition to, crystallization. Following the same procedures as this experiment, a temperature gradient could be applied during nucleation. This would allow for varying population of nuclei across the sample cross section. It could be possible to create such a gradient that nuclei are very populated at one surface and not at

all at the other surface. Homogeneous crystallization applied to this partially nucleated sample would grow crystals only where the nuclei have formed. In regions where the nuclei are very populated, the crystals would not grow very large before growing into surrounding crystals. In regions where nuclei are not very populated, crystals would grow larger before growing into surrounding crystals. Using this method, it could be possible to create a 100% crystalline material that is still microstructure graded due to the differing crystal sizes across the sample.

Lastly, another area of research could be to explore other material groups that contain glasses that readily crystallize. Groups of interest would include compositions that have similar coefficients of thermal expansion for the glass and crystal phases. If such a material group were to be converted into a microstructure graded glass-ceramic, it is possible that the stresses arising due the differences in coefficient of thermal expansion would not exceed the fracture strength of the material. It could also be possible that different material groups will provide beneficial properties when transformed into a microstructure graded glass-ceramic.

References

1. Mahmoud, M. (2007). *Crystallization of lithium disilicate glass using variable frequency microwave processing*. (Doctoral dissertation, Virginia Polytechnic Institute and State University), Available from Virginia Tech Digital Library and Archives. (etd-05012007-164214) Retrieved from http://scholar.lib.vt.edu/theses/available/etd-05012007164214/unrestricted/Morsidissertationfinal3.pdf
2. Shelby, J. E. (2005). *Introduction to glass science and technology*. (2 ed.). Cambridge, UK: The Royal Society of Chemistry.
3. Kingery, W. D., Bowen, H. K., & Uhlmann, D. R. (1975). *Introduction to ceramics*. (2 ed.). New York, NY: John Wiley & Sons.
4. Fang, L., Gao, Y., & Zhang, Z. (1999). Tribology of si3n4 with different glassy phase content sliding against grey cast iron lubricated with water. *Wear, 225*(2), 896-904. Retrieved from http://www.sciencedirect.com/science/article/pii/S0043164898004086
5. Neubrand, A. (2001). Functionally Graded Materials. *Encyclopedia of Materials - Science and Technology* (p. 3407-3413). Elsevier. Retrieved May 2, 2012, from http://www.knovel.com.ezproxy.lib.vt.edu:8080/web/portal/browse/display?_EXT_KNOVEL_DISPLAY_bookid=1871&VerticalID=0
6. Tilley, R. (2000). "Colour and the optical properties of materials." (pp. 151-155). West Sussex, England: John Wiley & Sons.
7. Rasband, W.S., ImageJ, U. S. National Institutes of Health, Bethesda, Maryland, USA, http://imagej.nih.gov/ij/, 1997-2011.
8. Vander, G. F. (2000). Microindentation hardness testing. In H. Kuhn & D. Medlin (Eds.), *ASM Handbook, Volume 8: Mechanical Testing and Evaluation* (pp. 221-231). ASM International.
9. Buchner, S., Lepienski, C. M., Soares Jr., P. C., & Balzaretti, N. M. (2011). Effect of high pressure on the mechanical properties of lithium disilicate glass ceramic. *Materials Science and Engineering*, (528), 3921-3924. Retrieved from http://www.sciencedirect.com/science/article/pii/S0921509311001171
10. Yamane, M., & Mackenzie, J. D. (1974). Vicker's hardness of glass. *Journal of Non-Crystalline Solids, 15*, 153-164. Retrieved from http://www.sciencedirect.com/science/article/pii/0022309374900441
11. Albakry, M., Guazzato, M., & Swain, M. V. (2003). Fracture toughness and hardness evaluation of three pressable all-ceramic dental materials. *Journal of Dentistry, 31*, 181-188. Retrieved from http://www.sciencedirect.com/science/article/pii/S0300571203000253
12. Bona, A. D., Mecholsky, J. J., & Anusavice, K. J. (2004). Fracture behavior of lithia disilicate- and lucite-based ceramics. Dental Materials, 20(10), 956-962. Retrieved from http://www.sciencedirect.com/science/article/pii/S01095641040